POLYHEDRAL OLIGOMERIC SILSESQUIOXANES (POSS) BASED POLYMER NANOCOMPOSITES

by

MPITLOANE JOSEPH HATO (M.Sc.)

Submitted in accordance with the requirements for the degree

DOCTOR OF PHILOSOPHY (Ph.D.)

Department of Chemistry

Faculty of Natural and Agricultural Sciences

at the

UNIVERSITY OF THE FREE STATE (QWAQWA CAMPUS)

SUPERVISOR: PROF A.S. LUYT

CO-SUPERVISOR: PROF S. SINHA RAY

November 2009

DECLARATION

We, the undersigned, hereby declare that the research in this thesis is Mr. Hato's own original work, which has not partly or fully been submitted to any other University in order to obtain a degree.

_____ _____

Mr MJ Hato Prof AS Luyt

_____

Prof S Sinha Ray

DEDICATION

I would like to dedicate this work to the memories of my late parents (Tankiso Piet and Masinuku Maria), late brothers (Moeketsi Elias and Kgauta David), late sister (Manana Elizabeth), and to my late grandmother (Makgokolotso Alinah Mothibeli)

ACKNOWLEDGEMENTS

- Firstly, I would like to give honour to the Almighty God for the strength he gave me to make this study a success.
- I would like to express my deep and sincere gratitude to my beloved supervisor, *Prof. Adriaan Stephanus Luyt,* for his meticulous guidance, congenial support during the tenure of the study. His broad knowledge, benevolent and compassionate treatment has been of great value to me to accomplish the target.
- I am grateful to my co-supervisor, *Prof. Suprakas Sinha Ray,* for his valuable advices all through my up and downs situations of this work. I also thank him for opening new vistas of my career (nanoscience). Above all, I am also grateful to him for his immense ideas not only from the science perspective but also as a colleague to me.
- My heartfelt appreciation goes to *Dr. Arjun Maity* (*Polymers and Composites, Council for Scientific and Industrial Research, Republic of South Africa)* for his fruitful discussions and constructive comments in this study.
- I am grateful to my friend *Dr. Mokhotjwa S. Dhlamini* from the *National Centre for Nano-Structured Materials, Council for Scientific and Industrial Research of the Republic of South Africa* for helping me to finalize my thesis. His comments were of vast help to me.
- I thank *Dr. Gerald F. Malgas* and *David E. Motaung (National Centre for Nano-Structured Materials, Council for Scientific and Industrial Research, Republic of South Africa)* for their immense help and kindness with x-ray diffraction analysis and discussion.
- I would like to thank *Mathew K. Moodley* for linguistic corrections of part of the work in this thesis.
- I thank *Jayita Bandyopadhyay* for helping me with the polarized optical microscopy and small-angle x-ray scattering measurements.
- I thank my friend *Dokie 'Kgots' Mofokeng* for his fascinating jokes that kept me going during hard times.
- I thank *Thabiso 'Malombo' Phillemon* for his constructive ideas and inputs all the time.
- Many thanks are offered to my wife, ***Mamatebele***, and our two daughters, ***Tankiso*** and ***Dimpho***, for letting me write on nights when I should have been an attentive husband

and father. My unique gratitude is due to my sisters (*Mamakgaola, Mapapiso, Malefi and Nthabiseng*) and my nephews and nieces for their moral support.

- I thank many friends over the years that have made me the person that I am today. I would in particular like to thank *George K. Tshabalala (Physics Department, University of the Free State, Republic of South Africa)*, *Dr. Jonathan Andrew 'Spirit' Molefi, Tshediso Sibiya, Malefu 'Shwalane' Mosia, Mphikeledi 'Skekete' Nhlapo, Walter 'Mashoto' Nhlapo, Ausi Regina Nhlapo, Dr. N.S. Nhlapo, Mojalefa I. Semase, Tshwafo E. Motaung, Dimaketse P. Motlohoneng, Sello P. Mbambo, Sabata 'Zoo' Mokhele, Mapula B. Mametja, Kwanele Tshapu, Segaula I. Manabile,* and others for making this an unforgettable experience.
- I am so blessed with the opportunity to meet both my promoters in my life. This work is a small tribute to them from a student who avidly still wants to learn more from them.
- I thank all staff members and my colleagues from the *National Centre for Nano-Structured Materials at the Council for Scientific and Industrial Research of the Republic of South Africa* for helping me in either way during laborious times.
- I am grateful to the *National Centre for Nano-Structured Materials* receptionist *Ms Simphiwe I. Mcineka* for arrangements of all my research trips I have undertaken during this study.
- Many thanks to my former school teachers of *Metsimatsho Senior Secondary School and Mapeka Senior Primary School* (*Thaba-bosiu village*) for their inspiration and encouragement.
- I thank all my collegeous at the *Chemistry Department* of the *University of the Free State (QwaQwa campus), Republic of South Africa,* for their moral support during my visits at the department.
- Finally, I am grateful for the financial support from the *Department of Science and Technology* and the *Council for Scientific and Industrial Research, Republic of South Africa,* which enabled me to complete my study.

'Modimo o mosa le lerato hlohonolafatsa ba nka karolo mosebetsing ona'

ABSTRACT

This work reports on the preparation and characterization of polyhedral oligomeric silsesquioxanes (POSS)-containing polymer nanocomposites. The nanocomposites investigated in this study consist of two different types of POSS particles [octamethyl-T_8-POSS and poly((propylmethacryl-heptaisobutyl-POSS)-*co*-(methyl-methacrylate))] dispersed in two different polymer matrices such as linear low-density polyethylene (LLDPE) and poly(methyl methacrylate) (PMMA). The melt-blending technique was used for the preparation of various nanocomposites. The morphology and structure of various nanocomposites were characterized by using x-ray diffraction (XRD), small angle x-ray scattering (SAXS), field-emission scanning electron microscopy (FE-SEM) and polarized optical microscopy (POM). The influence of different loadings of POSS particles on the thermal, thermomechanical, tensile, impact, and melt-state viscoelastic properties of nanocomposites was investigated.

The morphology of the freeze-fractured surfaces of the LLDPE/POSS nanocomposites investigated by means of FE-SEM, revealed a homogeneous dispersion of the octamethyl-T_8-POSS particles into the LLDPE matrix at a low filler content. The thermal properties of pure LLDPE and various nanocomposites showed double melting behaviour of the neat LLDPE matrix and the nanocomposite samples. The thermomechanical properties were investigated by stress-strain controlled rheometry using a solid-state rectangular fixture. The results showed a moderate improvement in both the storage and loss moduli of the neat LLDPE upon the incorporation of the POSS particles. The thermal stability of pure LLDPE and its nanocomposites was investigated in both air and nitrogen atmospheres. Two degradation steps were observed for all studied samples under nitrogen atmosphere. An improvement in the thermal stability of the samples studied in air in the high-temperature region was observed.

The melt-state rheological properties measurements showed that the POSS particles were highly immiscible with the LLDPE matrix. POSS-containing LLDPE composites did not show any improvement in tensile properties. A decrease in impact properties of the LLDPE at higher POSS loadings was observed. The heat distortion temperature of the LLDPE samples increased with increasing the POSS loading in the polymer matrix.

In the case of PMMA/POSS nanocomposites, the FE-SEM results did not give any information about the dispersion of the POSS particles in the PMMA matrix. However, the XRD studies indicated that the POSS particles were dispersed throughout the PMMA matrix. Both differential scanning calorimetry (DSC) and dynamic mechanical analysis (DMA) showed a single glass transition for all the investigated samples. A decrease in the glass transition temperature was observed with increasing POSS loading in the polymer matrix. The rheological studies showed a gel-like character for all the investigated samples. An increase in the storage modulus for the 5 wt % POSS-containing sample was observed when compared with pure PMMA.

LIST OF ABBREVIATIONS

AFM : Atomic force microscopy

AIBN : N,N-azobis(isobutyronitrile)

Al : Aluminium

ASTM : American standard testing method

CCD : Charge coupled device

CdS : Cadmium sulfide

CNT : Carbon nanotube

CoNaph : Cobalt naphthenate

DCP : Dicumyl peroxide

DDM : 4,4'-Diaminodiphenylmethane

DGEBA : Diglycidyl ether of bisphenol A

dH_c/dT : Heat flow rate

DSC : Differential scanning calorimetry

DMA : Dynamic mechanical analysis

DMSO : Dimethyl sulfoxide

DMTA : Dynamic mechanical thermal analysis

E : Young's modulus

E' : Elastic storage modulus

E'' : Elastic loss modulus

EDS : Energy dispersive spectroscopy or energy dispersive x-ray spectroscopy

EELS : Electron energy loss spectroscopy

EG : Ethylene glycol

EP : Ethylene propylene

FE-SEM : Field-emission scanning electron microscopy

G' : Storage modulus

G'' : Loss modulus

G_N^0 : Rubbery plateau modulus

g-PP : Grafted polypropylene

ΔH_m : Heat of fusion

ΔH_c : Heat of crystallization

HDPE : High-density polyethylene

HDT : Heat distortion temperature

ib-POSS : Isobutyl-POSS

i-PP : Isotactic polypropylene

LDPE : Low-density polyethylene

LLDPE : Linear low-density polyethylene

MAO : Metallocene-methalaluminoxane

MEKP : Methyl ethyl ketone peroxide

m-LLDPE : Metallocene linear low-density polyethylene

MA : Methacrylate

MDSC : Modulated DSC

MMA : Methyl methacrylate

MMD : Molecular mass distribution

MMT : Montmorillonite

$\overline{M}_n$: Number average molecular weight

$\overline{M}_w$: Weight average molecular weight

MWCNT : Multi-walled carbon nanotube

η^* : Complex viscosity

OA : Octaallylsilsequioxane

Oap-POSS : Octaaminophenyl POSS

Oib-POSS : Octaisobutyl-POSS

OnpPOSS : Octanitrophenyl-POSS

OG : Octaglycidyldimethylsiloxy

OPGE : Octa(propylglycidyl ether

PbS : Lead sulphide

PEDOT : Poly(3,4-ethylene dioxythiophene)

PEG : Poly(ethylene glycol)

PEO : Poly(ethylene oxide)

PE : Polyethylene

PET : Poly(ethylene terephthalate)

PMMA : Poly(methyl methacrylate)

PNVC : Poly(N-vinylcarbazole)

POM : Polarized optical microscopy

POSS : Polyhedral oligomeric silsesquioxane

POZO : Poly(2-methyl-2-oxazoline)

PP : Polypropylene

PPG : Poly(propylene glycol)

PS : Polystyrene

PBS : Poly(butylene succinate)

PBSA : Poly[(butylene succinate)-co-adipate]

PBT : Poly(butylene terephthalate)

PEEK : Poly(ether ether ketone)

PI : Polyimide

PT-15 : Cyanate ester

PTFE : Polytetrafluoroethylene

PTP : Polythiophene

PVA : Poly(vinyl alcohol)

PVDF : Polyvinylidene fluoride

PVP : Poly(vinyl pyrrolidinone)

$R'_8(SiO_{1.5})_8$: Octa-functional POSS

SAXS : Small angle x-ray scattering

SDS : Sodium dodecylsulfonate

SEM : Scanning electron microscopy

SiO_2 : Silicon dioxide

$Si(OCH_3)_3$: Sallyltrichlorosilane

SPM : Scanning probe microscopy

STXM : Scanning transmission x-ray microscopy

SWCNT : Single-walled carbon nanotube

T : Temperature

TA : Thermal analysis

tan δ : tan delta (loss factor)

TEM : Transmission electron microscopy

T_g : Glass transition temperature

TGA : Thermogravimetric analysis

THF : Tetrahydrofuran

T_m : Melting temperature

T_o : Crystallization onset temperature

$T_{p,c}$: Crystallization peak temperature

T_∞ : Crystallization end temperature

$R'Si(OR)_3$: Trialkoxysilanes

$R'SiCl_3$: Trichlorosilanes

VE : Vinyl ester

V_f : Free volume

WAXS : Wide angle x-ray scattering

XRD : X-ray diffraction

X_T : Relative degree of crystallinity (temperature or time)

Zn : Zinc

TABLE OF CONTENTS

LIST OF SCHEMES AND FIGURES

LIST OF TABLES

CHAPTER 1

INTRODUCTION

1.1 Background

Nanoscience is defined as the study of atoms, molecules and objects whose size is in the nanometer range [1], while nanotechnology is generally defined as a manufacturing technology to produce cost effective structures compatible with nature and prepared from molecules [2]. The concept of nanotechnology has been the subject of research for the past few decades. According to Dr. Mihail (Mika) Roco [3], nanotechnology can be described by four eras. The first era indicates the passive nanostructured materials designed to perform one task. The second era introduces active nanostructures for multiple tasks; for instance, actuators, drug delivery devices, and sensors. The third one is anticipated to begin emerging around 2010 and will feature nanosystems with thousands of interacting components. A few years later, the first integrated nanosystems, functioning (according to Roco) much like a mammalian cell with hierarchical systems within systems, are expected to be developed.

Knowledge in this new field of science is growing worldwide, which led to elementary scientific progresses [4]. This will lead to remarkable changes in various applications, such as micro-electronics, photovoltaics, and health care. For example, development is underway on a data storage machine that will be able to store a trillion bits of information on three centimetres, which is twenty times more than today's available technology. This figure is equivalent to 25 million printed pages on something the size of a postage stamp. It is predicted by many scientists that the developments in nanotechnology will affect almost every aspect of our lives, from medicines, the performance of the computers, the supply of energy, food, cars, buildings, and clothing [2]. For this reason, there are rapid increases in investments from governments and industries in each and every part of the world. Currently, billions of dollars have been invested in nanotechnology, of which the highest amount comes from the private sector [5]. In the long run, it is believed that nanotechnology will bring more efficient channels to manufacturing industries, which will use less raw materials and energy. It is also fundamentally important to substantiate such ideas [6].

Nanomaterials are categorized into nanoparticles and nanocrystalline materials. The former are ultrafine dispersive particles with diameters below 100 nm, while the latter are

polycrystalline bulk materials with grain sizes in the nanometer range (less than 100 nm) [7]. Generally, nanoparticles are considered as the building blocks of bulk nanocrystalline materials. Most of their applications are still in a fledging phase of technical development [8]. As a result, a lot of work still needs to be done for the full potential use of these materials in various sectors.

Recently, preparation of nanoparticles following various synthetic methods has shown an immense interest in research and development as well as academia. Different preparative methods may offer different internal structures that can affect the resultant properties of materials consolidated from them [1]. Nanoparticles have very high surface-to-volume ratios, i.e. large fractions of surface atoms. The large fractions of surface atoms together with ultra-fine size and shape effects make nanoparticles exhibit different properties from the bulk. Because nanoparticles contain high specific surface areas, they exhibit a high reactivity and strong tendency towards agglomeration. This particle agglomeration weakens the mechanical or optical properties of the resulting materials [8]. Nanomaterials exhibit peculiar and very fascinating final properties like improvement in the mechanical strength and higher specific heat capacity compared to their conventional coarse grained counterparts [9]. The percentage of surface atoms increases as the size of the nanoparticles decreases [1].

In this study, we mainly focus on the polyhedral oligomeric silsesquioxane (POSS) filled polymer composite systems. POSS is a hybrid material (organic-inorganic) which contains a basic polyhedral silicone-oxygen nanostructured skeleton or cage. POSS chemicals can form crystal domains when they are covalently bonded to a polymer backbone as pendant groups during grafting, polymerization, surface bonding, or other transformations [10]. Production of different POSS nanostructured chemicals has shown a rapid increase in recent years [11]. They are usually in the form of powders or oils [12,13], but in some other cases POSS nanomaterials are found in polymeric form as films, thin layers, or coatings. Polymeric POSS has excellent dielectric and optical properties. They are used in photoresists, interlayer dielectrics, and protective coating films for applications in semiconductor devices [13]. Unlike traditional organic compounds, they release no volatile components, so they are odourless and environmentally friendly [12,13]. These nanomaterials may be easily incorporated into different polymer systems using different methods such as melt-blending, copolymerization or grafting to produce lightweight composites without compromising properties such as optical behaviour or weight [14-17].

The use of nanostructured materials to prepare polymer composites is due to their special size-dependant specific properties, while the desired properties of the polymer remain preserved in the composites [18,19]. It was reported that the addition of these POSS hybrid materials into different polymeric systems enhances various properties such as the mechanical, thermal and processing properties that are appropriate to substitute materials like metals and other composite materials in many industrial fields [20]. In the case of POSS-containing polymer nanocomposite systems, homogeneous dispersion of POSS nano-sized particles can be obtained when small loadings of POSS nanofiller are used [16]. However, the incorporation of these hybrid materials may also result in phase separation of the hybrid particulate systems. For one to solve this problem, the use of a polymer which interacts (Van der Waals, dipolar, hydrogen bonding) with the particles as well as the attachment of initiation groups for grafting of polymer chains from the particle surface are needed [21]. Addition of POSS nano fillers into the polymer systems can influence the morphology of the composites. These morphological features of the resultant composites strictly depend on the processing conditions when the nanofillers may act as nucleating agent and influence the crystallization behaviour of the matrix [22].

1.2 Objectives of the study

The POSS particles have been used as reinforcing nanomaterials for many years and they can be molecularly dispersed within polymer matrices. POSS derivatives which contain unreactive functional groups can be physically mixed with polymer matrices to influence the morphological characteristics of the resultant composites. Therefore, the resultant properties of the polymer matrix can be improved by the addition of a small amount of POSS molecules into the polymer systems. For this reason, POSS derivatives are potential candidates as reinforcing nanomaterials for the fabrication of the polymer nanocomposites.

The main objective of this study is to prepare polymer nanocomposites based on thermoplastic and amorphous polymer resins with different types and loadings of POSS nanoscale fillers. The reason we opted for melt-blending in this investigation is because this is a very important method in industrial practices and it is performed to obtain unique properties that the individual materials fail to attain. In this study, linear low-density polyethylene (LLDPE) and poly(methyl methacrylate) (PMMA) were, respectively, melt-mixed with

octamethyl-POSS and poly(propyl methacryl-heptaisobutyl-POSS)-co-(methyl methacrylate) nanofillers. The specific objectives of this project were categorized as follows:

- Preparation of LLDPE/POSS and PMMA/POSS nanocomposites, containing different loadings of nano-scaled POSS particles.
- Determination of the influence of the POSS particles on the crystal growth behaviour of the different samples using a polarized optical microscope (POM).
- Determination of the morphological characteristics of various samples by means of scanning electron microscopy (SEM).
- Determination of the structure, crystallinity and miscibility of the different samples by wide angle x-ray scattering (WAXS) and x-ray diffraction (XRD).
- Determination of the melting and nonisothermal crystallization behaviour of the samples using differential scanning calorimetry (DSC).
- Determination of the influence of the presence of POSS nanoparticles on the thermal stability of the samples by thermogravimetric analysis (TGA).
- Determination of the influence of the presence of POSS nanoparticles on the thermomechanical properties of the samples using dynamic mechanical analysis (DMA).
- Determination of the melt-state viscoelastic properties of the different samples using rheometry.
- Determination of the effect of the POSS nanoparticles on the tensile properties of the samples using a universal testing machine.
- Determination of the effect of the POSS nanoparticles on the heat distortion temperatures (HDT) of the samples.
- Determination of the effect of the POSS nanoparticles on the impact properties of the samples.

1.3 Thesis layout

This study comprises of 7 chapters. Chapter 1 presents the background and objectives of this work. A literature survey relevant to the project is given in Chapter 2. A summary of all the materials and characterization techniques used in this study is given in Chapter 3. This includes a brief description on how each of these techniques works. The results generated on

the different polymer/POSS systems during the course of this research are presented and discussed in chapters 4, 5, and 6. Finally, in Chapter 7, a summary of the thesis and concluding remarks are presented.

1.4 References

1. M.S. Dhlamini. Luminescent properties of synthesized PbS nanoparticle phosphors. Ph.D dessertation, University of the Free State (2008).
2. S. Sinha Ray. A special issue on polymer nanocomposites. Journal of Nanoscience and Nanotechnology 2008; 8:1557-1558.
3. M.C. Roco, W.S. Bainbridge. Societal Implications of Nanoscience and Nanotechnology, Springer: Boston (2001).
4. Centre for Responsible Nanotechnology: http://www.crnano.org.2008
5. S.J. Fonash. Education and training of the nanotechnology workforce. Journal of Nanoparticle Research 2001; 3:79-82.
6. D. Bruce. The question of ethics. Nano Today 2006; 1:6-7.
7. S.C. Tjong, H. Chen. Nanocrystalline materials and coatings. Materials Science and Engineering Reports 2004; 45:1-88.
8. P.G. Sanders, J.R. Weertman, J.G. Barker. Structure of nanocrystalline palladium and copper studied by small angle neutron scattering. Journal of Materials Research. 1996; 11:3110-3120.
9. H. Gleiter. Nanocrystalline materials. Progress in Materials Science 1989; 33:223-315.
10. J.D. Lichtenhan, Y.A. Otonari, M.J. Carr. Linear hybrid polymer building blocks: Methacrylate-functionalized polyhedral oligomeric silsesquioxane monomers and polymers. Macromolecules 1995; 28:8435-8437.
11. G. Li, L. Wang, H. Ni, C.U. Pittman Jr. Polyhedral oligomeric silsesquioxane (POSS) polymers and copolymers: A review. Journal of Inorganic and Organometallic Polymers 2002; 11:123-154.
12. Nanostructured chemicals as alloying agents in polymers: http://www.patentstorm.us/patents/6716919/description.html 6th April 2004.
13. E.G. Shockey, A.G. Bolf, P.F. Jones, J.J. Schwab, K.P. Chafee, T.S. Haddad, J.D. Lichtenhan. Functionalized polyhedral oligomeric silsesquioxanes. New graftable POSS hydride, POSS-olefin, POSS epoxy, and POSS chlorosilane macromers and POSS-siloxane triblocks. Applied Organometallic Chemsitry 1999; 13:311-327.

14. R.H. Baney, M. Itoh, A. Sakakibara, T. Suzuki. Silsesquioxanes. Chemistry Reviews 1995; 95:1409-1430.
15. A. Fina, D. Tabuani, A. Frache, G. Camino. Polypropylene-polyhedral oligomeric silsequioxanes (POSS) nanocomposites. Polymer 2005; 46:7855-7866.
16. M. Joshi, B. S. Butola, G. Simon, N. Kukaleva. Rheological and viscoelastic behaviour of HDPE/octamethyl-POSS nanocomposites. Macromolecules 2006; 39:1839-1849.
17. M. Joshi, B.S. Butola. Isothermal crystallization of HDPE/octamethyl polyhedral oligomeric silsesquioxane nanocomposites. Journal of Applied Polymer Science 2007; 105:978-985.
18. G. Kickelbick. Concepts for the incorporation of inorganic building blocks into organic polymers on a nanoscale. Progress in Polymer Science 2003; 28:83-114.
19. M.Q. Zhang, M.Z. Rong, H.B. Zhang, K. Friedrich. Mechanical properties of low nano-silica filled high density polyethylene composites. Polymer Engineering and Science 2001; 43:490-500.
20. C. Jana, S. Jain. Dispersion of nano-fillers in high performance polymers using reactive solvents as processing aids. Polymer 2001; 42:6897-6905.
21. A.D. Pomagaila. Polymer-immobilised nano-scale and cluster metal particles. Russian Chemistry Reviews 1997; 66:679-716.
22. M. Pracella, D. Chionna, A. Fina, D. Tabuani, A. Frache, G. Camino. Polypropylene-POSS nanocomposites: Morphology and crystallization behaviour. Macromolecular Symposia 2006; 234:59-67.

CHAPTER 2

LITERATURE SURVEY

2.1 Introduction

New properties, low cost and reuse of polymers are fundamentally important parameters that are needed to meet the demands of today's society and of the polymer industry [1,1]. These polymers are of interest in many fields of science and engineering [3,2]. Unfortunately, for many applications, these demands need a set of properties that no polymers can fulfil. One method to satisfy these demands is by the addition of nanodimensional materials into a polymer matrix. These nanodimensional materials can be dispersed at nano or molecular level within the polymer matrix [5]. Processing methods include melt-blending [6], *in situ* curing [7], hydrolytic condensation [8], and *in-situ* polymerization [9]. However, melt-blending is of more interest because this method is regarded as an economical alternative and also one of the most important methods in industry for the preparation of new polymers. The advantages of polymer blending over other methods are its cost effectiveness and ease of processability. In addition, the unique properties that can be accomplished by melt-blending depend on the composition of the blend [10]. In most of the composites containing POSS nanofiller, studied by previous researchers, the focus was on the crystallization, morphological behaviour, as well as rheological, viscoelastic, thermal, and thermomechanical properties of these composites. However, the miscibility or compatibility and mechanical properties of these composites were not satisfactory.

This chapter is aimed at highlighting some aspects of the research on selective POSS-containing polymer nanocomposites.

2.2 Synthesis and characterization of POSS

POSS are low density (compared with conventional inorganic nanofillers), high performance hybrid materials that comprise of both organic (carbon) and inorganic (silicon) atoms. These molecules, which have been commercialized in the last decade, are intended to combine the most beneficial molecular properties of both organic and inorganic systems. POSS, owing to

their nanoscale size dimensions and their rigid inorganic framework, are potential candidates to be used for the preparation of hybrid nanocomposites.

Feher and coworkers [11] published a review on the synthesis of POSS macromers. Li *et al*. [12] also published a review describing the synthesis of both monofunctional and multifunctional POSS monomers and polymers. Generally, the synthesis of POSS depends on the nature of the starting materials to be used. These are very complex, multistep processes whereby an appropriate organosilicon precursor or monomer is converted into a series of polyhedral siloxanes *via* hydrolytic polycondensation [12]. The successful synthesis of POSS and its derivatives depends on the following factors [13]:

(i) Concentration of the initial monomer in the solution.
(ii) Nature of the solvent.
(iii) Type of catalyst used.
(iv) Temperature.
(v) Solubility of the polyhedral oligomers.
(vi) Quantity of water added and the rate of its addition.
(vii) Character of the substituent X and the functional group in the initial monomer.

There are two major methods for the synthesis of POSS compounds [14-16]. The first synthetic method was introduced by Scott in 1946. This method includes oligomeric silsesquioxanes containing the empirical formula $(CH_3SiO_{1.5})_n$ and synthesised by a thermolysis process of the polymeric products obtained from cohydrolysis of methyltrichlorosilane and dimethylchlorosilane shown in Scheme 2.1 [17]. The controlled hydrolysis and condensation of purified octaallylsilsequioxane (OA) obtained from allyltrichlorosilane is given in Figure 2.1 [18]. POSS compounds can also be derived from the manipulation of the substituents at the silicon atom without affecting the silicon-oxygen core of the molecule [12] as illustrated in Figure 2.2. This may be achieved via hydrosilylation of alkynes with $(HMe_2SiOSiO_{1.5})_8$ cages in the presence of a Pt (platinum) catalyst at 40 °C.

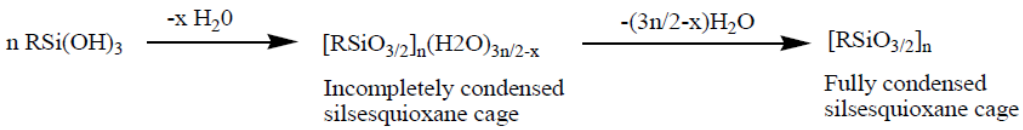

Scheme 2.1 Fabrication of POSS molecules using the hydrolytic condensation reactions of trifunctional organosilicon monomers

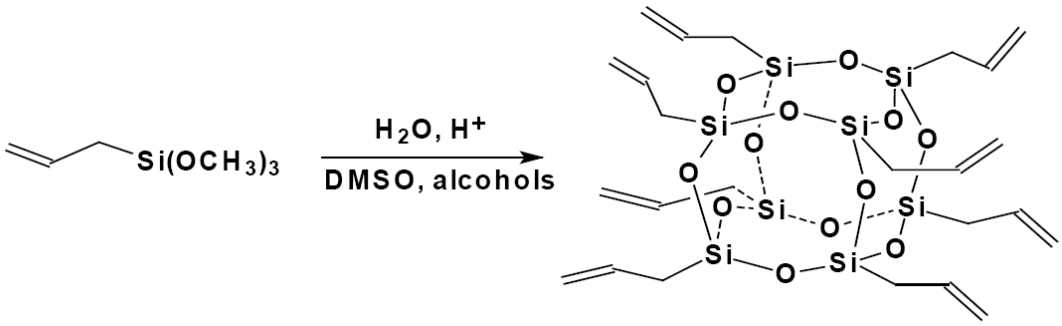

Figure 2.1 Synthesis of octaallylsilsesquioxane [19]

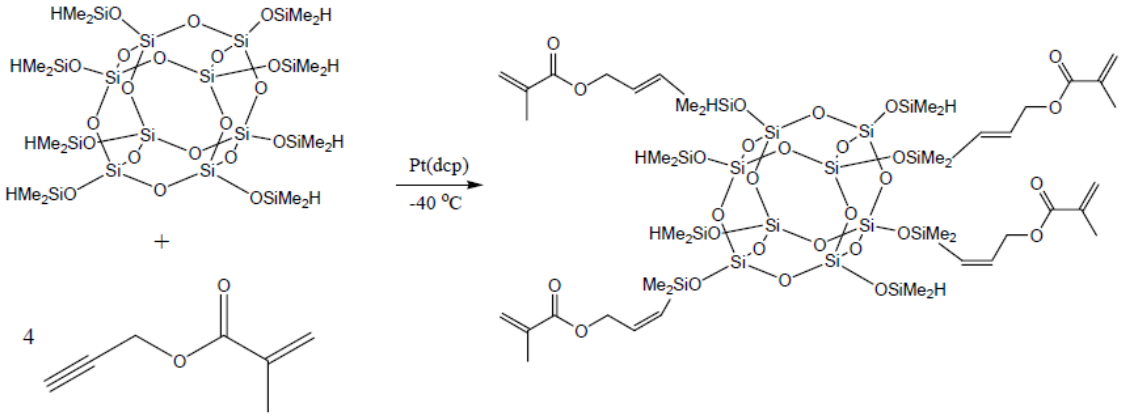

Figure 2.2 Synthesis of the multifunctional methacrylate (MA)-POSS [12]

2.3 Types of POSS

Silsesquioxanes are all structures with the general formula $RSiO_{1.5}$. Figure 2.3 depicts random, ladder, cage or cubic, and partially cage structures of silsequioxanes. The ladder-like and cage structures are the most common representations of silsesquioxanes. These compounds contain eight, ten or twelve silicon atoms attached on the vertices of the cage or core. POSS compounds contain a rigid framework which closely resembles that of silica and with a diameter of 1-3 nm. This framework is thermally and chemically robust and can stay intact up to 550 °C. The thermal stability of the organic substituents is compositionally dependent and ranges from 350 to 450 °C [20-22].

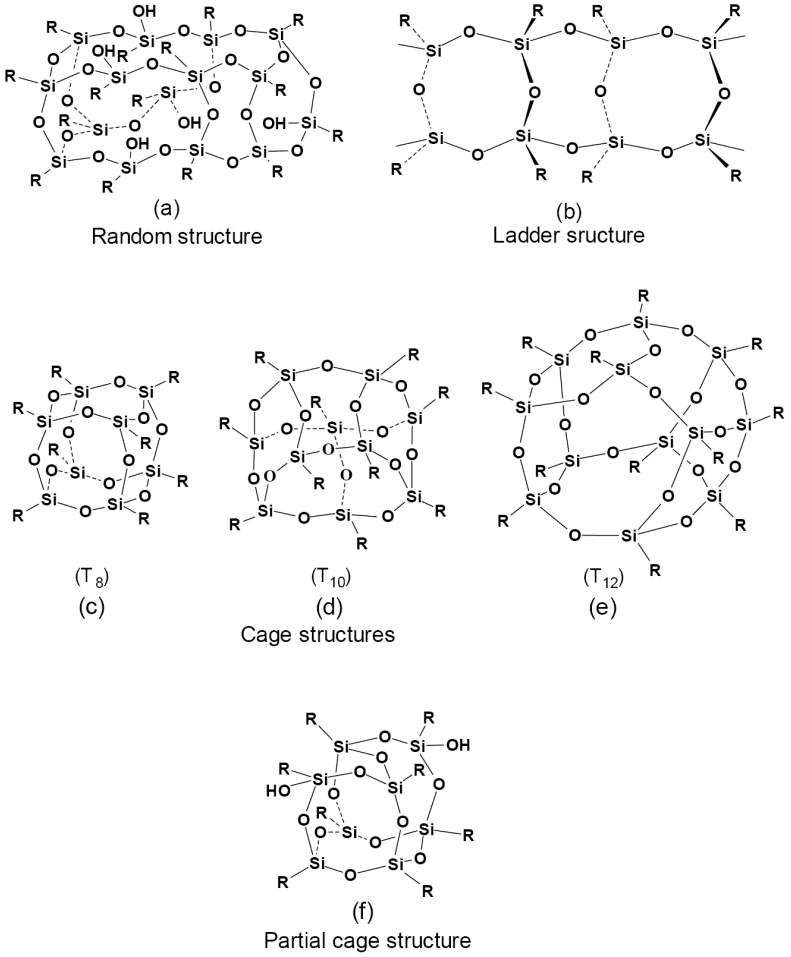

Figure 2.3 Structures of silsesquioxanes [12]

There are four general classifications of POSS-filled polymers and copolymers [23]:

(i) Star type: these are synthesized by the polymerization of a POSS cage containing multifunctional polymerizable groups which will form 3-D networks that are difficult to characterize.

(ii) Pendant type: these are POSS molecules with a single reactive functional group (e.g. vinyl) and can be polymerized as a monomer or co-monomer.

(iii) Bead type: a POSS core with two reactive functional groups is incorporated in the backbone of a polymer.

(iv) Non-reactive POSS molecules dispersed in a polymer matrix as filler.

Both bead and pendant types are highly soluble in common solvents (THF, toluene and chloroform).

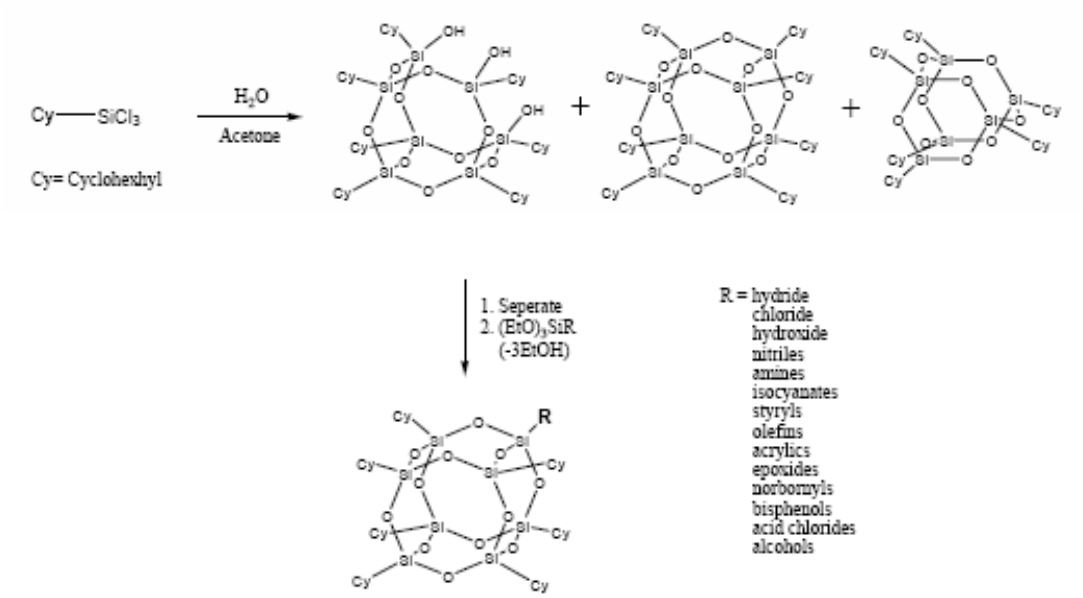

Figure 2.4 Synthesis of monofunctional POSS compounds [18]

In the reaction given in Scheme 2.1 both complete and incomplete condensed silsesquioxanes are produced. Complete condensed silsesquioxanes contain equivalent organic groups on each silicon atom, rendering them completely functionalized with non-reactive groups. Incomplete condensed ones contain reactive silanol functionalties and are the major products for producing monofunctional POSS compounds (see Figure 2.4). The reactivity of silanol groups makes incomplete condensed POSS molecules of interest as models for silica supported catalysts [18]. Multifunctional POSS molecules are another class of POSS derivatives. These molecules can be produced by hydrolysis and condensation of either trialkoxysilanes [$R'Si(OR)_3$] or trichlorosilanes ($R'SiCl_3$). R' is a reactive functional group. This reaction produces octa-functional POSS molecules, $R'_8(SiO_{1.5})_8$ as shown in Figure 2.2.

2.4 Modification of POSS structure

The organic groups ‘R’ attached on the Si atoms of the cage can be varied endlessly for further specific practical requirements [24] such as adhesion, light sensitization, binding catalyst species and surface bonding [21]. Although POSS can be thought of as the smallest particles of silica possible, they are physically large with respect to polymer dimensions and nearly equivalent in size to most polymer segments and coils.

POSS can be compatible or incompatible with different polymer matrices through copolymerization, grafting, or blending [25]. They can be applied in many important areas such as the preparation of polymer nanocomposites. In this case, the main aim is to obtain multifunctional materials with intermediate properties between those of the organic polymers and of ceramics. These intermediate properties fall into the "hybrids" category shown in Figure 2.5 [26].

POSS molecules can be used in other applications such as coatings, films and thin layers. They can be used in photoresists, magnetic recording media, liquid display elements and protective coating films for semiconductor devices, catalysis, precursors to silicates and preparation of copolymers. Polymeric POSS has remarkable dielectric and optical properties [27]. Its commercial availability has increased tremendously and this has recently led to an increase in intensity of research in this field.

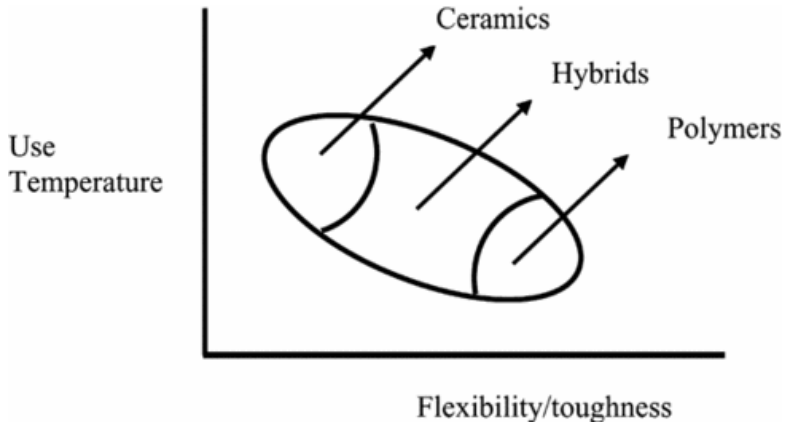

Figure 2.5 Performance of hybrids when compared with ceramics and polymers [26]

2.5 POSS containing polymer nanocomposites

2.5.1 Surface morphology

Introduction of nano-scaled fillers into polymers can affect the morphological characteristics of nanocomposites and these morphologies depend on the processing conditions and the type of reactive functional groups 'R' appended on the Si atom of the core. This could contribute largely to the resultant properties of the nanocomposites. A summary of the different processing routes used by previous researchers, and the influence of such processing methods

on the respective morphologies of composites, is given in this section. SEM analyses were mostly used for morphological characterization of POSS based polymer composite systems.

Li and co-workers [28] reported the viscoelastic and mechanical properties of vinyl ester (VE) resin nanocomposites containing chemically bonded multifunctional POSS, POSS-1 [$(C_6H_5CHCHO)_4(Si_8O_{12})CH{=}CHC_6H_5)_4$], nonfunctional octa-*i*-butyl-T_8-POSS (POSS-2) and dodecaphenyl-T_{12}-POSS (POSS-3) molecules prepared by solution blending. They used 5 and 10 wt % POSS contents and the synthesis reaction of these composites is illustrated in Figure 2.6. A good dispersion of the POSS-1 nanoparticles after mixed with VE (50 wt % styrene) resin was observed. Transmission electron microscopy (TEM), EDXS (energy dispersive X-ray spectroscopy) and EELS (electron energy loss spectroscopy) studies showed that the POSS-1 rich nanoparticles (75 nm to a few nm) are present in the 90/10 w/w VE/POSS-1 composite. Moreover, addition of both POSS-2 and POSS-3 into VE monomers exhibited much larger sized phase-separated morphology. A good miscibility was only observed when ≤5 wt % or ≤0.42 mol % of POSS-1 units in its styrene copolymers was used.

Preparation of cyanate ester composites containing monofunctional trisilanolphenyl-POSS ($C_{42}H_{38}O_{12}Si_7$) by direct blending followed by thermal curing at 250 °C was reported by Liang *et al.* [29] and the reaction is shown in Figure 2.7. The same research group also reported preparation, morphology and the viscoelastic properties of composites containing both octaaminophenyl-T_8-POSS [$(C_6H_4NH_2)(SiO_{1.5})_8$] (OapPOSS) and cyanopropylcyclopentyl-POSS [$(C_5H_9)_7(SiO_{1.5})_8CH_2CH_2CH_2CN$] incorporated in the same cyanate ester resin [30]. They prepared their samples by a solution blending technique (see Figure 2.8). In their studies, they generally used 1, 3, 5, 10 and 15 wt % POSS contents. SEM results exhibited phase-separated aggregates for composites containing 1 to 10 wt % of cyanopropylcyclopentyl-POSS. In the case of the trisilanolphenyl-POSS based composite systems, larger aggregates of POSS particles at higher loadings within the polymer matrix were observed. TEM studies revealed that POSS-enriched nanoparticles were present in these composites.

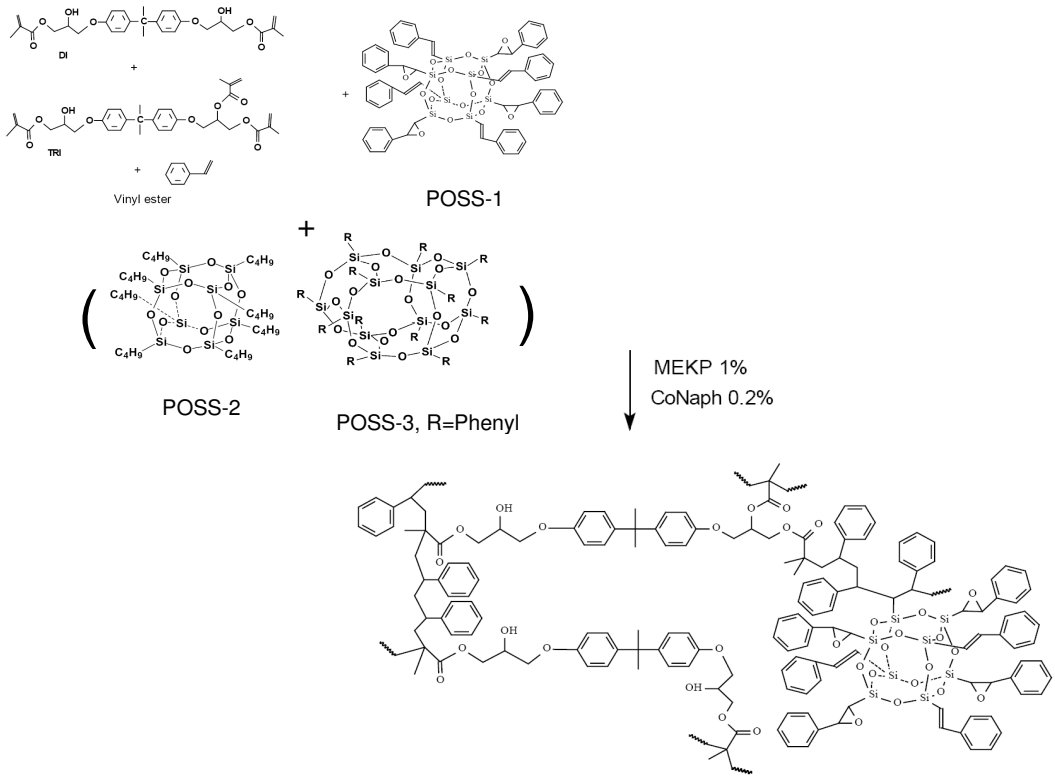

Figure 2.6 Synthesis of vinyl ester/POSS composites [29]

Chigwada *et al*. [31] investigated fire retardancy of vinyl ester nanocomposites in the presence of both clay and POSS nano-dimensional particles. Choi and co-workers [32,33] reported the preparation of epoxy nanocomposites containing octaglycidyldimethylsiloxy-octahedralsilsesquioxane (OG) using a series of octafunctionalized-T_8-POSS ($R_8Si_8O_{12}$) as reinforcing agents in the presence of aminophenyl and dimethylsiloxypropyl glycidyl moieties (see Figure 2.9). The number of organic tether links between POSS cages was varied by altering the amine to epoxy ratio (N) to control the structural design of the final epoxy nanocomposites. Molecular dispersion of multifunctional POSS $[(C_6H_5CHCHO)_4(Si_8O_{12})CH{=}CHC_6H_5)_4]$ units within the aliphatic epoxy resin network at high POSS content (25 wt %) studied by TEM was reported by Li *et al*. [34].

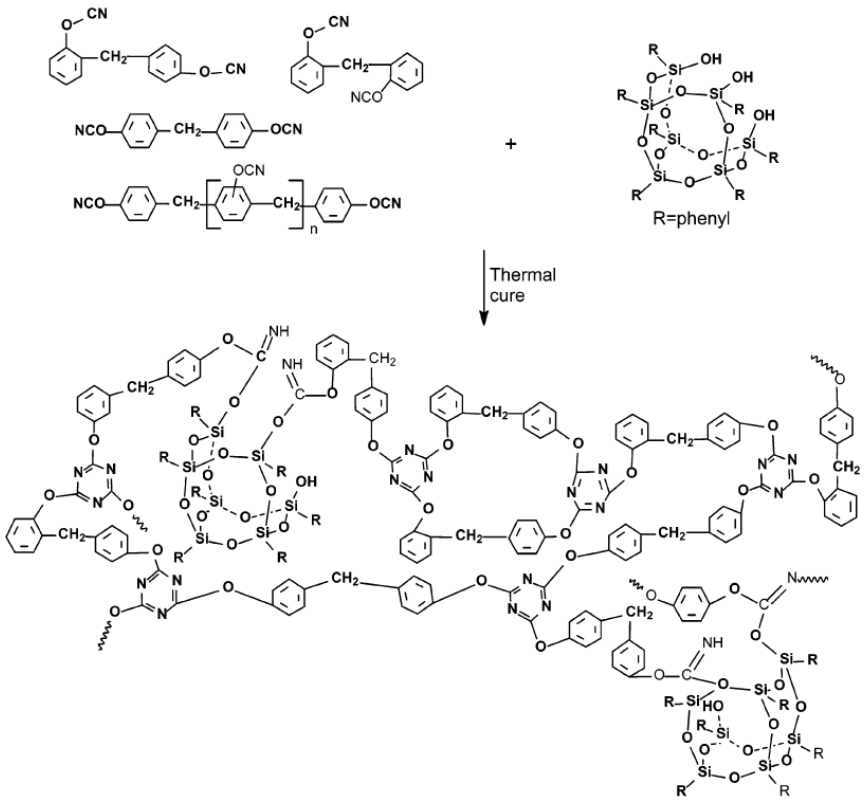

Figure 2.7 Cross-linked network formation of cyanate ester/POSS composites through triazine ring formation [30]

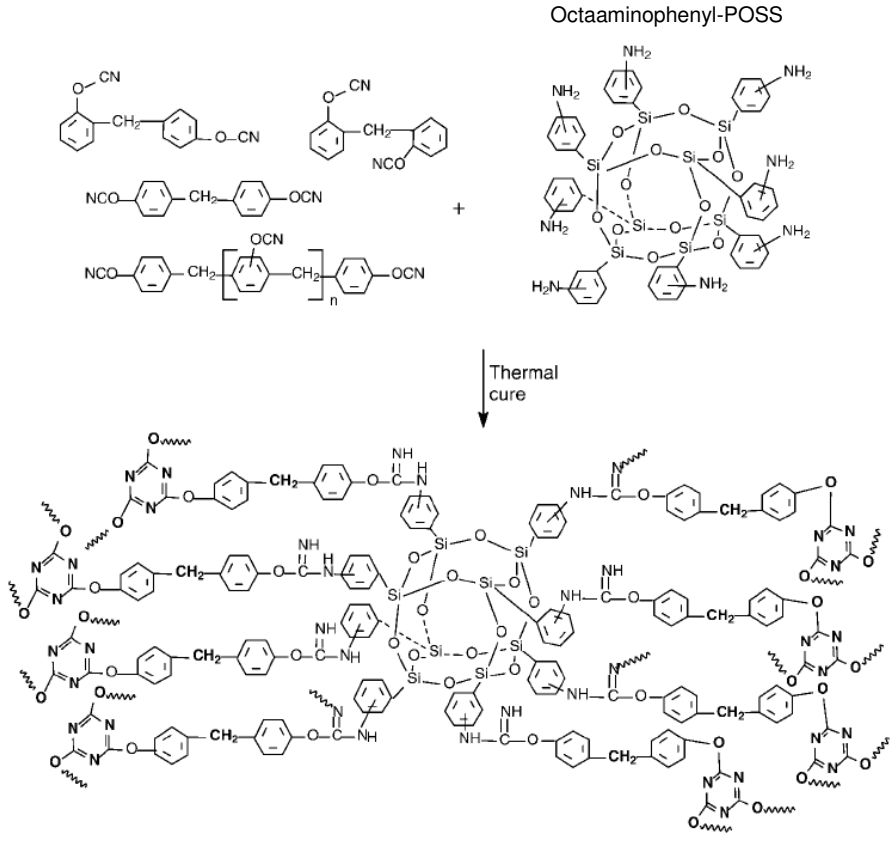

Figure 2.8 Synthesis of the PT-15/octaaminophenyl-POSS composites [30]

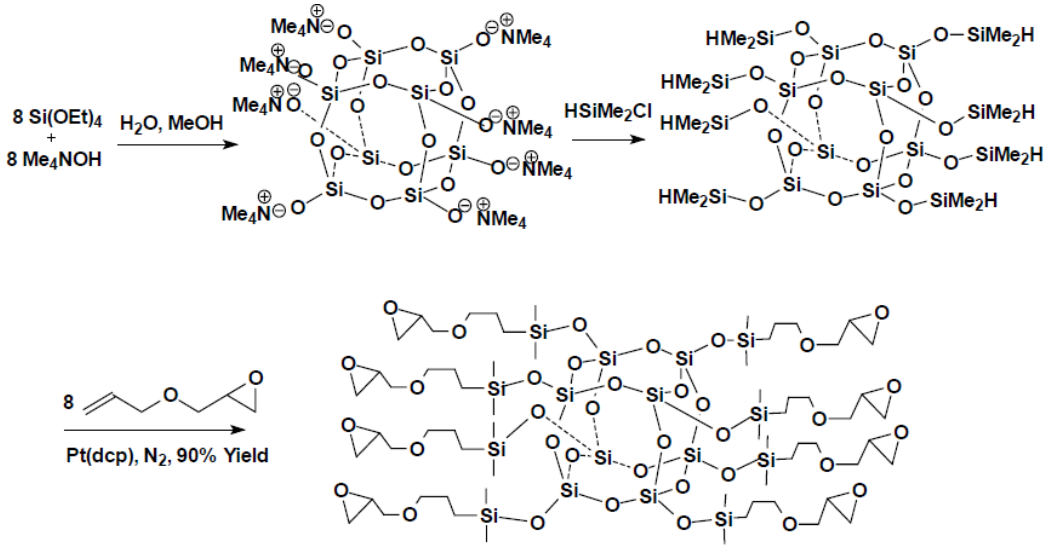

Figure 2.9 Synthesis of octaglycidyldimethylsiloxy-octasilsequioxane (OG) [32]

Ni and coworkers [9,35] investigated the morphological behaviour of epoxy resin based nanocomposites in the presence of octanitrophenyl $[(C_6H_4NO_2)_8(SiO_{1.5})_8]$ (OnpPOSS) and octaaminophenyl $[(C_6H_4NH_2)(SiO_{1.5})_8]$ (OapPOSS) *via in situ* polymerization of diglycidyl ether of bisphenol A (DGEBA) and 4,4'-diaminodiphenylmethane (DDM) (see Figure 2.10). The authors observed a homogeneous mixture of the starting materials (DGEBA, DDM and POSS monomers), suggesting the miscibility (or solubility) of POSS cages with the precursors of the epoxy resin. The morphologies of the resulting hybrids were dependent on the type of 'R' groups in the POSS macromers. SEM results exhibited a phase-separated morphology of the nanocomposites containing OnpPOSS, with spherical particle sizes of <0.5 μm in diameter, that were uniformly dispersed in the epoxy matrix. The epoxy-rich OapPOSS composites exhibited a homogeneous morphology.

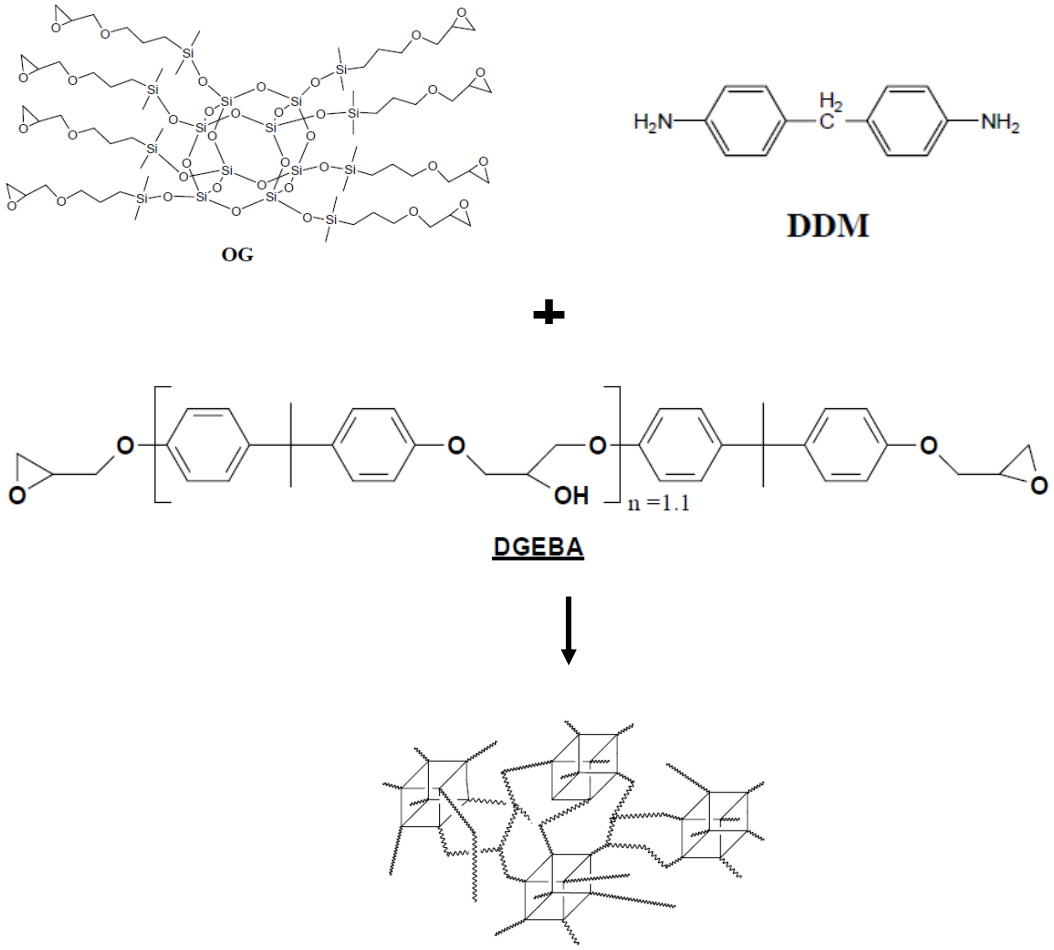

Figure 2.10 Synthesis of epoxy nanocomposites containing octa (propylglycidyl ether)-T_8-POSS [36]

Liu *et al.* [36] also observed a homogeneous dispersion of epoxy resin nanocomposites containing up to 40 wt % of octa(propylglycidyl ether)-T_8-POSS and [glycidyl-$(C_3H_6SiO_{1.5})_8$] investigated by SEM, TEM and atomic force microscopy (AFM). Zhang and co-workers [37] studied random copolymers of methyl methacrylate (MMA) and propylmethacrylheptacyclopentyl-POSS with both polystyrene (PS) and poly(methyl methacrylate) (PMMA) homopolymer systems through a conventional free radical polymerization process. Their results indicated efficient compatibilization of immiscible polymer blends caused by the copolymers. This compatibilization occurred when POSS was grafted onto the PMMA chains (see Figure 2.11). A strong interaction between cyclopentyl-POSS and the PS homopolymer was also observed. In the same paper, the morphology of polystyrene (PS)/PMMA blends with methyl methacrylate-POSS random copolymers (containing 5.5 % m/m-PMMA-POSS5, 8.0 % PMMA-POSS10 and 10.7 % m/m-PMMA/POSS15 cyclopentyl-POSS) as compatibilizer was examined using scanning

transmission x-ray microscopy (STXM) and scanning probe microscopy (SPM). Both STXM and SPM showed that a bicontinuous microemulsion structure with a well-defined wave vector was formed, indicating a reduction of the interfacial tension between the phases. The topographical images show that the size of the PS domains decreased when the POSS and PMMA copolymer were mixed.

When PMMA was mixed with both $[Si_8O_{12}(OSiMe_2)_8]$ and $[Si_7O_9(cyclohexyl)_7(OSiMe_2H)_3]$, a phase-separated morphology and self-assembly afforded *in situ* nanocubes with average diameters ranging from 25 nm to 500 nm were seen [38].

Kopesky *et al.* [39,40] investigated the miscibility and toughenability of PMMA based nanocomposite systems using different POSS nanocages. These nanocomposite systems were prepared by a solution blending method. The POSS macromers used in their study were unmodified acrylic-POSS, hydrogenated acrylic-POSS, cyclohexyl-POSS, methacryl-POSS and trisilanolphenyl-POSS and the PMMA resin used was Atoglas V920 with a weight average M_w = 80200 g.mol^{-1} and a polydispersity index of 1.7. The unmodified acrylic-POSS exhibited better miscibility with PMMA than the hydrogenated-POSS, approaching complete miscibility at volume fractions of $\Phi < 0.10$. A phase-separated morphology was observed when cyclohexyl-POSS was used. In the case of both methacryl-POSS and trisilanolphenyl-POSS, molecular dispersion of nanodimensional particles was reported.

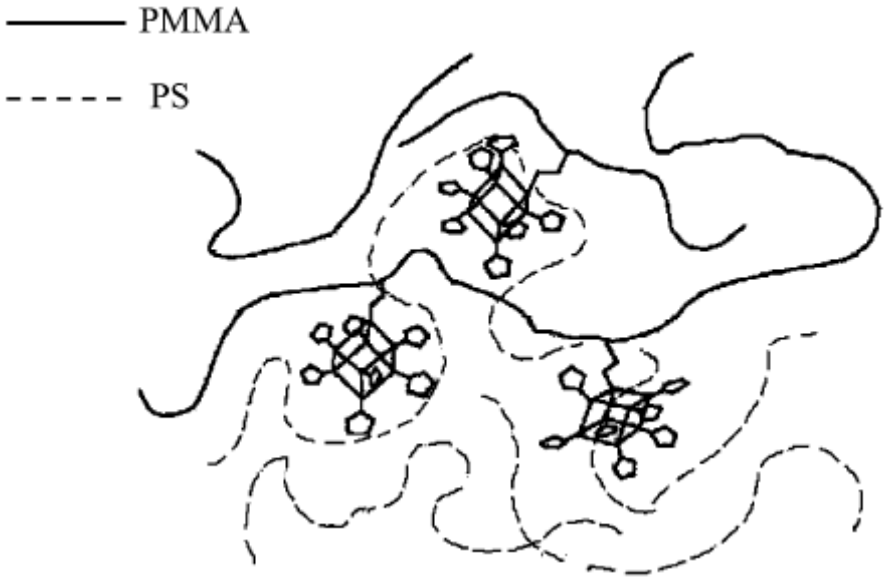

Figure 2.11 Schematic diagram of PMMA (solid) and PS (dashed) chains in a blend when functionalized POSS is grafted onto PMMA chains [37]

Kim *et al.* [41] prepared polymer hybrids by using three kinds of octasilsesquioxanes with hydroxyl groups and different polymers such as poly(2-methyl-2-oxazoline) (POZO), poly(*N*-vinylpyrrolidone) (PVP) and poly(*N*,*N*-dimethylacrylamide) (PDMAAm). Homogeneous and transparent hybrid films were obtained. The high homogeneity of the polymer hybrids was the result of hydrogen-bonding interaction between octasilsesquioxanes and organic polymers, as was confirmed by the carbonyl stretching shifts in IR measurements. The solubility of POSS and the transparency of polymer hybrids from POSS were closely dependent on this flexibility of the eight arms bound to the silica-like core of the polymer hybrids.

Morphological characteristics of polyolefins containing POSS molecules as reinforcing agents were reported by numerous researchers [5,6,42-48]. The majority of these publications paid attention to composite systems prepared by initially mixing isotactic polypropylene (*i*-PP) with POSS powders through the melt-mixing route in a Brabender internal mixer. A masterbatch of POSS in HDPE was also melt-mixed with the same type of POSS using a twin-screw extruder [5,42,43]. The 10 wt % POSS masterbatch was then used to prepare HDPE/POSS nanocomposites. In all these studies, the authors generally used loadings of POSS between 0.1 and 30 wt %. It was generally found that the octamethyl-T_8-POSS-containing nanocomposites exhibited phase-separated morphology and some crystalline aggregates on a micro-sized scale. In the case of composites of octaisooctyl-POSS and octaisobutyl-POSS with PP, homogeneous dispersion was only observed at low POSS contents. This was probably due to a more favourable interaction of the long alkyl groups with the polymer chains, as compared to octamethyl-T_8-POSS particles.

Zhou *et al.* [49,50] investigated different properties of PP/octavinyl-POSS nanocomposites by incorporating 0.1 wt % dicumyl peroxide (DCP) as a crosslinking agent in their powder mixtures using both physical and reactive blending methods. Before blending, both PP and POSS were dried at 70 °C under vacuum for 12 h. The SEM results of the physically blended composite (95/5 w/w PP/POSS) showed many agglomerates of POSS particles (0.2 to 1 μm) dispersed within the PP matrix. The reactively blended composite (95/5 w/w PP/POSS + 0.1 phr DCP) showed some uniform dispersion of POSS particles within the matrix with a size range of 50 to 200 nm.

Poly(ethylene terephthalate) (PET) was melt-mixed and *in situ* polymerized with triepoxy-POSS (5 wt %) [51]. In another publication, the same research group studied PET containing

composites using two types of POSS macromers (disilanolisobutyl-POSS and trisilanolisobutyl-POSS) prepared by only *in situ* polymerization [52]. In these studies, their composites were prepared in the presence of ethylene glycol (EG). The *in situ* polymerized triepoxy-POSS composite systems were prepared by polycondensation and the presumed reaction between the hydroxyl groups of PET and the epoxy groups of POSS is given in Figure 2.12. The loadings of POSS for the preparation of the nanocomposites were 1, 3 and 5 wt %, and the morphological characteristics of these nanocomposites were investigated. The SEM studies revealed that the melt-mixed composites had a phase-separated morphology, while the *in situ* polymerized samples showed a more homogenous morphology, particularly at low POSS contents with sizes ranging from 30 to 40 nm. This behaviour was attributed to the occurrence of interfacial interactions between PET and POSS during polymerization.

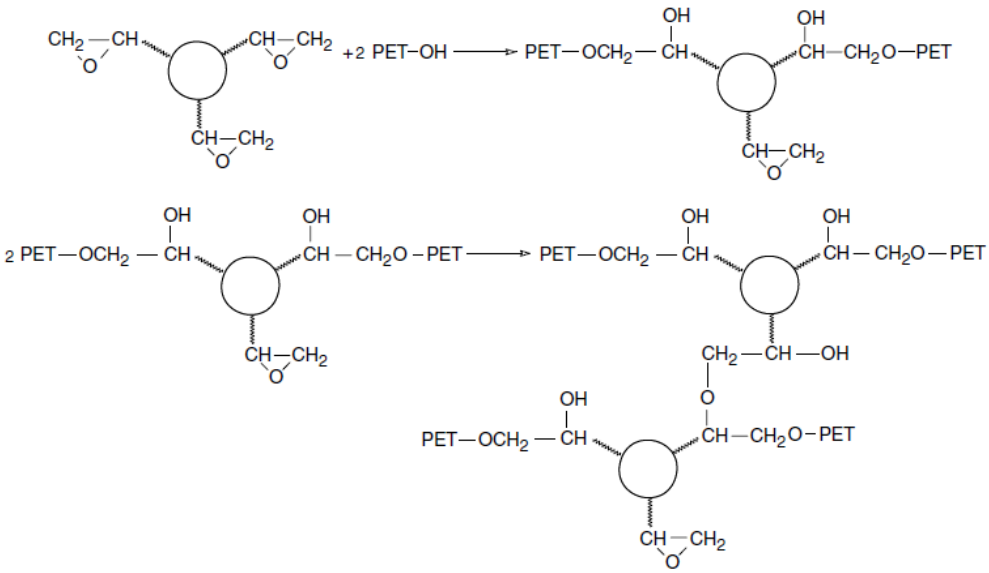

Figure 2.12 The reaction between the hydroxyl groups of PET and the epoxy groups of POSS [51]

2.5.2 Thermal properties

2.5.2.1 Melting, glass transition temperature and crystallization

It is well known that a polyolefin such as *i*-PP exhibits several crystalline forms at different processing conditions. These crystal forms could be affected by molecular mass, molecular mass distribution (MMD) and different blending compounds and preparation conditions used.

Nucleating agents in polymers were extensively used by many researchers. They are important because the control of the crystallization behaviour allows modification of the microstructure and retardation or enhancement of the thermal, mechanical and optical properties of the polymers. However, the relationship between the structure of nucleating agents and the physical properties of the polymer matrix is very complicated [53].

It is important for one to understand the nonisothermal processes of slowly crystallizing materials like polymers using simple models, because these processes are closest to the real industrial processing conditions. One advantage of nonisothermal DSC measurements over the isothermal ones is that these experiments are performed more rapidly and they can also be used to extend the temperature ranges of measurements beyond that accessible in isothermal experiments. Subsequently, nonisothermal crystallization behaviour can broaden and supplement the knowledge of the crystallization behaviour of polymers [54].

Numerous methods including the Ozawa [55], Avrami [56] and the combined Avrami-Ozawa methods [57] were developed for the treatment of nonisothermal DSC data in order to obtain kinetic parameters of polymers that reproduce the experimental data and predict the crystallization behaviour of the system under various conditions.

The absolute crystallinity of the material is not needed for the analysis of crystallization kinetics and the relative degree of crystallinity, X_T, as a function of temperature is defined as

$$X(T) = \frac{\int_{T_o}^{T} (\mathrm{d}Hc / \mathrm{d}T)}{\int_{T_o}^{T_\infty} (\mathrm{d}Hc / \mathrm{d}T)\mathrm{d}T} \tag{2.1}$$

where T_o and T_∞ are the onset and end crystallization temperatures, $\mathrm{d}H_c/\mathrm{d}T$ is the heat flow rate and T is the temperature used to determine X_T. In a nonisothermal crystallization analysis, the crystallization time (t) is related to the crystallization peak temperature $T_{p,c}$ (t = 0) according to the following equation:

$$t = \frac{(T_o - T_{p,c})}{\phi} \tag{2.2}$$

where ϕ is the cooling rate. This means that, according to equation (2), the relative degree of crystallinity with time can be developed [5].

Although the theory of Ozawa to describe the nonisothermal crystallization kinetics of polymers has been extensively used, it does not consider other factors such as secondary crystallization and dependence of fold length on temperature, and the exponent *m* is assumed to be constant independent of temperature. Effects such as transcrystallization are also not taken into account [54]. The Ozawa theory [55] states that the degree of conversion or relative degree of crystallinity, X_T, at a temperature *T*, can be written as:

$$1- X_T = \exp\left[\frac{-k(T)}{\varphi^m} \right] \tag{2.3}$$

where *m* is the Ozawa exponent that depends on the dimension of crystal growth and *k* is the cooling crystallization function, which is related to the overall crystallization rate and indicates the rate at which the crystallization occurs. Therefore, equation (3) can be written as

$$\ln [-\ln (1- X_T)] = \ln k(T) - m \ln \phi \tag{2.4}$$

Equation (4) describes the nonisothermal crystallization kinetics provided the plots of ln [-ln (1- X_T)] *versus* ln ϕ gives a straight line at a given temperature.

The analysis of the time dependent relative crystallinity function *X*(t) for a nonisothermal crystallization process is also conducted with the modified Avrami equation which can be written as:

$$X_t = 1 - \exp(-Z_t t^n) \tag{2.5}$$

Taking the double logarithm of this equation gives:

$$\ln[-\ln (1 - X(t))] = n \ln t + \ln Z_t \tag{2.6}$$

where *n* is the Avrami exponent (integer between 1 and 4) which depends on type of nucleation and growth process, Z_t is the Avrami rate constant involving nucleation and growth

parameters, and t is the crystallization time. Since the process is nonisothermal, Jeziorny [57] brought forward an idea that the Z_t should be corrected for the influence of cooling rate ϕ of the polymer. If one assumes that $\phi \approx$ constant, the final form of the parameter characterizing the kinetics of nonisothermal crystallization is given by the following equation:

$$\ln Z_c = \frac{\ln Z_t}{\phi} \tag{2.7}$$

where Z_c denotes the kinetic growth parameter. According to Jeziorny [57], Z_c does not have a constant value for different scanning rates. A modified Avrami-Ozawa model is valid if plots of ln[-ln (1 – X(t))] *versus* ln t give a straight line. One should be able to obtain the values of n and Z_t or Z_c from the slopes and intercepts, respectively.

Joshi and coworkers [5,43] discussed the effect of octamethyl-T_8-POSS on the nonisothermal and isothermal crystallization behaviour of high-density polyethylene (HDPE) resin using differential scanning calorimetry (DSC). They indicated that the POSS molecules exhibited nucleation activity only at 10 wt % loading in HDPE, and are not effective nuclei at lower loadings. The effect of the same type of POSS molecules (10, 20 and 30 wt %) on the crystallization behaviour of *i*-PP under quiescent and shear conditions were also investigated [44]. The addition of POSS during quiescent conditions increased the crystallization rate of *i*-PP. This suggested that octamethyl-T_8-POSS molecules could act as nucleating agents. At higher POSS content (30 wt %) a significant decrease in the crystallization rate was observed, suggesting that the growth mechanism was hindered. It was observed, under shear conditions, that the crystallization rate was significantly higher than those performed under quiescent conditions. The POSS molecules were assumed to act as weak physical crosslinks in the polymer melts and to increase the relaxation time of the PP chains under shear conditions. Under these conditions the oriented chain segments remained in the oriented state for a longer time, therefore acting as more effective nucleating sites. A higher crystallization rate and better overall orientation of the *i*-PP chains therefore resulted (see Figure 2.13).

The thermal behaviour of isothermally crystallized *i*-PP blended with various loadings of POSS molecules were investigated using DSC [48,58]. An increase in crystallization rate of *i*-PP with increasing loadings of POSS in the polymer matrix during crystallization was

reported. Moreover, the melting temperature of the *i*-PP/POSS nanocomposites slightly decreased, while the heat of fusion increased after addition of POSS molecules.

In the case of octaisooctyl-POSS molecules, reduction of the crystallization behaviour of PP was reported. This behaviour was attributed to the high dispersion of the filler as a liquid phase component. Octaisobutyl-POSS showed different behaviour depending on the loading amount in PP. At a lower content (3 wt %), the nano-dispersion of the POSS molecules hindered the PP crystal growth that resulted in a retarded crystallization behaviour. The presence of octaisobutyl-POSS crystal aggregates at a high content (10 wt %) counterbalanced the crystallization behaviour and induced polymorphism [6,46]. It was also reported that the length of the alkyl groups on the POSS molecules affected the filler dispersion. Chen *et al*. [58] reported that the crystallization behaviour of PP significantly changed with increasing loadings of POSS. POSS crystallized and aggregated together to form a thread or network-like morphology depending on its amount in the polymer matrix.

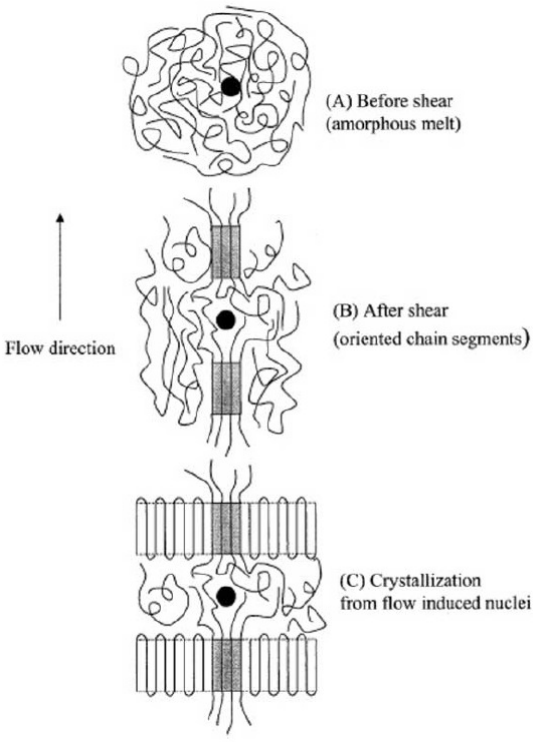

Figure 2.13 Schematic diagram of the shear-induced crystallization development in the presence of a POSS molecule [49]

Zheng and co-workers [59] prepared POSS/olefin copolymers by copolymerizing ethylene and propylene with norbornylene-substituted POSS macromers using a metallocene-

methylaluminoxane (MAO) cocatalyst system. A range of polyethylene (PE)/POSS (up to 56 wt % POSS loading) and PP/POSS (up to 73 wt % POSS loading) copolymers were prepared. The crystallinity of the PE/octamethyl-T_8-POSS nanocomposites decreased with increasing the POSS content.

Zhao *et al*. [60] investigated a series of PMMA containing octavinyl-POSS nanocomposites synthesized by solution polymerization. Only one glass transition was observed for all the nanocomposites and the neat PMMA. In comparison to neat PMMA, the T_g's of the nanocomposites increased with increasing the POSS content up to 12.27 wt %, but they decreased for the higher POSS content (14.06 wt %). The increase in the T_g's of the nanocomposites was due to the hindering effect of POSS, which inhibited the motion of the PMMA chains in the polymer matrix. It was also reported that the star-shaped structures with cubic silsesquioxane core is propitious to the T_g increase. The decrease in T_g was attributed to the increased incorporation of the low molecular weight species. The nanocomposite with 14.06 wt % POSS loading induced a greater steric hindrance of the POSS cages, which increased the internal free volume and decreased the reactivity of the MMA monomers. This led to relatively larger fractions of low molecular weight components. Huang and co-workers [61] reported a composition-dependent single T_g for all the blends investigated. Weickmann *et al.* [38] observed a glass transition temperature increase of 18 °C when PMMA was incorporated with octasilane-POSS loadings and 14 °C when tris(dimethylsilane) cyclo-pentyl-POSS was used.

Kopesky *et al*. [39] reported a decrease in the T_g and broadening of the glass transition region for POSS loadings up to $\phi = 0.30$ of the unmodified acrylic-POSS/PMMA blends. In the case of the $\phi = 0.30$ blend system, a second glass transition event was observed at -55 °C. This peak corresponds to the T_g of the pure POSS. This behaviour indicated a phase separated morphology of the two components at a particular unmodified acrylic-POSS loading. A similar trend of decreasing T_g with increasing hydrogenated acrylic-POSS loading was also reported. However, the drop in T_g was less pronounced in the case of hydrogenated acrylic-POSS systems.

2.5.2.2 Thermal stability

A number of studies also focused on the thermal stability of POSS containing polymer composites evaluated by means of thermogravimetric analysis (TGA) [31,45,46,48,51,52,59-62]. POSS molecules with different chain lengths (octamethyl-, octaisobutyl- and octaisooctyl-POSS) were incorporated into a PP matrix to investigate the thermal stability of the composites under nitrogen atmosphere [46]. The presence of octamethyl-POSS and octaisobutyl-POSS particles did not affect the degradation mechanism of the PP matrix. This behaviour was based on the fact that, when the degradation temperature of the PP matrix was reached, a negligible amount of octamethyl-POSS was present in the composite because of its lower volatilization temperature at 261 °C, compared to the 317 °C of the composites. A probable reason in the case of octaisobutyl-POSS containing composites is its complete evaporation at 265 °C. However, when 10 wt % octamethyl-POSS was used, two degradation steps were observed. This behaviour was the result of the maximum volatilization rate of octamethyl-POSS observed at 261 °C. No significant changes were observed in the thermodegradative behaviour of PP when octaisooctyl-POSS was used.

The thermal stability of PP/isobutyl trisilanol-POSS composites was investigated in inert and oxidative atmospheres [45]. Prior to TGA analysis, isobutyl trisilanol-POSS was functionalized with aluminium (Al) and zinc (Zn) metals by a deprotonation process. The weight loss maxima for Al functionalized-POSS and Zn-POSS studied in nitrogen atmosphere were, respectively, 342 °C and 490 °C, compared to the 265 °C of T_8-POSS. This behaviour indicated evaporation of Al-POSS, while the weight loss temperature delay was due to the higher molecular weight of the dimeric Al-POSS. The Al-POSS degraded in a single step, while the Zn-POSS showed a continuous weight loss in the range between 200 and 600 °C. The different behaviour in the thermal degradation of Zn-POSS was due to its resistance to evaporation. The residual amount of the Zn-POSS was 47 % of the initial weight, which was found to be stable up to at least 800 °C. This amount of residue was slightly lower than that of the inorganic fraction in Zn-POSS (56 %). This suggested that the thermal decomposition to volatiles of the isobutyl side chains and the reorganization of POSS in a thermally stable inorganic/carbonaceous phase were strongly predominant over the scission/evaporation process. In thermooxidative conditions, the thermal stability of the studied POSS molecules differed from that of the samples investigated under nitrogen atmosphere. This was due to the chemical interaction with oxygen. Different contents of metal functionalized POSS-

containing PP composites, investigated under nitrogen atmosphere, did not significantly change the thermal stability of these composites. However, for the composite samples investigated in air, the metal POSS molecules strongly effected the degradation pathways. Two degradation steps were observed for both metal functionalized POSS composites. The first step corresponded to the degradation of neat PP on the sample surface, while the second one was due to the degradation of the residue formed during the first step.

Chen and Chiou [48] observed similar degradation profiles for all the *i*-PP/POSS nanocomposites. This behaviour suggested the homogeneous dispersion of POSS nanocrystals in the *i*-PP matrix and the thermal stability of *i*-PP was reduced by addition of POSS particles. For pure *i*-PP, the initial decomposition temperature, defined as the 5 % mass loss temperature, was about 395 °C, while those for the nanocomposites were 320 to 348 °C. Even though the decomposition temperature of pure POSS is about 231 °C, a remarkable increase in decomposition temperature was observed after nanocomposites formation with POSS. This behaviour indicated that the thermal stability of POSS molecules increased remarkably when POSS is blended with an *i*-PP matrix, because of the decrease in the thermal vibrational motion of POSS molecules or the increase in the interaction between the POSS molecules and the *i*-PP matrix with increasing POSS loadings.

The influence of octavinyl-POSS on the thermal stability of a PP matrix was investigated by Zhou *et al*. [73]. It was found that all the TGA curves exhibited single step degradation, and all the values of the weight loss maximum and the initial decomposition temperature of the composites were lower than that of the neat PP. This was due to the lower thermal stability of the neat octavinyl-POSS. The degradation pathways of the POSS molecules showed a competition between evaporation and degradation mechanisms. A possible explanation was based on the polymerization effect of vinyl groups with evaporation, which was due to the free radicals produced by the scission/evaporation of octavinyl-POSS and which affected the degradation and decreased the initial decomposition temperature of PP.

For PMMA/octavinyl-POSS nanocomposites, the TGA curve of pure PMMA showed three main degradation steps [60]. The first and second degradation steps are associated with the scission of head-to-head and unsaturated chain ends of the polymer, while the third step is due to random scission. The first and second steps gradually disappeared with increasing the POSS contents lower than 12.27 wt %, while the 5 and 10 % mass loss temperatures increased

by 93 and 86 °C, respectively, for samples containing POSS contents up to 12.27 wt %. This indicated that the incorporated POSS particles retarded the scission of head-to-head linkage and vinylidene and chain-end initiation. The thermal stability decreased remakarbly when the amount of POSS content was increased to 14.06 wt %.

When vinyl-POSS molecules were incorporated into a vinyl ester resin, a slight change in the thermal stability of the prepared composites was observed. However, a significant amount of char formation in the presence of both POSS and phosphate was noticed [31]. Zhang *et al*. [74] investigated the thermal stability of phenolic resin/trisilanolphenyl-POSS composites in air atmosphere using 1, 3, 5, 7 and 10.4 wt % POSS loadings. Increasing amounts of trisilanol-POSS molecules in the phenolic resin caused an increase in the thermal stability of these composites.

2.5.3 Dynamic mechanical and mechanical properties

Ethylene copolymers with norbornylene-substituted POSS molecules, incorporated using a metallocene-methalaluminoxane (MAO) cocatalyst system, as well as *i*-PP containing POSS nanoparticles using a C_2 symmetric *ansa*-metallocene, were investigated by dynamic mechanical thermal analysis (DMTA) [59]. A plateau modulus at a temperature above 175 °C was observed. This behaviour indicated the suppression of melt flow for PE-POSS copolymers. Furthermore, the observation of a rubbery plateau at a temperature above 175 °C indicated that both impact and toughness properties of these PE/POSS composites were improved. Slightly higher values of the storage modulus of these composites in the rubbery region were observed, which suggested that the POSS nanoparticles had a better improvement on elastomers. This behaviour was due to the formation of POSS nanocrystals, which contributed to the confinement of polyethylene chains during β-relaxation. The γ-relaxation appeared at the same temperature for all the PE/POSS samples as a result of the "crankshaft" motion in the PE amorphous domain. The α-transition of the samples shifted to lower temperatures due to formation of thinner crystals in the PE/POSS samples.

DMTA results on ethylene propylene (EP)/POSS nanocomposites showed that the presence of 10 wt % POSS particles increased the storage modulus and shifted the T_g of the EP copolymer towards a higher value by 4.5 °C. These results suggested the presence of strong particle-particle interactions between the POSS crystals and weak particle-matrix interactions between

the POSS crystals and the EP matrix. This indicated a decrease of molecular mobility in EP, either due to the induced constrains of the EP chains, or due to the enhanced van der Waals bonding forces between the POSS and the EP chains. This behaviour suggested that the POSS nanocrystals exhibited some physical interactions with the EP polymer chains. Moreover, higher values of the storage modulus of the 10 wt % POSS containing composite were reported in the temperature range from -80 to 60 °C [63].

Li *et al*. [28] investigated the viscoelastic and mechanical properties of multifunctional POSS, $[(C_6H_5CHCHO)_4(Si_8O_{12})CH{=}CHC_6H_5)_4]$, units that were incorporated into an aliphatic epoxy resin and POSS-styrene copolymers. The presence of 10 wt % POSS particles in the VE network did not show any significant improvement in T_g as well as in the width of tan δ peak in the glass transition range. However, the incorporation of multifunctional POSS particles reduced the segmental motion of the small fraction of the segments which contributed to the T_g. There were no observable changes in the volume density of the VE resins after addition of POSS**,** since the VE resin could crosslink on its own. In contrast, the T_g values of the VE/POSS-styrene copolymers were substantially higher than that of the neat uncrosslinked PS. This behaviour was due to the crosslinking effect induced by the addition of these POSS units and to the restriction of segmental motion by the vast and bulky POSS moieties. The glass transition temperature values of both 5 and 10 wt % multifunctional POSS copolymers were almost the same. This was due to similar crosslinking densities for both the 5 and 10 wt % POSS contents. The E' values of the VE/POSS composites were higher than that of the neat VE resin over the entire temperature range investigated. The POSS-styrene composites have higher E' values. The incorporation of POSS increased the flexural modulus and hardness of the VE resin, and decreased the flexural strength. The presence of 5 wt % of octaisobutyl-POSS (OibPOSS) and dodecaphenyl-POSS in the VE resin gave rise to smaller flexural strength and modulus values for these composites.

Ni and co-workers [9] examined the dynamic mechanical properties of DGEBA epoxy resin/POSS nanocomposites in the presence of DDM as a curing agent. The POSS monomers used in their study were octanitrophenyl-T_8-POSS (OnpPOSS) and octaaminophenyl-T_8-POSS (OapPOSS) at loadings of 5, 10, 15, and 20 wt %. They reported lower glass transition temperatures of all the DDM cured composites containing octanitrophenyl-T_8-POSS and octaaminophenyl-T_8-POSS monomers over the temperature range investigated. However, in the case of the OnpPOSS composites, the T_g values were smaller than those obtained using

the OapPOSS monomer. The loss factor curve of the neat DDM cured DGEBA epoxy resin showed a well-defined relaxation peak at 177 °C. This peak was attributed to the glass rubbery transition of the polymer matrix. Similar behaviour was observed in the case of the composites at 130 °C. The storage moduli of these composites were higher than that of the neat epoxy resin in the glassy state observed at -50 to 100 °C, and E' increased with increasing POSS content. This behaviour was due to the reinforcement effect of the dispersed, spherical and rigid structure of OnpPOSS. Another possible reason was due to the nanoreinforcement effect of the POSS cages in the crosslinked polymer networks due the covalent bonding formation between OapPOSS and the epoxy resin.

Zhou *et al*. [50] reported that E' of all the physically blended PP composites decreased with increasing POSS loading at lower temperature in the glassy state between -60 and approximately 10 °C. The lower modulus was attributed to the lower stiffness of the β crystalline form and to the soft vinyl groups of POSS. The E' of all the reactive blended PP composites and POSS-g-PP were higher than that of pure PP, and reached a maximum when 2 wt % POSS content was used. This behaviour was associated with the grafting of POSS to the PP chains and the hindered chain mobility of the PP matrix. The loss factor results of the physically and reactively blended composites showed a well defined relaxation peak near 10 °C. This was attributed to the T_g of PP. All the composites showed slightly higher T_g's than PP, which indicated that the presence of POSS molecules resulted in a decrease of the molecular mobility of PP. When HDPE was used, a significant improvement in E' was reported for composites filled with lower POSS contents (0.25 to 0.5 wt %) [42]. Only one α-transition peak was observed for all the HDPE/octamethyl-POSS nanocomposites at higher temperatures than that of neat HDPE. The shift in peak transition was associated with the restriction of the movement of HDPE chain segments in the intercrystalline regions due to the presence of POSS macromers around the crystallite boundaries.

The DMTA properties of cyanate ester (PT-15) composites containing octaaminophenyl-T8-POSS (OapPOSS) and cyanopropyl cyclopentyl-POSS monomers were investigated by Liang *et al*. [30]. The PT-15/OapPOSS showed higher E' values than the neat PT-15 resin when 1 and 3 wt % OapPOSS contents were used. This behaviour was attributed to the generation of higher network crosslink densities around the OapPOSS moieties caused by amino functional groups that reacted with the liquid PT-15 resin. The loss factor peak intensities decreased and the peaks broadened after nanocomposite formation with OapPOSS. The glass transition

temperature of the PT-15 composite containing 1 wt % OapPOSS increased sharply, but decreased for both the 3 and 5 wt % OapPOSS contents. Similar behaviour was observed in the case of cyanopropyl cyclopentyl-POSS composites. However, both 5 and 10 wt % POSS contents produced opposite behaviour of the E' in the glassy region ($T<T_g$). The loss factor peak intensities decreased and they broadened upon addition of POSS at various loadings. Higher values of the storage bending modulus and the glass transition temperature of PT-15/trisilanolphenyl-POSS were reported by the same research group [29].

Pittman *et al.* [64] investigated the viscoelastic properties of phenolic resin nanocomposites containing four different types of POSS molecules using DMTA. They used dichloromethylsilylethyl heptaisobutyl-POSS, trisilanol heptaphenyl-POSS, poly(phenylsilsesquioxane) uncured POSS and octaisobutyl-POSS in different wt % contents of 1, 3, 5 and 10. Higher values of E' in the rubbery region ($T>T_g$) were observed in the presence of dichloromethylsilylethyl heptaisobutyl-POSS**,** and these values increased with increasing POSS loadings in the resin. Similar behaviour was observed in the case of the poly(phenylsilsesquioxane)-POSS containing composites in the rubbery region, but only for the 1 to 5 wt % contents. In the glassy region ($T<T_g$) of the phenolic resin, the values of E' were higher for the composites containing 1 to 5 wt % dichloromethylsilylethyl heptaisobutyl-POSS loadings. In the case of the trisilanol heptaphenyl-POSS composites, the E' values were higher in both the glassy and rubbery regions. Similar behaviour was seen in the glassy region ($T<T_g$) of the phenolic resin after addition of octaisobutyl-POSS, except for the 10 wt % octaisobutyl-POSS content. The glass transition temperatures of the composites containing dichloromethylsilylethyl heptaisobutyl-POSS increased with increasing POSS loadings. Higher values of T_g were also observed in the case of trisilanol heptaphenyl-POSS and poly(phenylsilsesquioxane)-POSS composites. However, opposite behaviour was observed when octaisobutyl-POSS was used.

The tensile properties of the polymers and polymer nanocomposites are also very important properties in many industrial applications. Significant for these properties is the compatibility between the different components. Only a few studies reported on the tensile properties of polymers filled with POSS. The tensile properties of nanosilica-filled PP composites containing 1 to 5 wt % fumed silica nanoparticles in the presence of PP/methyl-POSS as a compatibilizer were reported by Lin *et al*. [65]. It was found that PP/methyl-POSS effectively improved the tensile properties of the composites at a lower nanosilica content. This

behaviour was associated with a better dispersion of nanosilica and compatibility between the silica and the PP matrix in the presence of the PP/methyl-POSS compatibilizer.

The tensile properties of the melt-mixed and *in situ* polymerized PET filled triepoxy-POSS fibre composites were reported in another study [51]. It was found that the tensile strength and modulus of the melt-mixed fibre composites decreased when compared to that of the neat PET matrix. In the case of *in situ* prepared PET based composites, only bulk properties instead of fibre properties were reported. The reason for this was the poor spinnability of the *in situ* polymerized composites. Slightly higher values for both tensile strength and modulus were observed, even at 1 wt % POSS content. This behaviour was due to the homogeneous dispersion of the POSS particles in the PET matrix when prepared through *in situ* polymerization. The value of the storage modulus was higher for the *in situ* prepared composite throughout the temperature range. However, the authors observed no difference in the tan δ after composite formation with POSS particles. The same research group [52] reported an increase in both tensile strength and modulus when 1 wt % of both disilanol- and trisilanol-POSS molecules were incorporated into a PET matrix.

2.5.4 Rheological properties

Investigation of the rheological properties in the molten state is fundamentally important to understand the processability and structure-property relationships of polymer composite systems. These properties are strongly dependent on the degree of dispersion of the filler particles in the polymer matrix [42], while that of the polymer melt strongly rely on the temperature at which the measurement is carried out [66]. For this reason, it is important to study the rheological behaviour of a polymer matrix reinforced with filler particles, where the POSS nanoparticle size allows interactions with the polymer matrix at the molecular scale.

Joshi *et al*. [42] investigated the rheological properties of HDPE/octamethyl-T_8-POSS nanocomposites. POSS particles acted as lubricating agent at lower POSS contents (0.25 to 0.5 wt %) and reduced the complex viscosity, η^* of the nanocomposites, while high POSS loadings showed an increase in the viscosity. The presence of POSS particles caused gelation in the HDPE matrix at concentrations higher than 5 wt %. This was due to the segregated particle-particle interaction.

In another publication [67], the rheological behaviour of PP/octavinyl-POSS composites, prepared through reactive and physical blending in the presence of dicumyl peroxide (DCP), was investigated. It was found that the η^* of the physically blended composites decreased at a lower POSS content and increased with increasing POSS content. Furthermore, the samples showed a liquid-like rheological character after nanocomposite formation due to the strong particle-matrix interaction of PP and grafted POSS. In the case of the reactive blending, the composites showed a solid-like rheological behaviour at the low frequency region when the POSS content was higher than 1 wt %. Kopesky *et al*. [39] reported that the presence of tethered POSS within entangled PMMA reduced the rubbery plateau modulus (G_N^0) of the neat PMMA. Wu and his co-workers [68] reported on the linear viscoelastic properties of entangled random copolymers from styrene and isobutyl-POSS (^{i}Bu-POSS). A dramatic reduction in the G_N^0 values of the copolymers caused by the addition of ^{i}Bu-POSS particles was observed. Such behaviour suggested a strong dilatation effect on the entanglement density caused by the presence of isobutyl-POSS. Fu *et al*. [63] studied the rheological properties of nanocomposites prepared from an ethylene-propylene copolymer (EP) matrix and POSS particles. Their investigation revealed a transition from liquid-like rheological behaviour in the pure EP to solid-like rheological behaviour for the POSS composites.

Kim *et al*. [52] reported on the rheological behaviour of PET/POSS nanocomposites conducted at 280 °C. They used both disilanol- and trisilanol-POSS particles to prepare their composites. An increase in the amount of disilanol-POSS molecules in the PET matrix increased the η^* of the PET matrix at low frequencies. However, the opposite behaviour was observed with increasing frequency. This behaviour was due to a shear thinning effect. Similar behaviour was observed in the case of PET/trisilanol-POSS nanocomposites, with a slight difference in η^* with increasing the POSS content. A plateau region was observed for the PET/POSS composites containing 1 wt % POSS. This behaviour indicated strong interfacial interactions between the PET and POSS particles.

2.5.5 XRD analysis

The structure of HDPE [42] before and after nanocomposite formation with octamethyl-T_8-POSS was studied by x-ray diffraction (XRD). The XRD patterns of POSS showed a number of strong sharp peaks which indicated a highly crystalline structure. Fu *et al*. [72] observed

sharp peaks for both neat octacyclohexyl-POSS and hydromethylsiloxy-POSS molecules. However, the diffraction profiles of hydromethylsiloxy-POSS were broader than that of octacyclohexyl-POSS, which indicated that the crystal size became smaller or more disordered by the substituted group. Fina *et al*. [46] reported a very intense main diffraction peak at $2\theta = 10.5°$ for octamethyl-POSS, two major intensity diffraction peaks at 8° and 8.8° for octaisobutyl-POSS and one amorphous halo peak at $2\theta = 7°$ for liquid octaisooctyl-POSS. HDPE showed two sharp characteristics peaks at 21.3° and 23.5°. These reflections were assigned to the 110 and 200 reflections of the Bunn orthorhombic subcell. These values agreed well with the values reported for PE as 21.4° and 23.7°, 21.6° and 24.0° as well as 21.6° and 24.1° by Bhadrakumari and Predeep [69], Rizzo *et al*. [70] and Waddon *et al.* [62]. In the case of the HDPE/POSS nanocomposites similar diffraction patterns as that for the neat HDPE were observed. Similar positions of the 110 and 200 peaks indicated that the presence of POSS particles did not change the basic nature of the diffraction pattern of HDPE. However, it was noticeable that the diffraction peaks were not as sharp as the neat POSS peaks. This behaviour suggested imperfection of POSS crystals dispersed in the polymer matrix.

The small angle x-ray scattering (SAXS) pattern of an EP copolymer showed a weak scattering peak when studied at different temperatures [63]. This indicated that the EP had a lamellar structure. At a high temperature of 160 °C, this structure of EP was destroyed and no scattering peak was observed with increasing temperature. The same behaviour was observed in the case of the nanocomposite. However, when 30 wt % POSS was used, a very ill-defined lamellar peak at low temperature and after cooling from the melt was observed. This indicated that the formation of the crystalline lamellae was hindered at higher POSS content.

Nanocomposite systems containing PE and POSS nanoparticles were prepared and characterized using WAXS (wide angle x-ray scattering) [71]. The POSS nanoparticles in the PE-*co*-POSS copolymers formed a lattice separate from the PE lattice with characteristic diffraction signals. The POSS crystallized as anisotropically shaped crystallites. The anisotropic POSS crystallites were the primary component responding to draw, aligning with their major dimension parallel to the draw direction. WAXD studies of the cured PT-15/OapPOSS composites were reported by Liang *et al*. [30]. The OapPOSS pattern exhibited a broad amorphous peak at $2\theta = 7.8°$. However, this broad peak was not observed in the case of the PT-15/OapPOSS composites. All the nanocomposites exhibited one broad peak at $2\theta =$

19.5°, and this peak corresponded to the diffraction peak of the neat PT-15 resin. This indicated that dispersed OapPOSS was compatible with the PT-15 network. When a cyanopropyl cyclopentyl-POSS monomer was incorporated into the PT-15 resin, the crystalline features characteristic of cyanopropyl cyclopentyl-POSS and the amorphous features characteristic of the resin were observed. The intensity of the crystalline peaks increased with increasing the content of cyanopropyl cyclopentyl-POSS in the PT-15 resin.

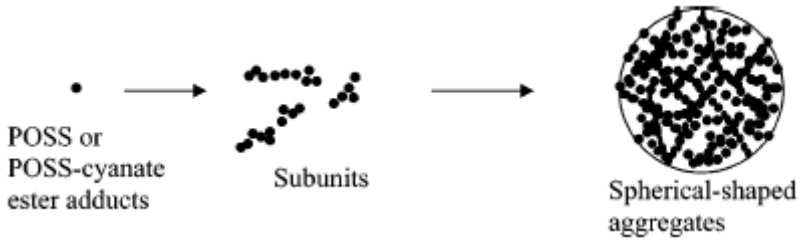

Scheme 2.2 Schematic representation of formation of POSS-enriched aggregated regions [29]

When PT-15/trisilanolphenyl-POSS nanocomposites were prepared [29], a similar WAXD peak was observed at $2\theta \approx 20°$ for the pure PT-15 resin. This peak was associated with cured amorphous PT-15. The incorporation of different amounts of trisilanol-POSS monomer into PT-15 produced WAXD patterns similar to those when OapPOSS and cyanophenyl cyclopentyl-POSS monomers were used. However, another small diffraction peak was observed at $2\theta \approx 7.5°$ for the nanocomposite containing 10 wt % POSS. This peak was attributed to the distance between the trisilanolphenyl-POSS moieties found in the neat solid sample of the POSS, which contributed to the formation of POSS aggregates into ordered particles that occurred at a higher POSS content. These POSS aggregates contributed to some regular structure that occurred when 10 wt % POSS was used as illustrated in Scheme 2.2.

2.6 References

1. A.J. Lester, P.S. Hope, European Symposium on Polymer Blends, Strasburg, 25-27 May (1987).
2. G. Allen, M.J. Bowden, G. Lewis, D.J. Blundell, G.M. Jeffs, J. Vyvoda. Composites formed by interstitial polymerization of vinyl monomers in polyurethane elastomers: 4.

Preparation, properties and structure of acrylonitrile and styrene based composites. Polymer 1974; 15:19-27.

3. Nurazreena, L.B. Hussain, H. Ishmail, M. Mariatti. Metal filled high density polyethylene composites – electrical and tensile properties. Journal of Thermoplastic Composite Materials 2006; 19:413-425.
4. Y.P. Mamunya, V.V. Davydenko, P. Pissis, E.V. Lebedev. Electrical and thermal conductivity of polymers filled with metal powders. European Polymer Journal 2000; 38:1887-1897.
5. M. Joshi, B.S. Butola. Studies on nonisothermal crystallization of HDPE/POSS nanocomposites. Polymer 2004; 45:4953-4968.
6. M. Pracella, D. Chionna, A. Fina, D. Tabuani, A. Frache, G. Camino. Polypropylene-POSS nanocomposites: Morphology and crystallization. Macromolecular Symposia. 2006; 234:59-67.
7. T. Seçkin, S. Köytepe, H. İbrahim, Adigüzel. Molecular design of POSS core star polyimides as a route to low-κ dielectric materials. Materials Chemistry and Physics. 2008; 112:1040-1046.
8. H. Mori, M.G. Lanzendörfer, A.H.E. Müller, J.E. Klee. Silsesquoxane-based nanoparticles formed via hydrolytic condensation of organotriethoxylane containing hydroxy groups. Macromolecules 2004; 37:5228-5238.
9. Y. Ni, S. Zheng, K. Nie. Morphology and thermal properties of inorganic–organic hybrids involving epoxy resin and polyhedral oligomeric silsesquioxanes. Polymer 2004; 45:5557-5568.
10. D.G. Dikobe, A.S. Luyt. Morphology and properties of polypropylene/ethylene vinyl acetate copolymer/wood powder blend composites. Express Polymer Letters 2009; 3:190-199.
11. F.J. Feher, R. Terroba, R.Z. Jin, , S. Lücke, F. Nguyen, R. Brutchey, K.O. Wyndham. Major advances in the synthesis of POSS monomers. Materials Research Society Proceedings 2000; 628:CC2.1.1-CC2.1.6.
12. G. Li, L. Wang, H. Ni, C.U. Pittman Jr. Polyhedral oligomeric silsesquioxane (POSS) polymers and copolymers: A review. Journal of Inorganic and Organometallic Polymers 2002; 11:123-154.
13. P.G. Harrison. Silicate cages: Precursors to new materials. Journal of Organometallic Chemistry 1997; 542:141-183.

14. J.F. Brown, L.H. Vogt. The polycondensation of cyclohexylsilanetriol. Journal of American Chemical Society 1965; 87:4313-4317.
15. C.L. Frye, W.T. Collins. Oligomeric silsesquioxanes, $(HSiO_{3/2})_n$. Journal of the American Chemical Society 1970; 92:5586-5588.
16. M.M. Sprung, F.O. Guenther. The partial hydrolysis of methyltriethoxysilane. Journal of the American Chemical Society 1955; 77:3990-3996.
17. D.W. Scott. Thermal rearrangement of branched-chain methylpolysiloxanes. Journal of the American Chemical Society 1946; 68:356-358.
18. F.J. Feher, D.A. Newman, J.F. Walzer. Silsesquioxanes as model for silica surfaces. Journal of the American Chemical Society 1989; 111:1741-1748.
19. L.H. Lee, W.C. Chen. Organic-inorganic hybrid materials from a new octa(2,3-epoxypropyl) silsesquioxane with diamines. Polymer 2005; 46:2163-2174.
20. R.A. Mantz, P.F. Johns, K.P. Chaffee, J.D. Lichtenhan, J.W. Gilman, I.M.K. Ismail, M.J. Burmeister. Thermolysis of polyhedral oligomeric silsesquioxane (POSS) macromers and POSS-siloxane copolymers. Chemistry of Materials 1996; 8:1250-1259.
21. A. Sellinger, R.M. Laine. Silsesquioxanes as synthetic platforms. Thermally curable and photocurable inorganic/organic hybrids. Macromolecules 1996; 29:2327-2330.
22. C.M. Leu, G.M. Reddy, K.H. Wei, C.F. Shu. Synthesis and dielectric properties of polyimide-chain-end tethered polyhedral oligomeric silsesquioxane nanocomposites. Chemistry of Materials 2003; 15:2261-2265.
23. H. Xu, S.W. Kuo, J.-S. Lee, F.C. Chang. Glass transition temperatures of poly(hydroxystyrene-*co*-vinylpyrrolidone-*co*-isobutylstyryl polyhedral oligo-silsesquioxanes). Polymer 2002; 43:5117-5124.
24. E.G. Shockey, A.G. Bolf, P.F. Jones, J.J. Schwab, K.P. Chaffee, T.S. Haddad, J.D. Lichtenhan. Functionalized polyhedral oligomeric silsesquioxanes: New graftable POSS hydride, POSS α-olefin, POSS epoxy, and POSS chlorosilane macromers and POSS-siloxane triblocks. Applied Organometallic Chemistry 1999; 13:311-327.
25. R.H. Baney, M. Itoh, A. Sakakibara, T. Suzuki. Silsesquioxanes. Chemical Reviews 1995; 95:1409-1430.
26. M. Joshi, B.S. Butola. Polymeric nanocomposites – Polyhedral oligomeric silsesquioxanes (POSS) as hybrid nanofiller. Polymer Reviews 2004; 44:389-410.
27. A. Lee, J.D. Lichtenhan. Thermal and viscoelatic properties of epoxy-clay and hybrid inorganic-organic epoxy nanocomposites. Journal of Applied Polymer Science 1999; 73:1993-2001.

28. G.Z. Li, L. Wang, H. Toghiani, T.L. Daulton, C.U. Pittman Jr. Viscoelastic and mechanical properties of vinyl ester (VE)/multifunctional polyhedral oligomeric silsequioxane (POSS) nanocomposites and multifunctional POSS-styrene copolymers. Polymer 2002; 43:4167-4176.
29. K. Liang, G. Li, H. Toghiani, J.H. Koo, C.U. Pittmann Jr. Cyanate ester/polyhedral oligomeric silsesquioxane (POSS) nanocomposites: Synthesis and characterization. Chemistry of Materials 2006; 18:301-312.
30. K. Liang, H. Toghiani, G. Li, C.U. Pittmann Jr. Synthesis, morphology, and viscoelastic properties of cyanate ester/polyhedral oligomeric silsesquioxane nanocomposites. Journal of Polymer Science, Part A: Polymer Chemistry 2005; 43:3887-3898.
31. G. Chigwada, P. Jash, D.D. Jiang, C.A. Wilkie. Fire retardancy of vinyl ester nanocomposites; Synergy with phosphorus-based fire retardants. Polymer Degradation and Stability 2005; 89:85-100.
32. J. Choi, S.G. Kim, R.M. Laine. Organic/inorganic hybrid epoxy nanocomposites from aminophenylsilsesquioxanes. Macromolecules 2004; 37:99-109.
33. J. Choi, J. Harcup, A.F. Yee, Q. Zhu, R.M. Laine. Organic/inorganic hybrid composites from cubic silsesquioxanes. Journal of the American Chemical Society 2001; 123:11420-11430.
34. G.Z. Li, L. Wang, H. Toghiani, T.L. Daulton, K. Koyyama, C.U. Pittmann. Viscoelastic and mechanical properties of epoxy/multifunctional polyhedral oligomeric silsequioxane nanocomposites and epoxy/ladderlike polyphenylsilsesquioxane blends. Macromolecules 2001; 34:8686-8693.
35. Y. Ni, S. Zheng. Epoxy resin containing octamaleimidophenyl polyhedral oligomeric silsesquioxane (POSS). Macromolecular Chemistry and Physics 2005; 206:2075-2083.
36. Y. Liu, S. Zheng, K. Nie. Epoxy nanocomposites with octa(propylglycidyl ether) polyhedral oligomeric silsesquioxane. Polymer 2005; 46:12016-12025.
37. W. Zhang, B.X. Fu, Y. Seo, E. Schrag, B. Hsiao, P.T. Mather, N.L. Yang, D. Xu, H. Ade, M. Rafailovich, J. Sokolov. Effect of methyl methacrylate/polyhedral oligomeric silsesquioxane random copolymers in compatibilization of polystyrene and poly(methyl methacrylate) blends. Macromolecules 2002; 35:8029-8038.
38. H. Weickmann, R. Delto, R. Thomann, R. Brenn, W. Döll, R. Mülhaupt. PMMA nanocomposites and gradient materials prepared by means of polysilsequioxane (POSS) self-assembly. Journal of Materials Science 2007; 42:87-92.

39. E.T. Kopesky, T.S. Haddad, G.H. McKinley, R.E. Cohen. Miscibility and viscoelastic properties of acrylic polyhedral oligomeric-poly(methyl methacrylate) blends. Polymer 2005; 46:4743-4752.
40. E.T. Kopesky, G.H. McKinley, R.E. Cohen. Toughened poly(methyl methacrylate) nanocomposites by incorporating polyhedral oligomeric silsesquioxanes. Polymer 2006; 47:299-309.
41. K.M. Kim, T. Inakura, Y. Chujo. Organic-inorganic polymer hybrids using octasilsesquioxanes with hydroxyl groups. Polymer Bulletin 2001; 46:351-356.
42. M. Joshi, B.S. Butola, G. Simon, N. Kukaleva. Rheological and viscoelastic behaviour of HDPE/octamethyl-POSS nanocomposites. Macromolecules 2006; 39:1839-1849.
43. M. Joshi, B.S. Butola. Isothermal crystallization of HDPE/octamethyl polyhedral oligomeric silsesquioxane nanocomposites: Role of POSS as nanofiller. Journal of Applied Polymer Science 2007; 105:978-985.
44. B. X. Fu, L. Yang, R.H. Somani, S.X. Zong, B.S. Hsiao, S. Phillips, R. Blanski, P. Ruth. Crystallization studies of isotactic polypropylene containing nanostructured polyhedral oligomeric silsesquioxane molecules under quiescent and shear conditions. Journal of Polymer Science, Part B: Polymer Physics 2001; 39:2727-2739.
45. A. Fina, H.C.L. Abbenhuis, D. Tabuani, A. Frache, G. Camino. Polypropylene metal functionalised POSS nanocomposites: A study by thermogravimetry analysis. Polymer Degradation and Stability 2006; 91:1064-1070.
46. A. Fina, D. Tabuani, A. Frache, G. Camino. Polypropylene-polyhedral oligomeric silsesquioxanes (POSS) nanocomposites. Polymer 2005; 46:7855-7866.
47. O.H. Lin, M. Ishak, H.M. Akil. Preparation and properties of nanosilica-filled polypropylene composites with PP-methyl POSS as compatibiliser. Materials and Design 2009; 30:748-751.
48. J.H. Chen, Y.D. Chiou. Crystallization behaviour and morphological development of isotactic polypropylene blended with nanostructured polyhedral oligomeric silsesquioxane molecules. Journal of Polymer Science, Part B: Polymer Physics 2006; 44:2122-2134.
49. Z. Zhou, L. Cui, Y. Zhang, Y. Zhang, N. Yin. Isothermal crystallization kinetics of polypropylene/POSS composites. Journal of Polymer Science, Part B: Polymer Physics. 2008; 46:1762-1772.

50. Z. Zhou, L. Cui, Y. Zhang, Y. Zhang, N. Yin. Preparation and properties of POSS grafted polypropylene by reactive blending. European Polymer Journal 2008; 44:3057-3066.
51. K.H. Yoon, M.B. Polk, J.H. Park, B.G. Min, D.A Schiraldi. Properties of poly(ethylene terephthalate) containing epoxy-functionalized polyhedral oligomeric silsesquioxane. Polymer International 2005; 54:47-53.
52. J.K. Kim, K.H. Yoon, D.S. Bang, Y.B. Park, H.U. Kim, Y.H. Bang. Morphology and rheological behaviour of poly(ethylene terephthalate) nanocomposites containing polyhedral oligomeric silsesquioxanes. Journal of Applied Polymer Science 2008; 107:272-279.
53. J. Tang, Y. Wang, H. Liu, L.A. Belfiore. Effects of organic nucleating agents and zinc oxide nanoparticles on isotactic polypropylene crystallization. Polymer 2004; 45:2081-2091.
54. C. Cazé, E. Devaux, A. Crespy, J.P. Cavrot. A new method to determine the Avrami exponent by DSC studies of nonisothermal crystallization from the molten state. Polymer 1997; 38:497-502.
55. T. Ozawa. Kinetics of nonisothermal crystallization. Polymer 1971; 12:150-158.
56. M. Avrami. Kinetics of phase change. I. General theory. The Journal of Chemical Physics 1939; 7:1103-1107.
57. A. Jeziorny. Parameters characterizing the kinetics of the nonisothermal crystallization of poly(ethylene terephthalate) determined by DSC. Polymer 1978; 19:1142-1144.
58. J.H. Chen, B.X. Yao, W.B. Su, Y.B. Yang. Isothermal crystallization behaviour of isotactic polypropylene blended with small loading of polyhedral oligomeric silsesquioxane. Polymer 2007; 48:1756-1769.
59. L. Zheng, R.J. Farris, E.B. Coughlin. Novel polyolefin nanocomposites: Synthesis and characterizations of metallocene-catalyzed polyolefin polyhedral oligomeric silsesquioxane copolymers. Macromolecules 2001; 34:8034-8039.
60. C. Zhao, X. Yang, X. Wu, X. Liu, X. Wang, L. Lu. Preparation and characterization of poly(methyl methacrylate) nanocomposites containing octavinyl polyhedral oligomeric silsesquioxane. Polymer Bulletin 2008; 60:495-505.
61. C.F. Huang, S.W. Kuo, F.J. Lin, W.J. Huang, C.F. Wang, W.Y. Chen, F.C. Chang. Influence of PMMA-chain-end tethered polyhedral oligomeric silsesquioxanes on the miscibility and specific interaction with phenolic blends. Macromolecules 2006; 39:300-308.

62. A.J. Waddon, L. Zheng, R.J. Farris, E.B. Coughlin. Nanostructured polyethylene-POSS copolymers: Control of crystallization and aggregation. Nano Letters 2002; 2:1149-1155.
63. B.X. Fu, M.Y. Gelfer, B.S. Hsiao, S Phillips, B. Viers, R. Blansky, P. Ruth. Physical gelation in ethylene-propylene copolymer melts induced by polyhedral oligomeric silsesquioxane (POSS) molecules. Polymer 2003; 44:1499-1506.
64. C.U. Pittman Jr, G.Z. Li, H.S. Cho. Chemical bonding between phenolic resins and polyhedral oligomeric silsesquioxanes (POSS) in inorganic-organic hybrid nanocomposites. Journal of Inorganic and Organometallic Polymers and Materials 2006; 16:43-59.
65. O.H.Lin, Z.A. Mohd Ishak, H.M. Akil. Preparation and properties of nanosilica-filled polypropylene composites with PP/methyl-POSS as compatibiliser. Materials and Design 2009; 30:748-751.
66. S. Sinha Ray, K. Okamoto, M. Okamoto. Structure-property relationship in biodegradable poly(butylene succinate)/layered silicate nanocomposites. Macromolecules 2003; 36:2355-2367.
67. Z. Zhou, Y. Zhang, Y. Zhang, N. Yin. Rheological behaviour of polypropylene/octavinyl polyhedral oligomeric silsesquioxane composites. Journal of Polymer Science, Part B: Polymer Physics 2008; 46:526-533.
68. J. Wu, T.S. Haddad, G.M. Kim, P.T. Mather. Rheological behavior of entangled polystyrene-polyhedral oligosilsesquioxane (POSS) copolymers. Macromolecules 2007; 40:544-554.
69. S. Bhadrakumari, P. Predeep. Synthesis, characterization and A.C. susceptibility of $YBa_2Cu_3O_{7-x}$/polyethylene composites. Journal of Superconductivity and Novel Magnetism 2008; 21:409-414.
70. P. Rizzo, F. Baione, G. Guerra, L. Martinotto, E. Albizzati. Polyethylene unit cell and crystallinity variations as a consequence of different cross-linking processes. Macromolecules 2001; 34:5175-5179.
71. L. Zheng, A.J. Waddon, R.J. Farris, E. Coughlin. Bryan X-ray characterizations of polyethylene polyhedral oligomeric silsesquioxane copolymers. Macromolecules 2002; 35:2375-2379.
72. B.X. Fu, B.S. Hsiao, S. Pagola, P. Stephens, H. White, M. Rafailovich, J. Sokolov, P.T. Mather, H.G. Jeon, S. Phillips, J. Lichtenhan, J. Schwab. Structural development during

deformation of polyurethane containing polyhedral oligomeric silsesquioxanes (POSS) molecules. Polymer 2001; 42:599-611.

73. Z. Zhou, Y. Zhang, Z. Zeng, Y. Zhang. Properties of POSS-filled polypropylene: Comparison of physical blending and reactive blending. Journal of Applied Polymer Science 200; 110:3745-3751.

74. Y. Zhang, S. Lee, M. Yoonessi, K. Liang, C.U. Pittman. Phenolic resin-trisilanolphenyl polyhedral oligomeric silsesquioxane (POSS) hybrid nanocomposites: Structure and properties. Polymer 2006; 47:2984-2996.

CHAPTER 3

SAMPLE PREPARATION AND EXPERIMENTAL TECHNIQUES

3.1 Introduction

The experimental techniques used in this study include melt-mixing in a Thermohaake-mixer, hot-melt pressing, injection moulding, differential scanning calorimetry (DSC), thermogravimetric analysis (TGA), dynamic mechanical analysis (DMA), rheometry, polarized optical microscopy (POM), field-emission scanning electron microscopy (FE-SEM), small angle x-ray scattering (SAXS), x-ray diffraction (XRD), heat distortion temperature (HDT), pendulum impact and tensile testing. A detailed discussion of these techniques for the preparation and characterization of the neat polymers and their nanocomposites is provided in section 3.3.

3.2 Materials

3.2.1 Polyhedral oligomeric silsesquioxane (POSS)

POSS derivatives used in this study, octamethyl-T_8-POSS and poly((propylmethacryl-heptaisobutyl-POSS)-*co*-(methyl-methacrylate)), were purchased in powder form from Sigma Aldrich, Republic of South Africa. Octamethyl-T_8-POSS has a molecular weight of 537 $g.mol^{-1}$ and a decomposition temperature of about 230 °C. Poly((propylmethacryl-heptaisobutyl-POSS)-*co*-(methyl methacrylate)) has a T_g of 97 °C. The octamethyl-T_8-POSS is slightly soluble in common solvents such as tetrahydrofuran (THF) and chloroform, while poly((propylmethacryl-heptaisobutyl-POSS)-*co*-(methyl-methacrylate)) is soluble in both solvents. The molecular structures of poly((propylmethacryl-heptaisobutyl-POSS)-*co*-(methyl-methacrylate)) and octamethyl-T_8-POSS are illustrated in Figure 3.1.

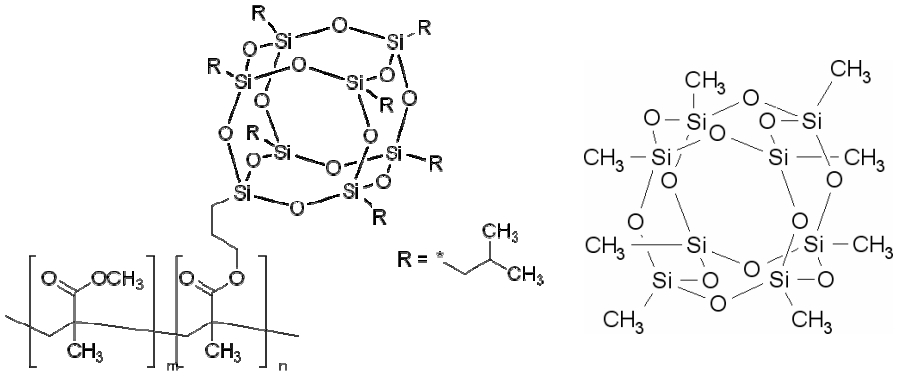

(a) (b)

Figure 3.1 Molecular structures of (a) poly((propylmethacryl-heptaisobutyl-POSS)-*co*-(methyl methacrylate)) and (b) octamethyl-T_8-POSS

3.2.2 Linear low-density polyethylene (LLDPE)

DOWLEX 2045G (Dow Chemical) linear low-density polyethylene (LLDPE) pellets were supplied by Plastomark (Pty) Ltd, Republic of South Africa, and has a melt flow index (MFI) of 1 g.10 min^{-1} (ASTM D-1238), a melting point of 121 °C and a density of 0.920 $g.cm^{-3}$.

3.2.3 Poly(methyl methacrylate) (PMMA)

The PMMA resin was supplied in pellet form by Rohm and Haas Co. (Plexiglas V-811). It has a weight average molecular weight $\overline{M}_w$ = 130 000, number average molecular weight $\overline{M}_n$ = 52 900 and a T_g of 108 °C.

3.3 Methods

3.3.1 Preparation of nanocomposites

The LLDPE/octamethyl-T_8-POSS and PMMA/poly((propylmethacryl-heptaisobutyl-POSS)-*co*-(methyl methacrylate)) nanocomposite systems were mixed at 150 °C and 180 °C (set points) for LLDPE and PMMA, respectively, in a twin-rotor thermohaake-mixer (Haake Polylab OS system) (Figure 3.2 (a)) at 60 rpm for 8 min. LLDPE and PMMA with different POSS loadings from 5 to 25 wt % were prepared according to the desired ratios (Table 3.1).

Prior to use, both LLDPE and PMMA were dried under vacuum at 80 °C for 4 hours and 100 °C for 24 hours, respectively. The POSS powders were used as received and slowly added into the mixer after 2 minutes (time zero) of melting of the LLDPE and PMMA in the mixer. The mixing of the samples was followed by melt-pressing for 5 min at 150 °C for LLDPE and 180 °C for PMMA using a pressure of 2 tons in the Carver hot-melt press (Figure 3.2 (b)).

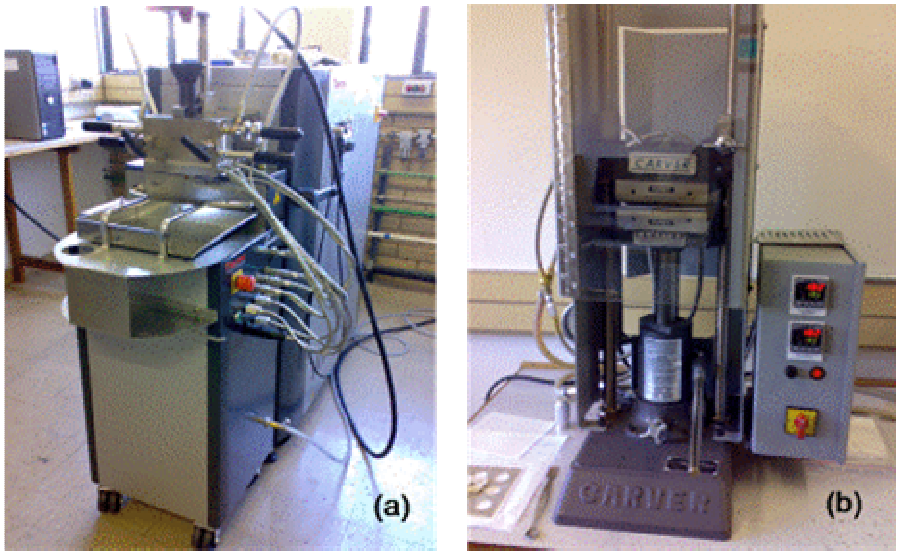

Figure 3.2 (a) Haake Polylab OS rheomixer 600 model system and (b) Carver hot-melt press

Table 3.1 Sample compositions used in this study

LLDPE/octamethyl-T_8-POSS (w/w)	**PMMA/poly((propylmethacryl-heptaisobutyl-POSS)-*co*-(methyl-methacrylate)) (w/w)**
100/0	100/0
95/5	95/5
92.5/7.5	90/10
90/10	85/15
-	75/25

3.3.2 Small angle x-ray scattering

Small angle x-ray scattering (SAXS) is an accurate non-destructive analytical technique used to investigate the structure of the particle systems with respect to the average particle sizes or shapes. In the SAXS, x-rays are produced by either an x-ray tube or a synchrotron source by irradiating a sample. The first one is mostly preferred in SAXS studies, while the latter is used when high beam intensities or unusual wavelengths are needed. SAXS can be used to test different materials in the solid or liquid phase. It can also be used to tests materials that contain solid, liquid or gaseous domains (called particles) of the same or another material in any combination. It is, therefore, perfectly suitable to be utilized in various applications from cement, oils, polymers, food and in pharmaceutical industries. This method can also be helpful for quality control purposes. The advantage of SAXS over other analytical techniques is that it can test particles of high atomic numbers which can exhibit higher contrast and give better detection limits. Particle or structures ranging from 1 to 100 nm can be resolved in a typical set-up. The range of measurements can be extended on either side by taking measurements at smaller (i.e. ultra small-x-ray scattering or larger q region) or larger angles (i.e. wide-angle x-ray scattering, WAXS or smaller q region) [1].

Figure 3.3 Anton-Paar small-angle x-ray scattering spectrometer

In order to determine the structural modification during heating, WAXS spectra of the samples were collected on a SAXS instrument (Anton-Paar, Figure 3.3) with a wide-angle attachment (SAXSess, Germany, CuK_{α} radiation), operated at an accelerating voltage of 40 kV and a current of 50 mA. The sample thickness was ≈ 0.4 mm and the temperature was controlled by a TCU50 (Anton-Paar) temperature control unit.

3.3.3 Optical microscopy

An optical microscope, often referred to as a light microscope, is a type of microscope which uses visible light and a system of lenses to magnify images of small samples. Optical microscopes are the oldest and simplest of the microscopes. When they are accompanied by a charge coupled device (CCD) camera, a sample is examined and the image is shown directly on a computer screen without the use of optics like eye-pieces. Optical microscopes are used for identification of metals, composite construction, as well as the assessment of the homogeneity of nanoparticles dispersion in the polymer matrix [2]. A schematic illustration of the optical path in a typical microscope is shown in Figure 3.4.

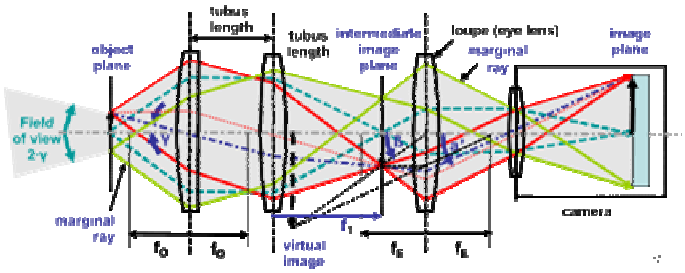

Figure 3.4 A schematic drawing of the optical path in a typical optical microscope [3]

The microstructures of the samples were investigated with a Carl Zeiss imager Z1 model polarized optical microscope (POM) shown in Figure 3.5. Prior to taking the POM micrographs, compression-moulded thin films (sample thickness was ≈ 0.4 mm) were placed between two covering glasses and placed on a Linkam hot-stage (Linkam Scientific Instruments Ltd, UK) mounted on the microscope.

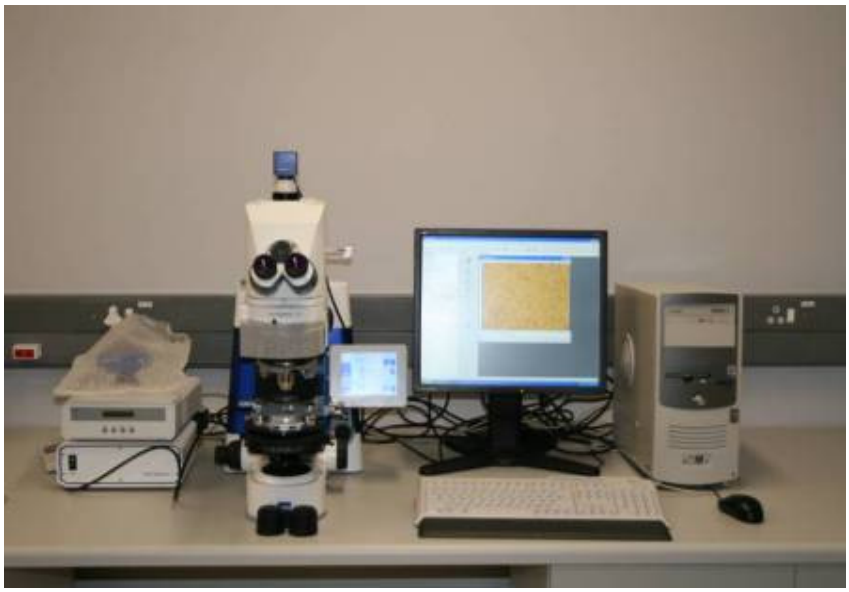

Figure 3.5 Carl Zeiss Imager Z1 model polarized optical microscope

3.3.4 X-ray diffraction

X-ray diffraction (XRD) is an efficient non-destructive analytical technique used to determine structural properties of crystalline materials. It is also used in applications such as phase identification, determination of grain size, compositions of solid solutions, lattice constants, and degree of crystallinity in a mixture of amorphous and crystalline substances. A diffraction pattern is produced when a material is irradiated with a collimated beam of x-rays. The x-ray patterns generated by this technique provide a structural fingerprint of the unknown material. The relative peak height is generally proportional to the number of grains in a preferred orientation, and peak positions are reproducible. The intensity of the diffracted x-rays is measured with respect to the diffraction angle 2θ and the sample's orientation [4].

The X'pert PRO (PANalytical) PN 3040/60 x-ray diffractometer shown in Figure 3.6 was used for the analyses of the samples in this study. A monochromated Cu-K_α (λ = 0.154 nm) radiation source, operated at an acceleration voltage of 45.0 kV and a current of 40.0 mA were used. XRD data were collected in the 2θ geometry ranging from 5 to 40° with a step size of 0.02 and a scanning rate of 4° min^{-1}.

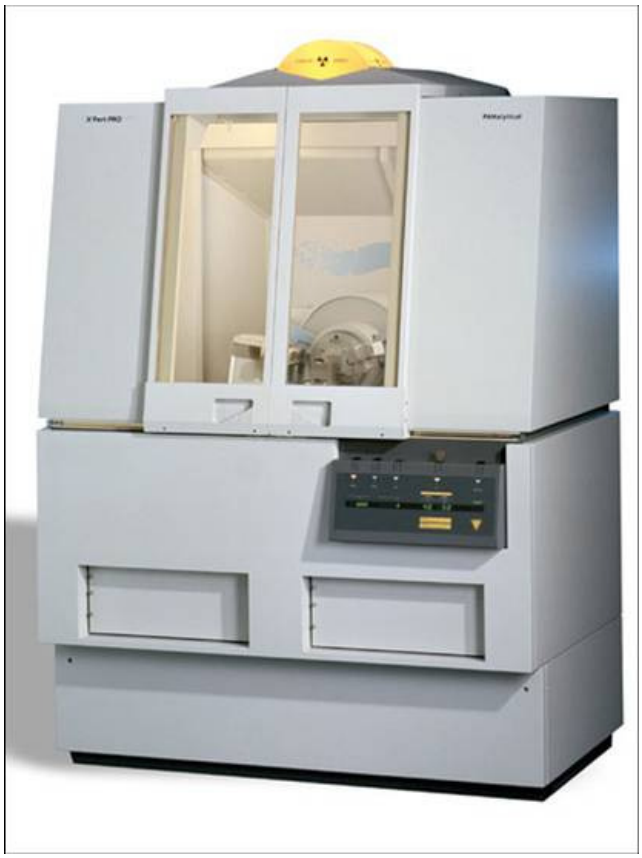

Figure 3.6 X'Pert PRO PN3040/60 model (PANalytical) x-ray diffractometer

3.3.5 Scanning electron microscopy

Scanning electron microscopy (SEM) is a technique whereby a beam of energetically well-defined and highly focused electrons is scanned across a sample. The microscope uses a lanthanum hexaboride (LaB_6) source and is pumped using turbo and ion pumps to maintain the highest possible vacuum. The technique can provide information about the topography, morphology and crystallography of the material [4]. If the system is equipped with an energy dispersive x-ray spectrometer (EDS), it can also provide information about the chemical composition of the material [5]. The basic principle of the system is that the electron beam impinges the surface and generates a splash of electrons, called secondary electrons, with kinetic energies much lower than the primary incident electrons. An image of the sample surface is constructed by measuring the secondary electron intensity as a function of the primary beam position. Advantages of the SEM over traditional microscopes are (i) its large depth of field, which allows more of a sample to be in focus at one time and much higher

resolution, so that closely spaced samples can be magnified at much higher levels, and (ii) its use of electromagnetic lenses which give much more control on the degree of magnification. A simplified layout of a SEM is shown in Figure 3.7.

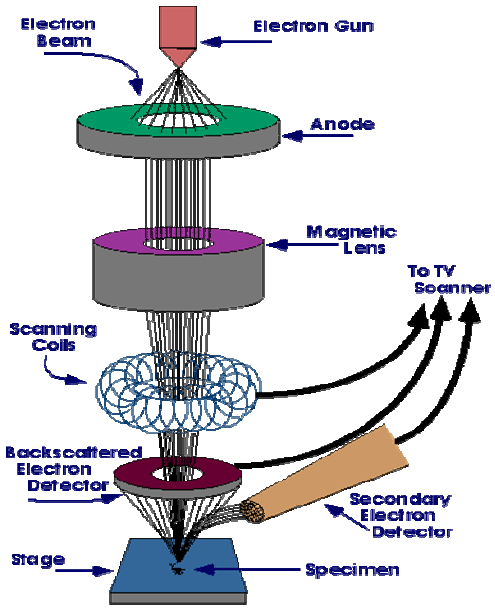

Figure 3.7 A simplified layout of the scanning electron microscope [4]

The SEM micrographs were obtained by the JEOL JSM 7500F field-emission scanning electron microscopy (FE-SEM), shown in Figure 3.8. Before the images were taken, all the samples were frozen in liquid nitrogen for 24 hours, and fractured by simply breaking the samples in an appropriate size to fit in the sample chamber, and then mounted onto the holder. The surfaces of the samples were coated with carbon by an electro-deposition method to impart electrical conduction before recording the SEM micrographs. This was done to prevent the accumulation of static electric charge on the sample during electron irradiation.

Figure 3.8 JEOL JSM 7500F model field-emission scanning electron microscopy (FE-SEM)

3.3.6 Differential scanning calorimetry

Differential scanning calorimetry (DSC) is a thermoanalytical technique in which the difference in the amount of heat required to increase the temperature of a sample and reference are measured as a function of temperature (nonisothermal) or time (isothermal). DSC techniques are widely used in the polymer industry. It is mainly applied in studying phase transitions such as melting, crystallization, oxidation, glass transitions, curing, as well as the composition and compatibility of plasticized polymers, polymer blends and composites. The transitions involve energy or heat capacity changes that can be detected by the DSC with great sensitivity. The most commonly used DSC type in analytical laboratories is based on the heat flux principle, illustrated in Figure 3.9. Both the sample and reference are maintained at nearly the same temperature throughout the experiment. Generally, the temperature program for a DSC analysis is designed in such a way that the temperature of the sample holder increases linearly with respect to time. The reference sample has a well-defined heat capacity over the range of temperatures to be scanned [6,7].

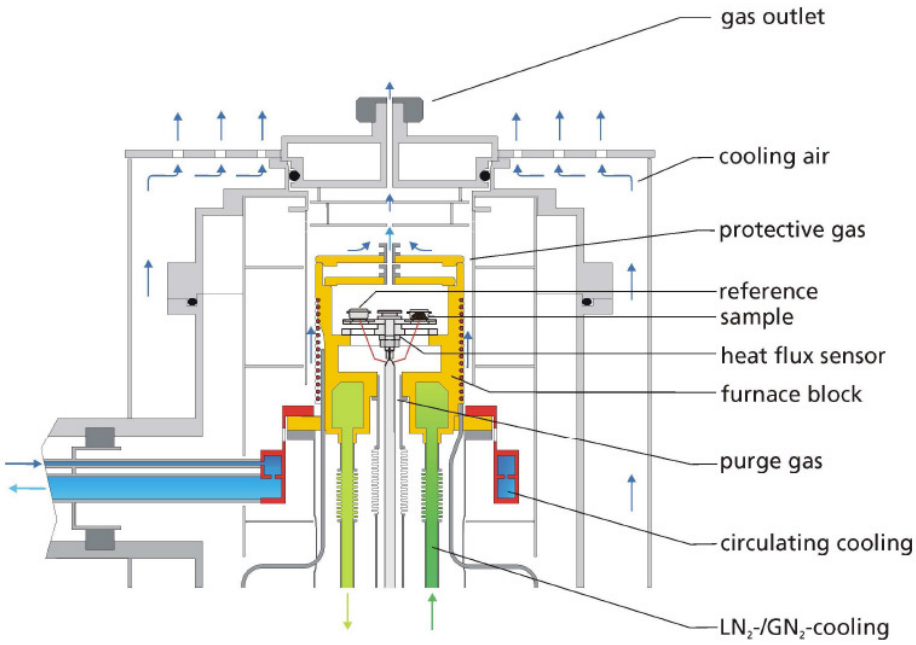

Figure 3.9 Schematic diagram of a differential scanning calorimeter [8]

DSC analyses were done on a TA Q2000 model (TA Instruments) differential scanning calorimeter (Figure 3.10) under constant flowing nitrogen (flow rate 50 ml min^{-1}). The samples were weighed such that all the samples had an identical LLDPE and PMMA content. Approximately 7-10 mg of each sample was loaded in an aluminium pan in order to minimize any possible thermal lag during the scans. The instrument was calibrated by employing the temperature and heat-of-fusion of an indium standard, and the baseline was checked according to the TA Instruments protocols. The thermal histories of all the samples were the same prior to each experiment.

To study the nonisothermal crystallization behaviour and the T_g, the samples were first heated to 150 °C for LLDPE and 180 °C for PMMA at a heating rate of 20 °C.min^{-1}, held at that temperature for 3 min. to eliminate any previous thermal history, and then cooled to -60 °C at a constant cooling rate of 10 °C.min^{-1}. For the second scan, the samples were heated and cooled under the same conditions.

Figure 3.10 Q2000 model (TA instrument) differential scanning calorimetry

To separate the heat capacity and kinetic-related components during re-crystallization and the subsequent melting of the pure LLDPE and the nanocomposite systems containing 5 wt % POSS, a TMDSC (temperature-modulated DSC) analysis of the samples was carried out using the same DSC instrument with a constant nitrogen flow of 50 $ml.min^{-1}$. TMDSC generally applies a sinusoidal temperature oscillation (modulation) on a conventional heating DSC and allows the total heat flow (as obtained from conventional DSC) to be separated into the heat capacity related (reversible) and kinetic (non-reversible) components. The heat capacity was calibrated with a sapphire sample. Different underlying rates, modulations and periods were applied. The most suitable parameters were a heating rate of 2 $°C.min^{-1}$, an amplitude of ±0.318 °C and a period of 60 s.

3.3.7 Thermogravimetric analysis

Thermogravimetric analysis (TGA) is an analytical technique used to determine a material's thermal stability and its fraction of volatile components by monitoring the weight changes that occur in relation to temperature, time or both in a controlled atmosphere such as air or inert gas. TGA is commonly used in research to determine the characteristics such as degradation temperatures, absorbed moisture content of materials, the level of inorganic and organic components in materials, decomposition points of explosives, and solvent residues of

polymers, composites, films, fibers, coatings and paints. It is also often used to estimate the corrosion kinetics in high temperature oxidation. In addition to weight changes, some instruments also record the temperature difference between the sample and one or more reference pans such as differential thermal analysis (DTA) [9,10].

Figure 3.11 Q500 model (TA instrument) thermogravimetric analysis

Figure 3.11 shows the TGA Q500 model (TA Instruments) used for studying the thermal degradation behaviour of the samples. The measurements were carried out at a heating rate of 10 °C.min^{-1} under thermo-oxidative and nitrogen atmospheres from room temperature to 700 °C. Samples ranging from 5 to 10 mg were analyzed.

3.3.8 Injection moulding

Injection moulding is a technique used to produce different parts using different thermosetting and thermoplastic materials. The principle of the process is that the material is supplied into a heated barrel, mixed and forced through the sprue into a mould cavity where it cools and hardens to the configuration of the mould cavity. It is widely used for manufacturing of parts, from the smallest component (e.g. packaging bottles) to entire body panels of vehicles [11]. Figure 3.12 depicts a schematic diagram of the injection moulder.

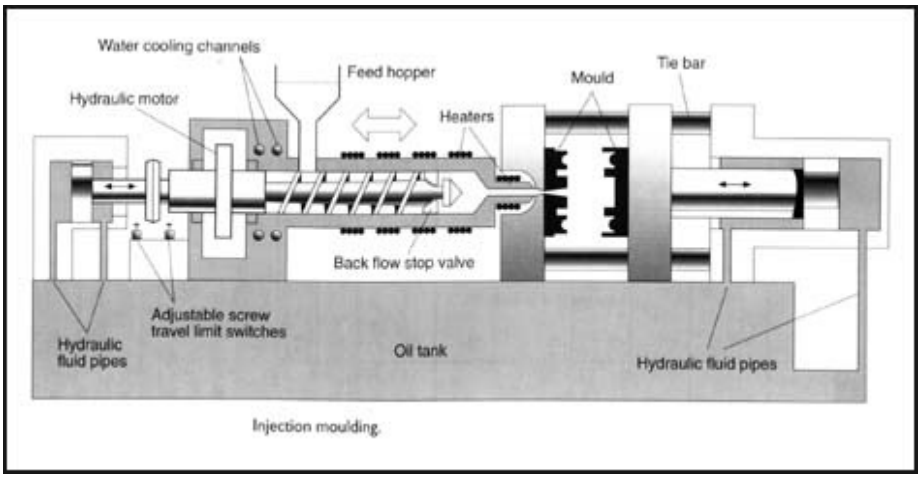

Figure 3.12 Schematic diagram of an injection moulder [11]

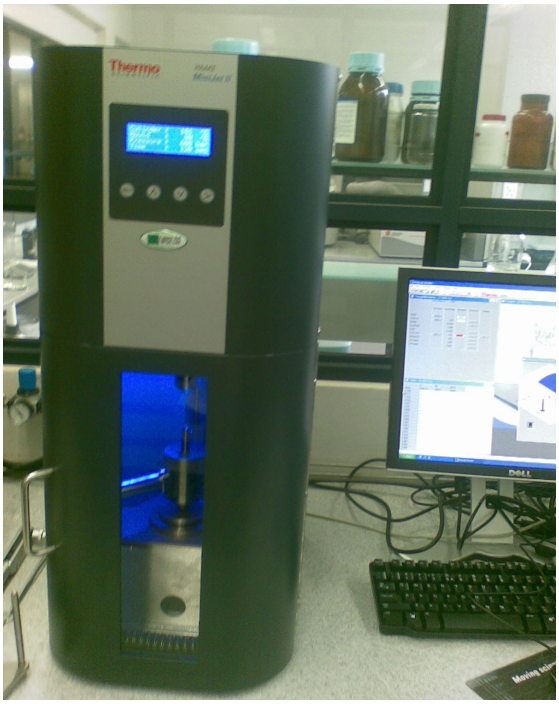

Figure 3.13 ThermoHaake Scientific Minijet II injection moulder

3.3.9 Tensile testing

Tensile testing is used to determine the modulus of elasticity (or Young's modulus), the tensile strength, stress at break and sample elongations at yield and break. In a typical tensile

test a sample of known dimensions is firmly tightened between two grips. The tensile tester pulls the sample from both ends and measures the force needed to pull the sample apart as well as the elongation of the sample. The product of a tensile test is a load versus elongation curve which is then converted into a stress-strain curve, from which the required tensile values are determined [7]. The tensile properties of composites can be influenced by the aspect ratio of the inclusions [12,13]. The modulus of elasticity of reinforced polymer composites can be predicted by using various models, which are mainly based on either hydrodynamic considerations, for example, Guth-Smallwood, the Kerner equation and its modifications such as Hashin-Shtrikman or Halpin-Tsai [14-18].

The dumbbell-shaped samples for LLDPE/POSS composites were prepared at 180 °C (cylinder temperature), an injection pressure of 400 bar and a mould temperature of 60 °C using a ThermoHaake Minijet II injection moulding machine (ASTM D-638) as shown in Figure 3.13. Samples of thickness = 3.00 mm, width = 3.0 mm and length = 64 mm were used. Five measurements were carried out for each composition and the results were averaged to obtain a mean value. A Hounsfield H10KT (Tinius Olsen Ltd) tensile tester was used for the tensile properties of the samples at room temperature (Figure 3.14). The settings of the instrument used for the tensile analysis are shown in Table 3.2.

Table 3.2 The settings of the tensile tester used for the analysis

Load range	250.0 N
Extension range	500.0 mm
Gauge length	25.0 mm
Stretching speed	10.0 $mm.min^{-1}$
Approached speed	0.02 $mm.min^{-1}$

The dimensions and shape of the moulded dumbbell-shaped (ASTM D-638) sample for tensile testing were as follows:

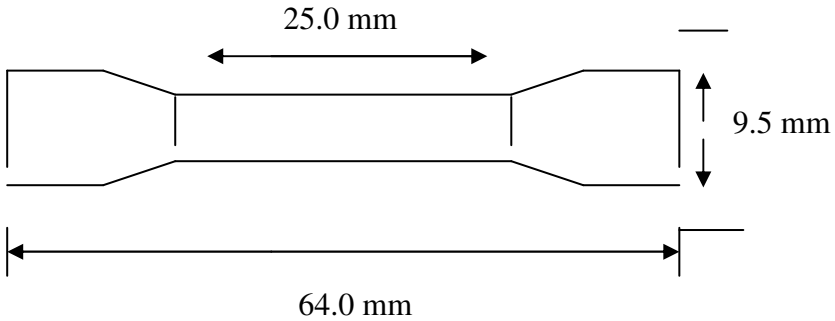

Figure 3.14 Tinius Olsen H10KT model tensile testing

3.3.10 Dynamic mechanical analysis

Dynamic mechanical analysis (DMA) is a technique that yields information about the mechanical properties such as the storage modulus, loss modulus and damping factor of a sample. In a typical DMA test, an oscillation force is applied to a sample as a function of time and temperature and the system analyzes the response of the material to the applied force. Depending on various factors such as the type of the sample, as well as dimensions and sample behaviour, different measuring setups ranging from compression, 3-point bending, shear, tension, single and dual cantilever modes can be performed by DMA [19].

DMA can be used to study the viscoelastic behaviour of polymers and their composites, as well as powders, coatings, and liquids. Since all polymers are viscoelastic in nature, this method is perfectly suited for the task of evaluating a complex array of phenomena that polymers present to us, focusing on solid state transitions [7,19].

Polymers and their corresponding composites may exhibit three thermal transitions that can be described in terms of free volume changes or relaxation times. These transitions are classified as the γ-, β- and α-transitions by their types of motion [7,20-22]. When DMA tests are performed from a very low temperature where the molecules are tightly compressed, to higher temperatures, the free volume, v_f starts increasing so that localized bond movements (bending and stretching) and side chain movements occur. This transition is known as the γ-transition. With increasing the temperature, the v_f increases to a point where there is enough space and mobility of the whole side chains and localized groups of 4-8 backbone atoms. For this reason, the sample develops some toughness. This type of transition is called the β-transition. When studying a blend system, this is referred to as the T_g of a secondary component in that blend. The α-transition is associated with the chain segment mobility in the crystalline phase, probably due to the reorientation of defect areas in crystals. The α-transition appears to be a composite process of two transitions labeled as α and α' [7,23-25].

The dynamic mechanical analysis of the samples was done using the Perkin-Elmer DMA 8000 shown in Figure 3.15. Table 3.3 shows the instrumental settings used for the DMA measurements.

Table 3.3 The settings of the instrument and sample dimensions used for DMA analysis

Frequency	6.28 rad s^{-1}
Temperature range	LLDPE/POSS samples (-50 to 150 °C), PMMA/POSS samples (0 to 180 °C)
Heating rate	5 °C.min^{-1}
Normal force	-1.0 N
Length	29.0 mm
Width	9.8 mm
Thickness	1.6 mm

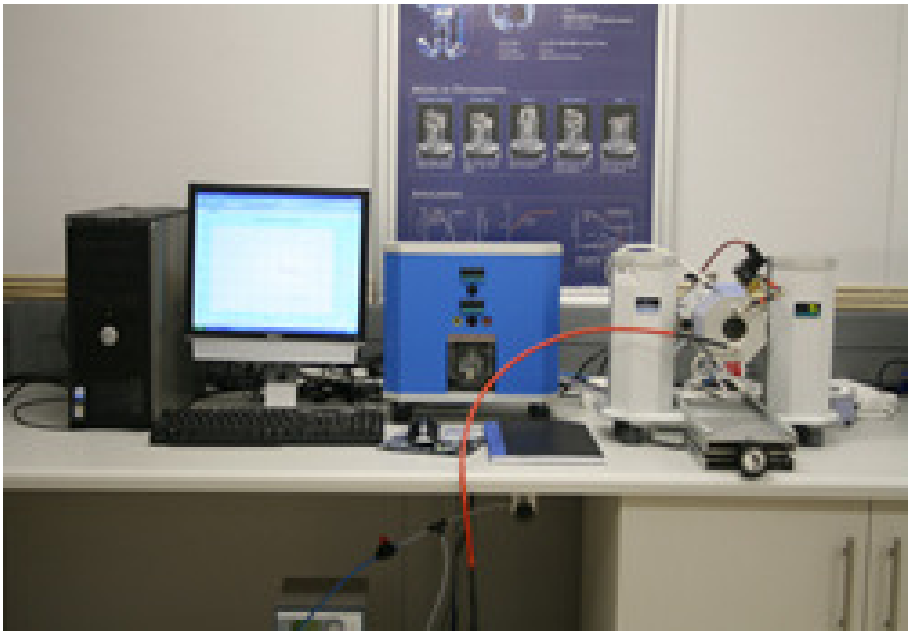

Figure 3.15 Perkin Elmer DMA 8000 dynamic mechanical analyzer

3.3.11 Heat deflection temperature

Heat deflection temperature or heat distortion temperature (HDT) is defined as the temperature at which a standard test bar (rests on two supports of a specified span) deflects a specified distance under a specific load. It is an essential piece of information for product design. If connected with vicat stations, softening temperatures can also be determined [26]. It is also defined as a non-direct reflection of the intrinsic property of the material, as well as a measurement of the upper boundary of the dimensional stability of a plastic material under a normal load and thermal effect [27]. The interpretation of HDT data is often related to the mechanical behaviour of the materials of concern [28].

The HDT of the samples was measured using a Ceast 6 HDT/Vicat tester (Figure 3.16). The dimensions of the test bars and the procedure all conformed to those specified in ISO 75-2 (1993).

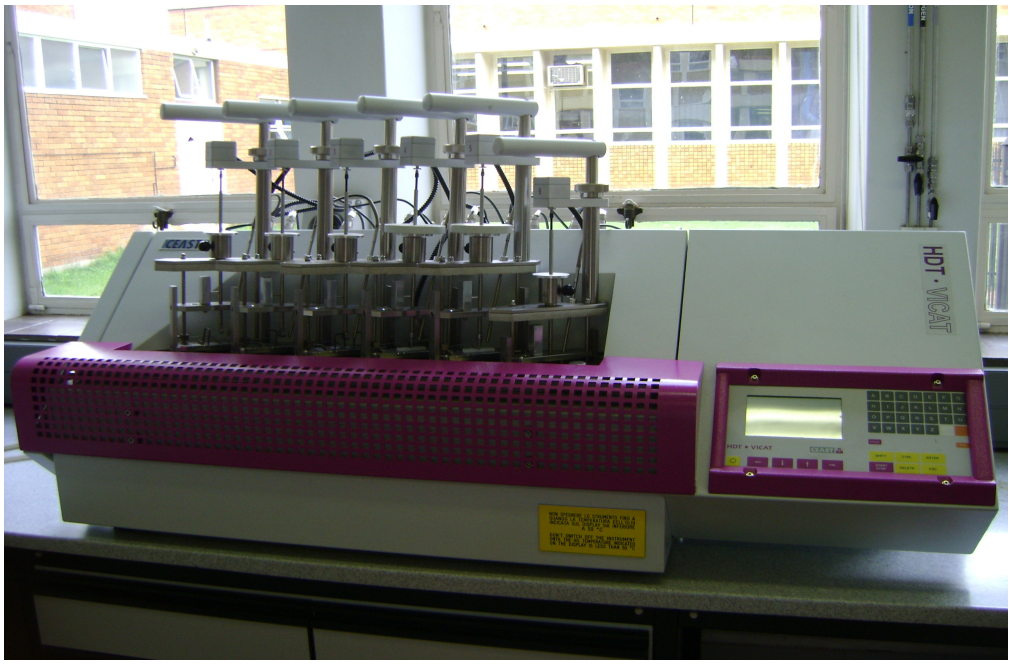

Figure 3.16 The Ceast P/N 6921.000 model HDT6/VICAT system

The rectangular samples for the LLDPE/POSS composites were prepared at 180 °C (cylinder temperature), an injection pressure of 400 bar and a mould temperature of 60 °C using the ThermoHaake Minijet II injection moulding machine (ASTM D-638) shown in Figure 3.13. Samples of thickness = 10.00 mm, width = 4.0 mm and length = 80 mm were used. At least five measurements were performed for each sample and the results were averaged to obtain a mean value.

3.3.12 Rheometry

Rheology is defined as the science of deformation and flow of materials such as polymers and composites. It is a branch of physics and physical chemistry since the most important variables come from the field of mechanics. Rheological experiments reveal information about the flow behaviour of liquids and the deformation behaviour of solids. These experiments are done using a rheometer. There are two types of rheometers used in research nowadays, namely (1) rotational and (2) oscillatory rheometers. Liquids and solid materials can be investigated using both rheometers. Rotational tests are performed to characterize the viscous behaviour of materials, while creep and viscoelastic behaviour, as well as relaxation tests can be carried out using oscillatory tests [29].

Figure 3.17 Anton-Paar Physica MCR 501 rheometer

The Anton-Paar Physica MCR 501 rheometer (Figure 3.17) was used to investigate the rheological properties of all the samples in this study. It was equipped with 25 mm diameter parallel plates in an oscillatory shear mode. To preserve the structure of the sample, the gap between the two plates (1.1 mm) was adjusted while the sample was being melted at 150 °C for LLDPE and 180 °C for PMMA samples, so that no material was squeezed out between the plates. The following tests were carried out: (i) a strain amplitude sweep at a frequency of ω = 6.28 rad s^{-1}, for a strain, γ, ranging from 0.01 to 100 % and (ii) a frequency sweep at strains, γ = 1 and 5 % within an ω range from 0.01 to 100 rad s^{-1}. In the rheological tests during the melt-state, G' symbolizes the strain energy reversibly stored by the sample, while G'' represents the amount of energy irreversibly dissipated by the material to its surroundings.

3.3.13 Pendulum impact testing

An impactor is a technique designed to determine the mechanical and physical properties of polymers and their corresponding composites. The impactor is designed to perform three different configurations, e.g. Charpy, Izod and tensile impact properties of a sample according to international standards. The impact test involves a pendulum with a known weight at its arm swinging down and striking the notched sample clamped in a horizontal or vertical position. When the sample is horizontally clamped, the test is called the Charpy test. The Izod

test is performed when a sample is clamped in a vertical position. The Charpy test is regarded as a high speed fracture test in which a sample is laid horizontally on two supports against an anvil and the notched side of the sample is positioned away from the pendulum. The Izod tests involve the sample mounted in a vice fixture with the notch facing the pendulum.

The outputs of all these tests are expressed in terms of kinetic energy consumed by the pendulum in order to break the sample. The energy required to break a standard sample is actually the sum of different contributions such as the energy to deform the sample, to initiate the fracture, to propagate the fracture across sample and the energy spent in order to toss the broken ends of the sample. The energy lost through the friction and vibration of the apparatus is usually very small and it can be neglected. The impact strength (resilience) is the loss of momentum in the pendulum while breaking the sample off at the notch. Advantages of the Charpy test over the Izod test are (i) the sample does not have to be clamped and it is free of variations in clamping process, (ii) its easily applicability, (iii) short testing times, and (iv) low cost consumption materials during the test [30].

The CEAST Automatic Notchvis Plus and the Pendulum Resil Impactor II (Figure 3.18) were used to (a) prepare the notched samples and (b) measure the Charpy impact properties of the samples at room temperature.

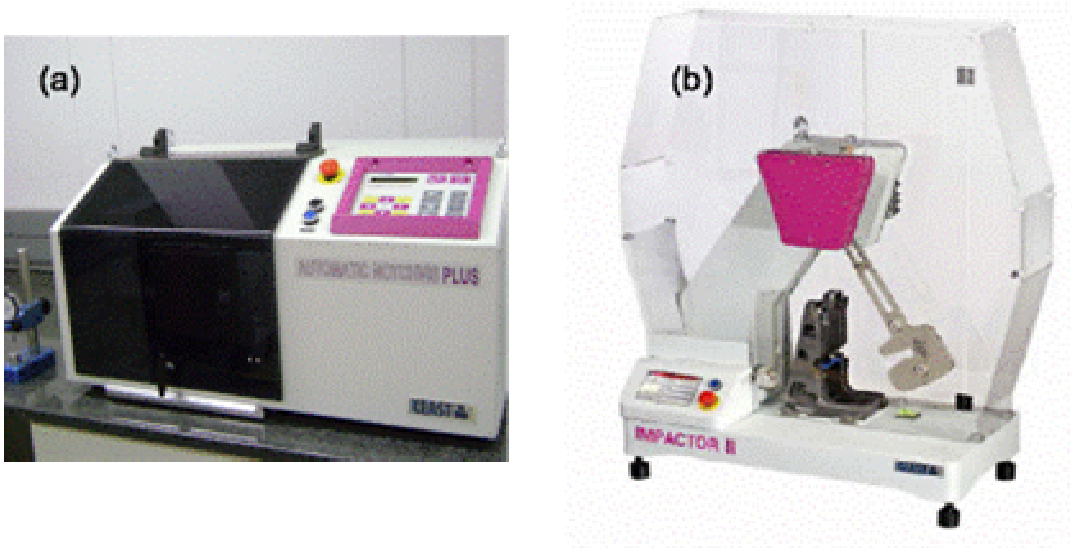

Figure 3.18 Configurations of Charpy edgewise impact sample with single notch

The dimensions and shape of the Charpy moulded rectangular-shaped (ISO 179) of the pendulum impact sample were as follows:

Length	80 mm
Height	10 mm
Breadth	4 mm
Notch root radius	0.125 mm
Span between supports	40 mm

3.4 References

1. H. Schnablegger, Y. Singh. A practical guide to SAXS: Getting acquitted with the principles. Anton Paar GmbH Publishers: Austria (2006).
2. B.K. Choi. Optical microscopy study on the crystallization of PEO-salt polymer electrolytes. Solid State Ionics 2004; 168:123-129.
3. C. Timothy, V.M. Kriss. History of the Operating Microscope: From magnifying glass to microneurosurgery. Neurosurgery 1998; 42:899-907.
4. M.S. Dhlamini. Luminiscent properties of synthesized PbS nanoparticles phosphors. Ph.D dissertation, University of the Free State, Republic of South Africa (2008).
5. Binghamton University: Nanotechnology for undergraduate education: http://nue.clt.binghamton.edu/semtem.html.
6. J. Holubová, Z. Černošek, E. Černošková. Kinetic analysis of nonisothermal DSC data. Journal of Thermal Analysis and Calorimetry 2000; 62:715-719.
7. J.A. Molefi. Investigation of phase change conducting materials prepared from polyethylenes, paraffin waxes and copper. PhD dissertation, University of the Free State, Republic of South Africa (2008).
8. G. Ehrenstein, G. Riedel, P. Trawiel. Thermal Analysis of Plastics. Carl Hanser: Munich (2004).
9. A. Galíková, J. Pola. Highly sensitive TGA, diagnosis of thermal behaviour of laser-deposited materials. Thermochimica Acta 2008; 473:54-60.
10. T.A. Manley. Thermal analysis of polymers. Pure and Applied Chemistry 1989; 61:1353-1360.
11. R. Dominick, R. Marlene, R. Donald. Injection Moulding Handbook, 3rd Ed. Kluwer Academic Publishers: Massachusetts (2000).
12. T.M. Malik, M.I. Faroogi, C. Vachet. Mechanical and rheological properties of reinforced polyethylene. Polymer Composites 1992; 13:174-178.

13. M.A. Osman, A. Atallah, M. Muller, U.W. Suter. Reinforcement of poly(dimethylsiloxane) networks by mica flakes. Polymer 2001; 42:6545-6556.
14. H.M. Smallwood. Limiting law of the reinforcement of rubber. Journal of Applied Physics 1944; 15:758-764.
15. E. Guth. Theory of filler reinforcement. Journal of Applied Physics 1945; 16:20-27.
16. E.H. Kerner. The elastic and thermo-elastic properties of composite media. Proceedings of the Physical Society 1956; B69:808-813.
17. Z. Hashin, S. Shtrikman. A variational approach to the theory of the elastic behaviour of multiphase materials. Journal of the Mechanics of Physics and Solids 1963; 11:127-140.
18. J.C. Halpin. Stiffness and expansion estimates for oriented short fibre composites. Journal of Composite Materials 1969; 3:732-734.
19. M. Doi, S. Edwards. The Dynamics of Polymer Chains, Oxford University Press: New York (1986).
20. J.M.G. Cowie. Polymers: Chemistry and Physics of Modern Materials, Intertext Books: Aylesbury, United Kingdom (1973).
21. T. Murayama. Dynamic Mechanical Analysis of Polymeric Materials, Elsevier: New York (1977).
22. R.H. Boyd. Relaxation processes in crystalline polymers: Molecular interpretation- A review. Polymer 1985; 26:1123-1133.
23. K.P. Menard. Dynamic Mechanical Analysis: A Practical Introduction, 2nd Ed. CRC Press: Boca Raton, New York (2008).
24. C.A. Mahieux, K.L. Reifsnider. Property modeling across transition temperatures in polymers: Application to filled and unfilled polybutadiene. Journal of Elastomers and Plastics 2002; 34:79-89.
25. A.C. Quental, M.I Felisberti. Phase behavior of the blends of linear low density polyethylene and poly(ethane-propene-1-butene). European Polymer Journal 2005; 41:894-902.
26. A.C.Y. Wong. Heat deflection characteristics of polypropylene and polypropylene/ polyethylene binary systems. Composites: Part B 2003; 34:199-208.
27. D. Jarus, A. Scheibelhoffer, A. Hiltner, E. Baer. The effect of skin-core morphology on the heat deflection temperature of polypropylene. Journal of Applied Polymer Science 1996; 60:209-219.

28. M. Saha, D. Basu, A.N. Banerjee. Heat distortion temperature of unidirectional polyethylene glass fiber PMMA hybrid composite laminates. Journal of Applied Polymer Science 1999; 71:541-545.
29. T.G. Mezger. The Rheology Handbook, 2nd Ed. Hannoprint: Germany (2006).
30. Materials Testing Solutions. Charpy and Izod pendulum impact test (Instron): http://www.instron.co.uk/wa/products/impact/charpy_izod.aspx.

CHAPTER 4

MORPHOLOGY, THERMAL AND THERMOMECHANICAL PROPERTIES OF POLYETHYLENE FILLED POSS NANOCOMPOSITES

4.1 Introduction

Polyethylene (PE) is one of the polymers produced in large quantities in the world compared to other polymers. PE is produced in different forms, each of which possesses different valuable properties such as low cost, ability to be recycled, good processability, non-toxicity and bio-compatibility. These properties give polyethylene the strongest platform to be used in different engineering applications including vehicles, sporting goods, etc. However, because of its apolar chemical nature, its low temperature toughness and stiffness, it is not suitable for some industrial applications [1]. In this chapter different properties of LLDPE, prior to and after nanocomposites formation with POSS macromonomers, are discussed.

4.2 Results and discussion

4.2.1 Scanning electron microscopy (SEM)

The morphological characteristics of the freeze-fractured surfaces of LLDPE and three different nanocomposite systems were investigated by field-emission SEM (FE-SEM). Parts (a) – (d) of Figure 4.1 show the fractured surfaces of the PE nanocomposites containing (a) 0 wt %, (b) 5 wt %, (c) 7.5 wt %, and (d) 10 wt % POSS loadings. It can be seen that the compatibility between the POSS and the LLDPE matrix is very low, leading to the formation of micro-aggregates for all the compositions. The homogeneous dispersion of phase-separated POSS particles can be seen in Figure 4.1(b). The phase-separated morphology becomes more pronounced with increasing the loadings of POSS in the polymer matrix. At the higher POSS loading of 10 wt % many small crystallites as well as micron-sized POSS agglomerates are observed (Figure 4.1(d)). In all the images there seem to be a large degree of debonding, which is shown by some voids in the interface between the POSS aggregates and the polymer

matrix. These voids are clearly observed at the higher POSS loadings (7.5 and 10 wt %), suggesting a weak interfacial interaction between the POSS particles and the LLDPE matrix.

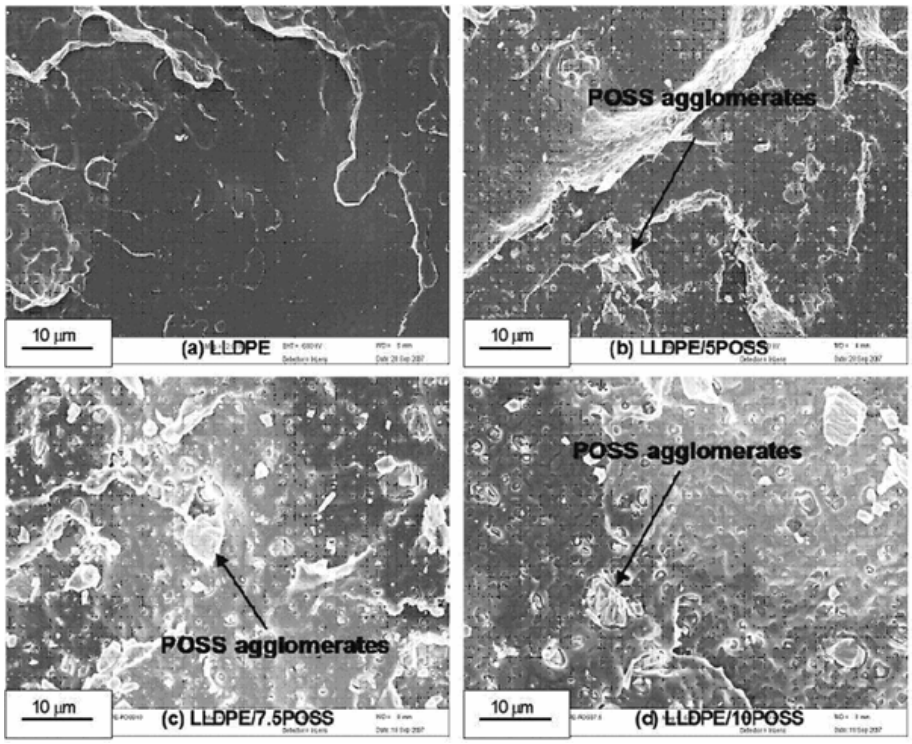

Figure 4.1 FE-SEM images of freeze-fractured surfaces of neat LLDPE and various nanocomposite samples

4.2.2 Polarized optical microscopy (POM)

To further elucidate the degree of dispersion of the POSS particles in the LLDPE matrix, POM studies were carried out at 150 °C. Before taking the POM photographs, the samples were held at the same temperature for 6 min. Figure 4.2 shows the POM images of the neat LLDPE matrix and the different nanocomposite systems at 150 °C. It is clear from the images that the POSS particles forming micro-aggregates are homogeneously dispersed in the LLDPE matrix. Furthermore, the degree of formation of micro-aggregates systematically increases with increasing the loading of POSS into the initial feed. However, it is very difficult to reach a conclusion on the extent of agglomeration.

POM studies during nonisothermal crystallization conditions were also carried out to determine the effect of the POSS particles on the crystal growth behaviour of the LLDPE

matrix. To perform these studies, a thin sample, sandwiched between two covering glasses, was placed inside the hot-stage mounted onto the optical microscope. The temperature was first raised to 150 °C at a heating rate of 30 °C.min^{-1}, and kept constant for 12 min to ensure complete melting of the samples. The samples were then cooled to 80 °C at a cooling rate of 10 °C.min^{-1}.

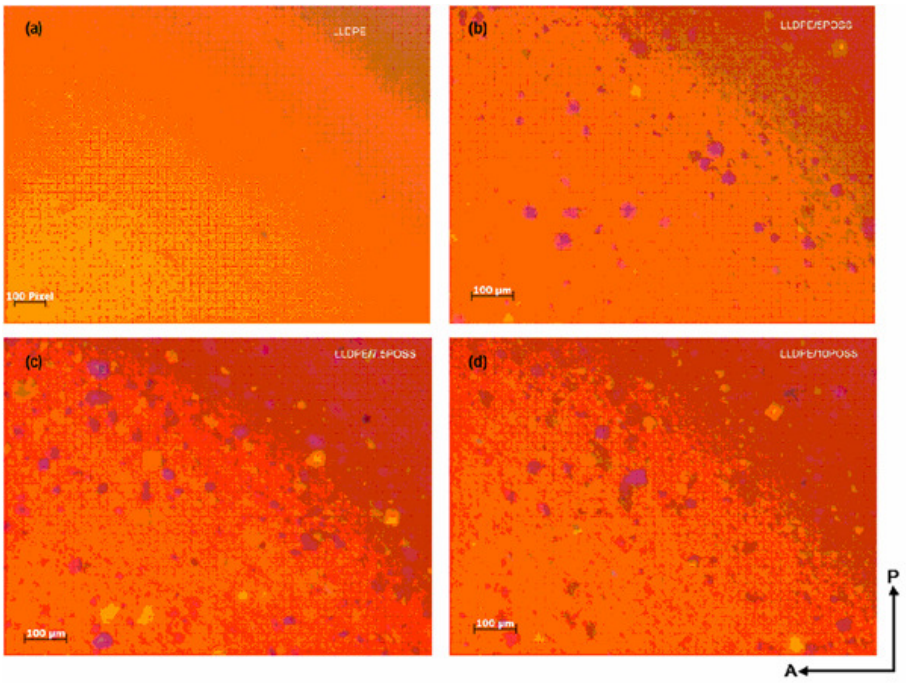

Figure 4.2 Optical microscopy images of (a) neat LLDPE, (b) LLDPE/5POSS, (c) LLDPE/7.5POSS and (d) LLDPE/10POSS nanocomposite samples at 150 °C

Figure 4.3 shows the POM images of neat LLDPE and three different nanocomposite samples taken during the nonisothermal crystallization process. It is clear from the POM image of the neat LLDPE (Figure 4.3(a)) that the spherulites are fairly large and perfectly grown. In the case of the nanocomposite samples, the sizes of the spherulites are very little affected by the different loadings of the POSS particles (Figures 4.3 (b)-(d)). This is more pronounced in the high-magnification POM images (100x) of the neat LLDPE and the nanocomposite samples presented in Figure 4.4. This suggests that the nucleating role of the dispersed POSS phase is not that active during the crystallization of the LLDPE matrix from the melt.

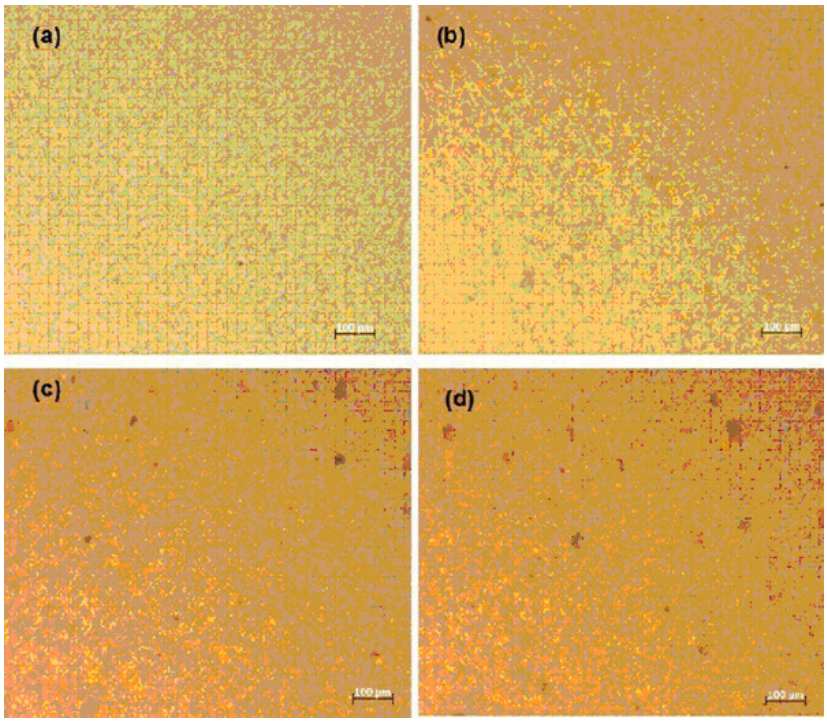

Figure 4.3 POM images of (a) neat LLDPE, (b) LLDPE/5POSS, (c) LLDPE/7.5POSS and (d) LLDPE/10POSS nanocomposites taken at 80 °C during nonisothermal crystallization

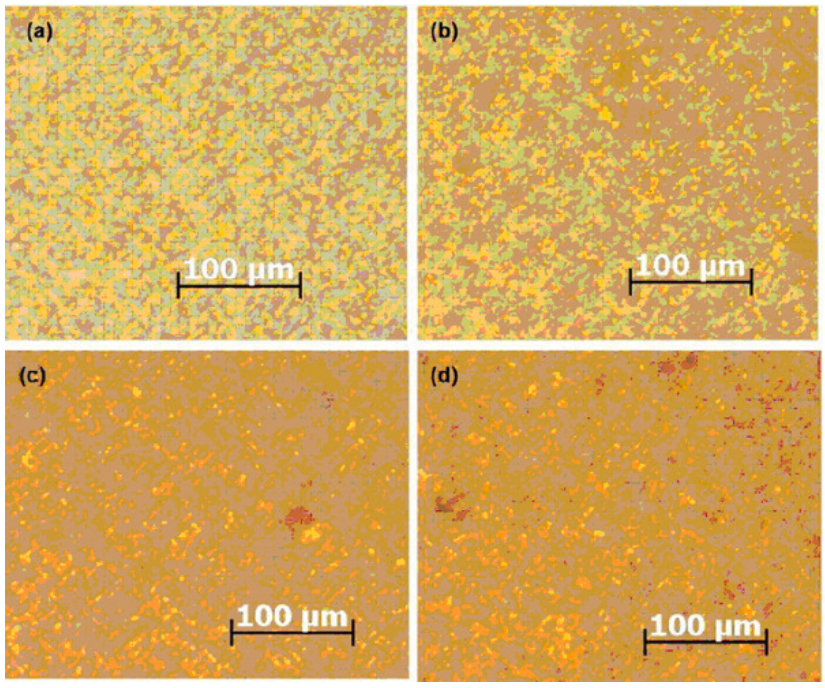

Figure 4.4 High magnification POM images (100x) of (a) neat LLDPE, (b) LLDPE/5POSS, (c) LLDPE/7.5 POSS and (d) LLDPE/10POSS nanocomposites

4.2.3 Differential scanning calorimetry (DSC)

4.2.3.1 Melting behaviour of compression moulded samples

The typical melting behaviour of neat LLDPE and the different nanocomposite samples are presented in Figure 4.5 and the results are summarized in Table 4.1. The DSC curves exhibit two distinct melting peaks of LLDPE labelled 'I' and 'II' from low to high temperatures. These multiple melting peaks indicate the presence of two different populations of crystalline lamella [2]. The temperature positions of the 'I' and 'II' melting peaks of the neat LLDPE are 110.8 °C and 121.4 °C. Addition of POSS particles into LLDPE did not change these peak temperatures. At the highest POSS loading (10 wt %), the second melting peak temperature (T_{mII}) shifts to a lower temperature by only 0.8° compared to that of the pure LLDPE. This observation indicates that the crystalline lamellar thickness of the LLDPE matrix remains almost the same in the presence of POSS. However, the total heat of fusion (ΔH_m) of the two melting peaks of LLDPE, estimated by the integration of the area under these peaks, decreases with the addition of POSS (see Table 4.1). This behaviour indicates that the degree of crystallinity decreases by the incorporation of the inorganic phase into the polymer matrix. This is due to the high level of dispersion of POSS particles in the LLDPE matrix as revealed by the POM and FE-SEM images, which consequently acts as obstacles for the mobility and flexibility of the polymer chains to fold and join the crystallization growth front.

Several authors reported on the multiple melting behaviour of various semi-crystalline thermoplastic polymers such as PET [3-7], poly(butylene terephthalate) (PBT) [8-11], PE [12], semi-crystalline polyimides (PI) [13], poly(ether ether ketone) (PEEK) [14,15], poly(butylene succinate) (PBS) [2], and poly[(butylene succinate)-co-adipate] (PBSA) [2,15]. There are a number of models to explain this behaviour of polymers. The two most important ones are: (a) the presence of melting, re-crystallization, and re-melting phenomena [17-19], and (b) the crystal structure modification during the heating scan. According to the first model, the first step is melting and re-crystallization of the low-melting crystallites with lower thermal stability, followed by the melting of the crystallites with higher thermal stability along with the modified crystals formed through re-crystallization. The discussion below will consider the applicability of the above two models in addressing the double-melting behaviour of LLDPE in the light of the available experimental evidence.

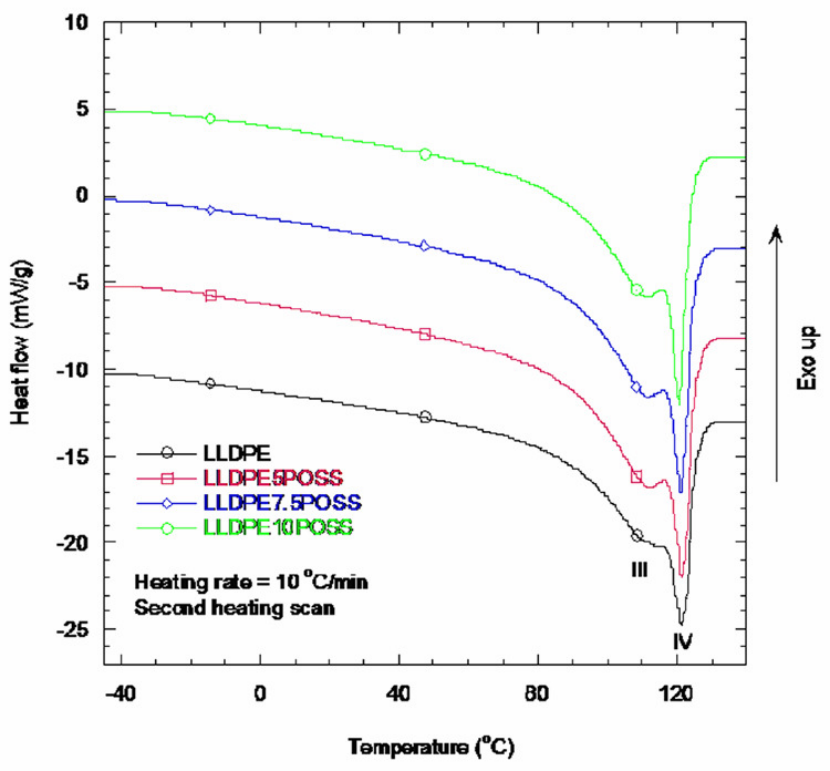

Figure 4.5 **Melting behaviour of neat LLDPE and nanocomposite samples**

Table 4.1 **Reported data are taken from the second scan to ascertain reproducible thermograms free of prior thermal history**

Sample	Area under characteristic LLDPE peaks, calculated from WAXS patterns	T_{mI} (°C)	T_{mII} (°C)	ΔH_m ($J.g^{-1}$)	T_c (°C)	ΔH_c ($J.g^{-1}$)
LLDPE	18.5 ± 0.11	110.8	121.4	123.8	107.1	83.6
LLDPE/5POSS	17.5 ± 0.13	110.8	121.6	122.3	108.8	81.2
LLDPE/7.5POSS	16.8 ± 0.16	110.8	121.1	120.5	108.7	80.6
LLDPE/10POSS	16.1 ± 0.10	110.8	120.6	110.6	109.1	74.1

T_{mI}, T_{mII}, ΔH_m, and ΔH_c are the first melting temperature, second melting temperature, heat of melting of the two melting peaks of LLDPE and heat of crystallization, respectively

To verify the first model, *i.e.* the presence of melting, re-crystallization, and re-melting phenomena, Figure 4.6 depicts the pure LLDPE and the LLDPE/5POSS nanocomposite samples heated at different heating rates of 1, 2, 5, 10, 15 and 20 °C.min^{-1}. It can be seen in Figure 4.6(a) that with increasing heating rate, the endotherm 'II' of the pure LLDPE (see Figure 4.5) developed into two endothermic peaks designated as 'III' and 'IV'. These endothermic peaks appear at 117.4 and 120.8 °C. It is clear that 'IV' corresponds with 'II' and shifts towards lower temperatures while its intensity decreases, whereas the endotherms 'II' and 'III' became more prominent and remained in the same positions. There is also a development of another endotherm 'I' in the low-temperature region with increasing heating rate. Another interesting observation is that the re-crystallization phenomenon between endotherms 'III' and 'IV' became less pronounced with increasing heating rate, but was still visible. At a very slow heating rate, the sample passes through the re-crystallization process very slowly, and there is more than enough time for the molten sample to reorganise into new crystals. The endotherms 'III' and 'IV' are therefore well resolved at a slow heating rate (5 °C.min^{-1}). However, at higher heating rates (more than 5 °C min^{-1}), the sample passes through the re-crystallization region so rapidly that there is not enough time for the molten sample to reorganise into new crystals. Therefore, the reorganisation process is largely inhibited as the heating rate increases which consequently decreases the fraction of perfect crystals and finally contributes to the decrease in the peak temperature of endotherm 'IV'. These observations indicate the presence of melting, re-crystallization, and re-melting phenomena that are partly responsible for the multiple melting behaviour of LLDPE.

The LLDPE/5POSS sample also shows the same type of melting behaviour. However, all the melting endotherms are less intense and slightly moved towards lower temperatures (at low heating rates). This may be due to a decrease in the overall crystallinity of the LLDPE in the presence of the POSS particles as observed in the previous paragraphs.

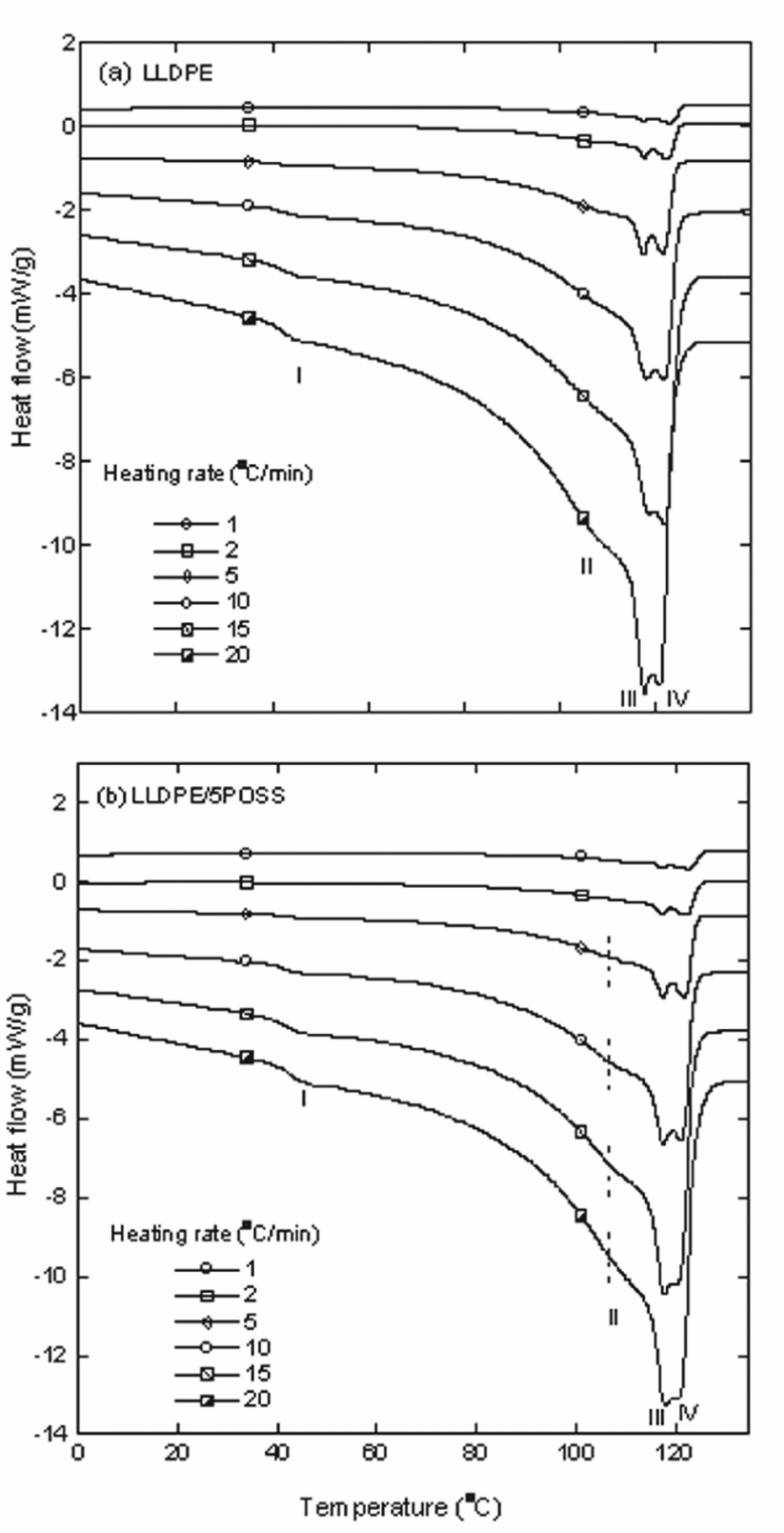

Figure 4.6 Heating rate dependence of DSC thermograms of compression moulded samples. All samples had identical LLDPE content

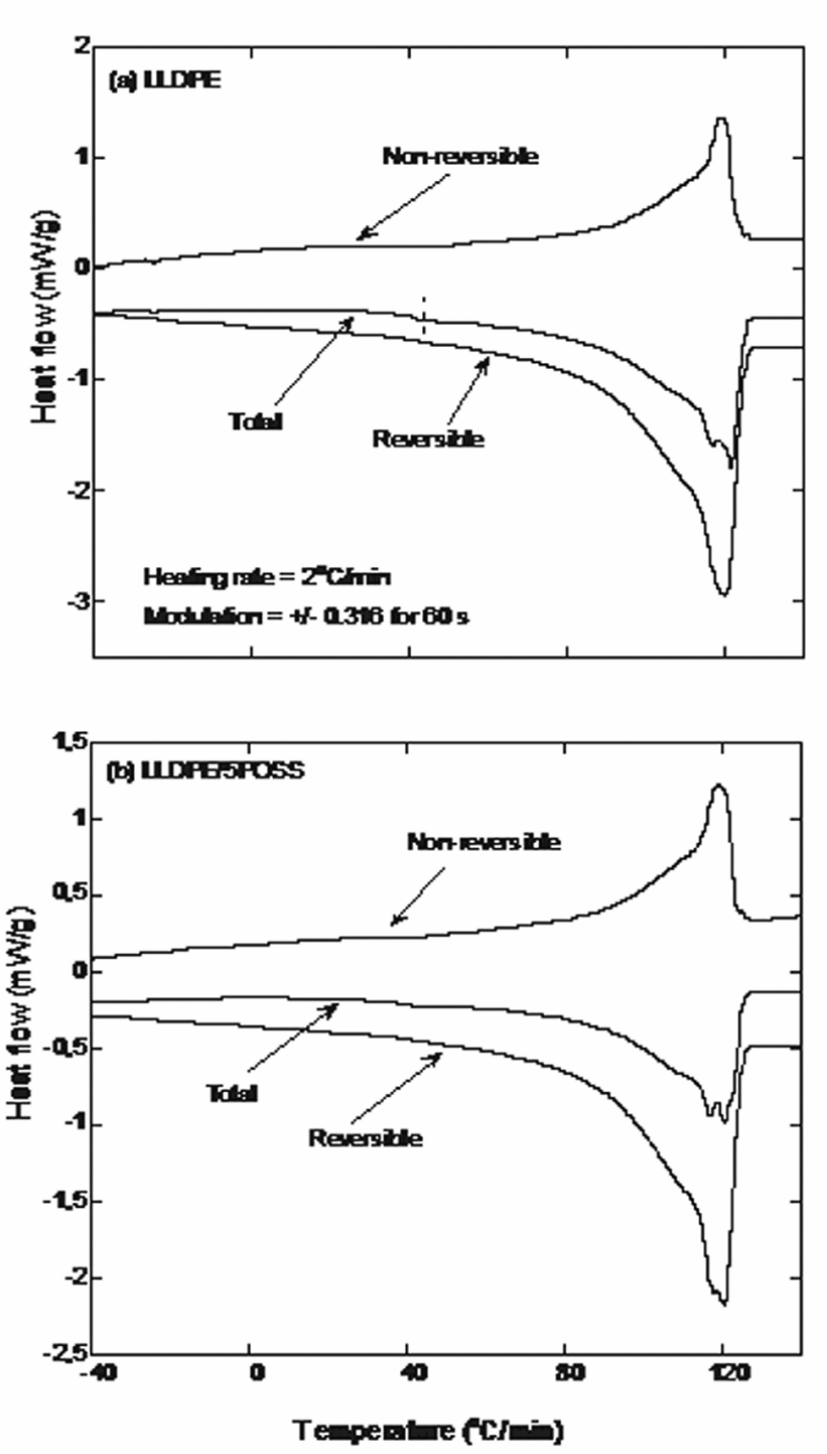

Figure 4.7 Heat only MDSC of compression moulded LLDPE and LLDPE/5POSS samples. Heating rate of 2 °C.min^{-1}, an amplitude of ± 0.318 °C and a period of 60 s. All samples had identical LLDPE content

To further support the melting, re-crystallization and re-melting phenomena of LLDPE, modulated DSC (MDSC) analyses were performed. MDSC generally applies a sinusoidal

temperature oscillation (modulation) on the heating in a conventional DSC and separates the total heat flow (as obtained from the conventional DSC) into heat-capacity-related (reversible) and kinetic (non-reversible) components. Therefore, MDSC allows one to see that some re-crystallization occurs as soon as the LLDPE begins to melt. Figure 4.7 shows the MDSC curves of the neat LLDPE and LLDPE/5POSS nanocomposite samples obtained at a heating rate of 2 °C min^{-1}. For both samples, the total heat flow (middle curve) is separated into well-defined reversible heat flow (bottom) and non-reversible heat-flow (top) curves.

For the neat LLDPE sample, the following behaviour was observed. Firstly, the lower melting endotherm in the non-reversible signal curve begins at the same temperature as the melting endotherm observed in the total heat-flow curve. Secondly, the small peak shoulder, corresponding to the endotherm 'II' in Figure 4.6, appears in the reversible curve. Finally, a well-distinguished re-crystallization signal is only observable in the non-reversible curve. A sharp melting peak is also observed in the reversible curve. This observation supports the conclusion that re-crystallization operates simultaneously with the high-temperature melting.

The MDSC curves of the LLDPE/5POSS nanocomposite also show the same type of behaviour, but the main endo- and exotherms are less intense. The melting peak shoulder, corresponding to the endotherm II (see the dashed line in Figure 4.7), is more prominent for the LLDPE sample. This behaviour suggests the presence of a high concentration of crystallites in the LLDPE sample, which is responsible for the endotherm II. A very weak re-crystallization phenomenon is observed in the reversible curve of the nanocomposite. This observation may be due to the continuous partial melting and perfection of a higher fraction of crystals responsible for the melting endotherm II before their final melt.

On the basis of the above observations, for both neat LLDPE and nanocomposite samples, it can be confirmed that the multiple melting behaviour of LLDPE originates from the melting and re-crystallization of the lower melting crystallites with a lower thermal stability. The melting of the crystallites with a higher thermal stability, along with the modified crystals formed through the re-crystallization, then occurs.

4.2.3.2 Nonisothermal crystallization behaviour

The crystallization exotherms of neat LLDPE and the three different nanocomposite samples during nonisothermal crystallization from their melt at the same cooling rate are presented in Figure 4.8. The characteristic parameters of the nonisothermal crystallization exotherms of all the samples are summarised in Table 4.1.

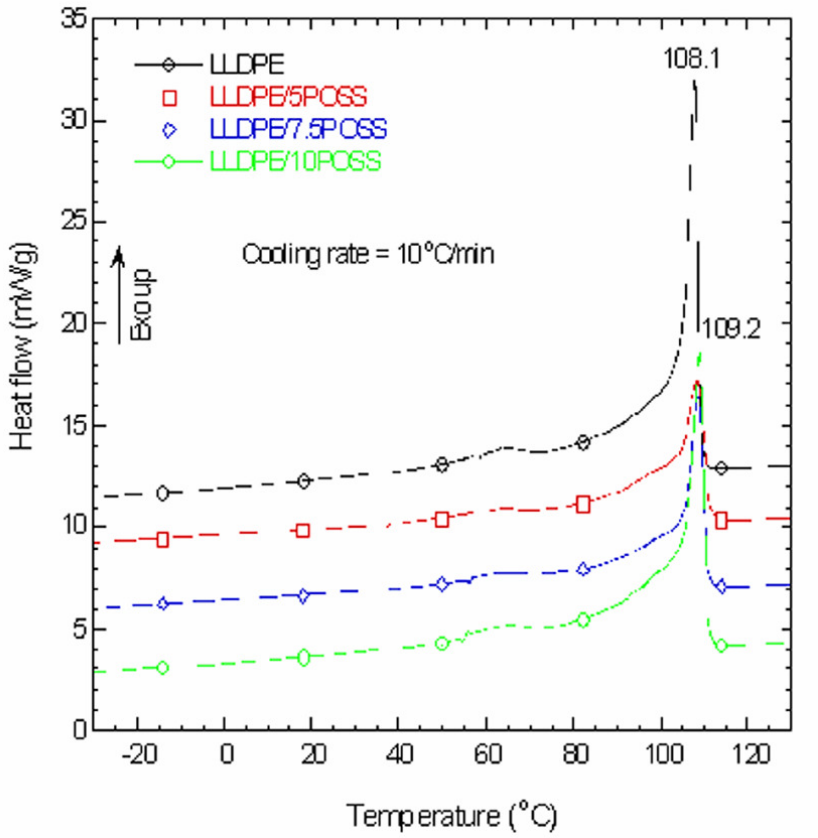

Figure 4.8 Nonisothermal crystallization behaviour of neat LLDPE and various nanocomposite samples

It can be seen that the crystallization peak temperature (T_c) of the neat LLDPE slightly moves towards a higher temperature region. In the case of the LLDPE/10POSS nanocomposite system, this peak appears at 109 °C. A very small increase in the crystallization peak temperature of the nanocomposite sample compared to the neat LLDPE sample implies that the POSS particles do not really nucleate the crystallization of the LLDPE matrix, and that the POSS loading does not play any role. This may be due to either the poor compatibility between the LLDPE matrix and the POSS particles (see Figure 4.1), or the smaller available surface area of the spherical structure of the POSS particles, as well as the observed

agglomeration, that will less effectively initiate the crystallization process as nucleation centres. This conclusion also confirms the POM studies obtained at a particular crystallization temperature. However, the total heat of crystallization (ΔH_c), estimated by integration of the area under the exothermic peak in the DSC curves, decreases with the addition of the POSS particles (Table 4.1). This result indicates that the POSS particles influence the crystallization behaviour of LLDPE. There are different factors that can determine the influence of an inorganic phase on the crystallization behaviour of PE [20]. These include the sizes and size distribution of the filler particles, the dispersion of the particles in the polymer matrix, the effective surface areas of the particles, the extent of interaction between the matrix and the filler particles and the crystallinities and crystallization mechanisms of the respective polymers. Depending on these factors, the filler particles will immobilize the polymer chains (reduce crystallinity) and/or act as nucleating agents (increase crystallinity). We can therefore attribute this behaviour to the high level of dispersion of POSS particles in the LLDPE matrix.

4.2.4 Wide angle x-ray scattering (WAXS)

The microstructure of LLDPE before and after nanocomposite formation was studied by WAXS with a scattering angle (2θ) varying from 2 to 40°. The normalized WAXS patterns of pure POSS powder, neat LLDPE and various nanocomposite compression-moulded films are presented in Figure 4.9 (sample thickness was ≈ 0.4 mm). The WAXS pattern of pure POSS macromonomer powder with eight methyl groups attached to a main silicon skeleton is presented in Figure 4.9(a). It is clear from the figure that the POSS macromonomer shows a number of strong peaks that indicate a highly crystalline structure. Figure 4.9(b) depicts the WAXS pattern of neat LLDPE which exhibits two sharp characteristic peaks at 21.3° and 23.7°. These two observable peaks are assigned to the 110 and 200 reflections of the Bunn orthorhombic subcell [21]. Similar crystalline peaks have earlier been reported by Rizzo *et al*. [22] and Heinemann *et al*. [23] for PE. Another broad background scattering is observed for the WAXS pattern of neat LLDPE. This behaviour suggests the presence of an amorphous structure in the polymer. It is interesting to note that the intensity of the characteristic peaks of the LLDPE crystalline structure decreases with increasing the POSS loading in the LLDPE resin. The decrease was more pronounced when 5 wt % POSS particles were used. The positions of the two peaks remained unchanged after nanocomposite formation, indicating that the crystal lattice of the LLDPE did not expand in the presence of the POSS particles.

The area calculated under the crystallization peaks from the WAXS patterns (rough estimation within the range of 2θ =10-28°) decreases systematically with increasing POSS particle loadings. This observation is in good agreement with the DSC observations (Table 4.1).

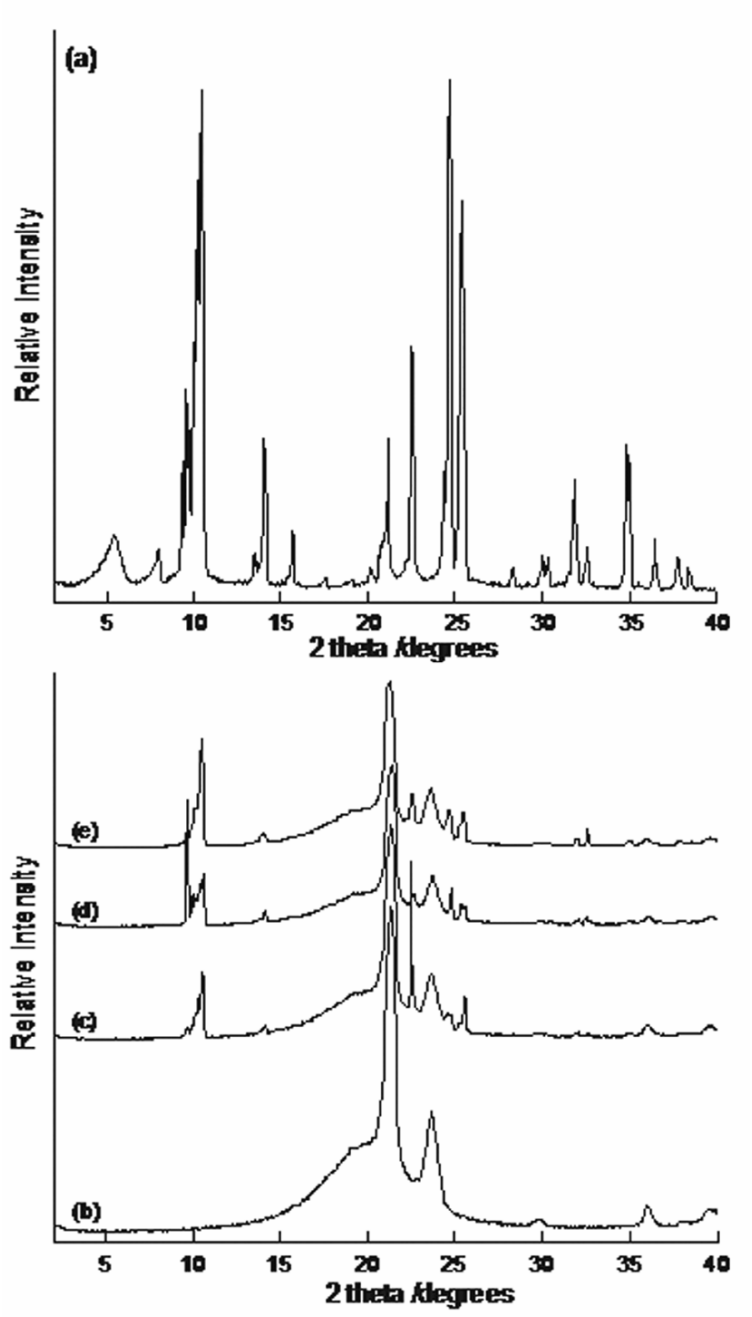

Figure 4.9 Wide angle x-ray scattering patterns of (a) pure octamethyl-T_8-POSS, (b) neat LLDPE, LLDPE/5POSS, LLDPE/7.5POSS and (d) LLDPE/10POSS nanocomposite samples

The average crystallite size, $D_{(hkl)}$, for the broadening of diffractions was determined using Equation 4.1. Table 4.2 shows the values of $D_{(hkl)}$ calculated from the characteristic dominant scattering peak of POSS at $2\theta = 10.4°$, which corresponds to the 011 reflection.

$$D_{(hkl)} = \frac{K}{\cos} \tag{4.1}$$

where β is the half-width of the diffraction peak in radians, K is equal to 0.94, θ is the Bragg angle, and λ is the wavelength of the x-rays. It can be seen that crystals from the dispersed POSS in the nanocomposites are smaller than the pure POSS crystals. This suggests that the dispersed POSS crystals are not as perfect as the pure POSS crystals. However, the value of β increases with increasing the loading of POSS particles into the LLDPE matrix, indicating that the crystalline perfection decreases after nanocomposites formation with POSS particles.

Table 4.2 Estimation of crystallite sizes of POSS nanocrystals in LLDPE/POSS nanocomposites obtained from WAXS data

Sample	hkl	2θ	β (degree)	β (rad)	cos θ	D_{hkl} (nm)
POSS	011	10.47	0.1664	0.002904	0.9960	50.05
LLDPE/5POSS	011	10.51	0.1907	0.003328	0.9960	43.70
LLDPE/7.5POSS	011	10.54	0.1985	0.003465	0.9960	42.00
LLDPE/10POSS	011	10.46	0.2957	0.005161	0.9960	28.20

Since the crystallinity of the pure LLDPE matrix is affected by the incorporation of POSS, one can assume that the POSS particles are mostly dispersed in the LLDPE crystalline phase [21,22]. From Figure 4.9(a) it is clear that the POSS is highly crystalline and have a characteristic dominant scattering peak at $2\theta = 10.4°$. In Figures 4.9 (c) – (e) this dominant characteristic peak appears for all the nanocomposites. This suggests that the POSS exists as separate crystals or that the POSS particles are able to crystallize when they are dispersed in the polymer matrix. However, there is a sudden increase in the peak intensity for both 7.5 and 10 wt % POSS incorporation in the LLDPE matrix, which may be due to the POSS particles starting to agglomerate and crystallize more easily at higher concentrations. The increasing intensity clearly shows the progressive development of a different ordered POSS lattice. This conclusion supports the POM and FE-SEM results discussed in the previous paragraphs.

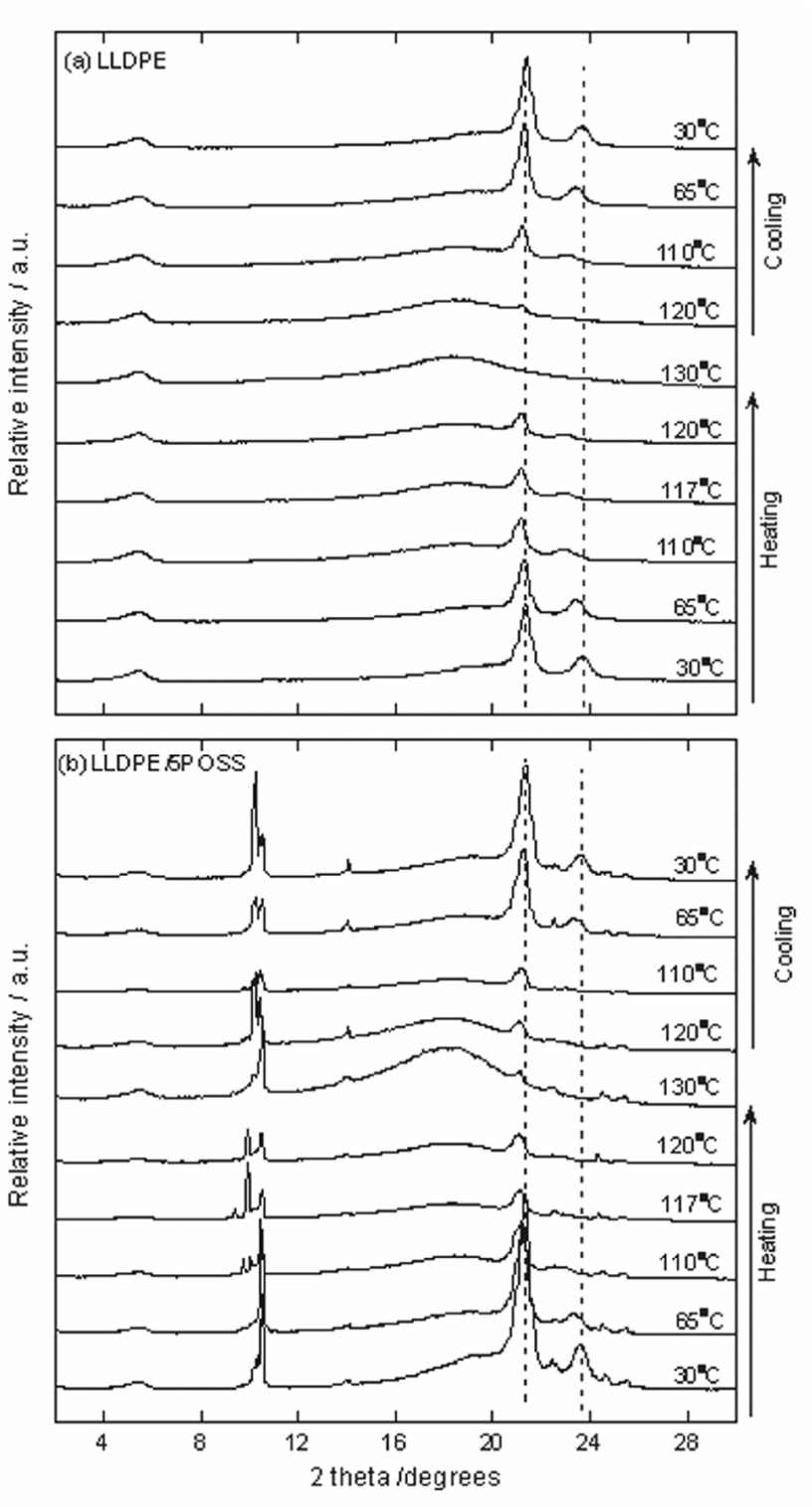

Figure 4.10 Temperature dependence of WAXS patterns of (a) neat LLDPE and (b) LLDPE/5POSS nanocomposites. The samples were kept at each temperature for 5 min, including 1 min exposure time

To identify the different crystal structure modifications, i.e. phase changes, during the heating scan that may have been responsible for the multiple melting endotherms of the LLDPE, WAXS studies were performed on neat LLDPE and LLDPE/5POSS samples that were both crystallised for 5 min above and below the temperature of each DSC endothermic peak. Figure 4.10 shows the WAXS patterns of the compression moulded LLDPE and LLDPE/5POSS samples crystallised at different temperatures of 30, 65, 110, 117, 120, 130, 120, 110, 65 and 30 °C (sample thickness was ≈ 0.4 mm). The WAXS patterns of both samples show that the intensity of the main characteristic peaks of the LLDPE matrix decreases during heating and increases during cooling. This observation is ascribed to the melting and re-formation of crystals from the melt.

On the other hand, the characteristic peak positions of the LLDPE crystals move slightly towards lower 2θ angles during the heating scans, and move in opposite direction during the cooling process from the melt. It is also interesting to note that for both samples, the peak positions remain unchanged for a particular temperature. This slight shift in the scattering 2θ angle may be due to the thermal expansion of the crystallites and not to the formation of new types of crystals. Therefore, on the basis of the WAXS patterns, it is contended that the presence of multiple melting endotherms is the result of the presence of melting, re-crystallization, and re-melting phenomena as well as to the presence of two different populations of crystals, and not because of the formation of different crystal structures during the heating or cooling process.

Figure 4.11 shows the 2-D small and wide angle x-ray scattering (SWAXS) temperature dependence of the crystal growth behaviour of the neat LLDPE and the LLDPE/5POSS nanocomposite obtained at four different temperatures during nonisothermal crystallization studies. The 2-D SWAXS images show that both samples are highly crystalline at room temperature and maintain their spherulitic structure up to 65 °C, probably because the spherical POSS particles have a preferential orientation (i.e. anisotropic structure) and this orientation is also maintained in nanocomposite. At 130 °C the LLDPE is molten and all crystallinity is lost. When POSS is present in the LLDPE matrix, there is still some crystallinity visible at 130 °C, which is probably the result of the crystallinity and orientation of the POSS particles in the molten LLDPE matrix.

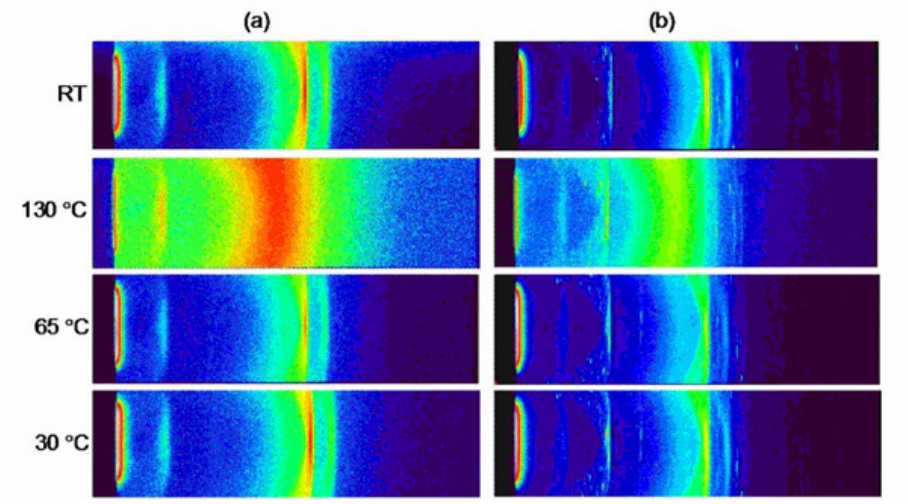

Figure 4.11 2-D small and wide angle x-ray scattering (SWAXS) patterns of (a) neat LLDPE and (b) LLDPE/5POSS nanocomposite samples obtained at four different temperatures. The samples were kept at each temperature for 5 min including 1 min exposure time.

4.2.5 Thermal stability

Figure 4.12 presents the typical TGA curves of the POSS powder, the neat LLDPE and the three different nanocomposite samples measured under an air atmosphere. It is clear that the thermal stability of pure POSS is much lower than that of the neat LLDPE matrix. The temperatures at 5% weight ($T_{0.05}$) loss are 345.1, 301.6, 315.4, and 302.6°C for LLDPE, LLDPE/5POSS, LLDPE/7.5POSS, and LLDPE/10POSS, respectively. This behaviour is due to the lower thermal stability of the POSS particles. However, the LLDPE/7.5POSS nanocomposite shows a higher value of $T_{0.05}$. This behaviour is difficult to explain at this point in time because one would expect a lower thermal stability due to the lower thermal stability of the POSS. In the temperature range of 390-500 °C, the thermal stability of nanocomposites systematically increases with POSS loading. This increase in the thermal stability may be attributed to the dispersion of the POSS particles in the LLDPE matrix, which actually decelerates the degradation of polymer chains *via* char formation.

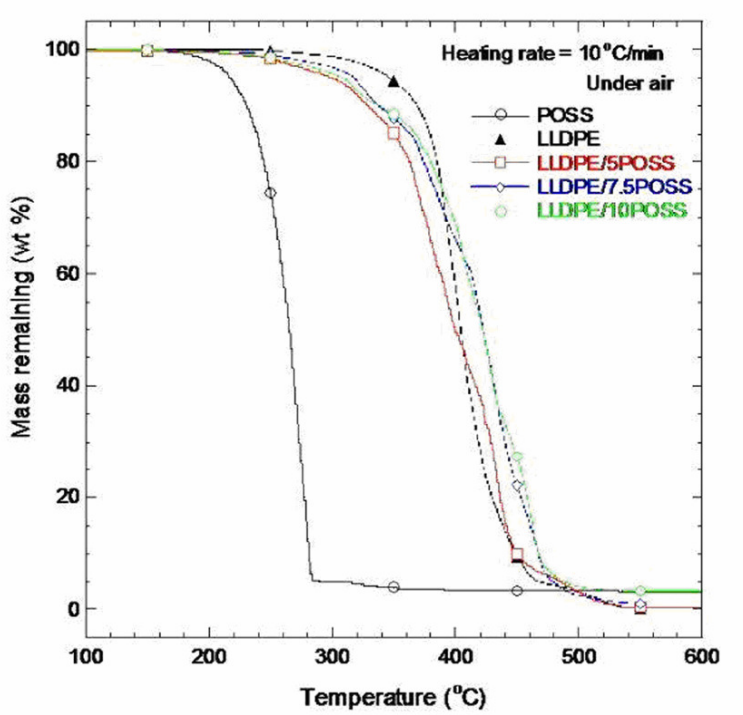

Figure 4.12 TGA curves of neat POSS, neat LLDPE and various nanocomposite samples obtained in an air atmosphere

Figure 4.13 depicts the TGA curves of the pure POSS powder, the neat LLDPE and the three different nanocomposite systems investigated in nitrogen atmosphere. It can be seen that all the composite samples exhibit two degradation steps. Similar behaviour was reported by Fina *et al*. [25] when 10 wt % octamethyl-POSS was incorporated into a PP matrix. A probable reason for this behaviour is due to the maximum volatilization rate of octamethyl-POSS around 270 °C. However, no significant change in the thermal stability of the composites was observed after addition of different POSS loadings in the LLDPE matrix. Similar behaviour was reported when metal functionalized POSS molecules were incorporated into a PP matrix when measured under an inert atmosphere [26]. However, in this study, no definite explanations were given. Since the neat octamethyl-POSS does not undergo any oxidation process, the lower volatilization temperature observed in air still occurs in nitrogen atmosphere at the same temperature. Therefore, when LLDPE starts degrading, a negligible amount of octamethyl-POSS is still present in the composite, and its evaporation is not yet completed. Based on this argument, we can assume that octamethyl-T_8-POSS protects LLDPE by forming a surface layer preventing oxygen diffusion within the polymer matrix.

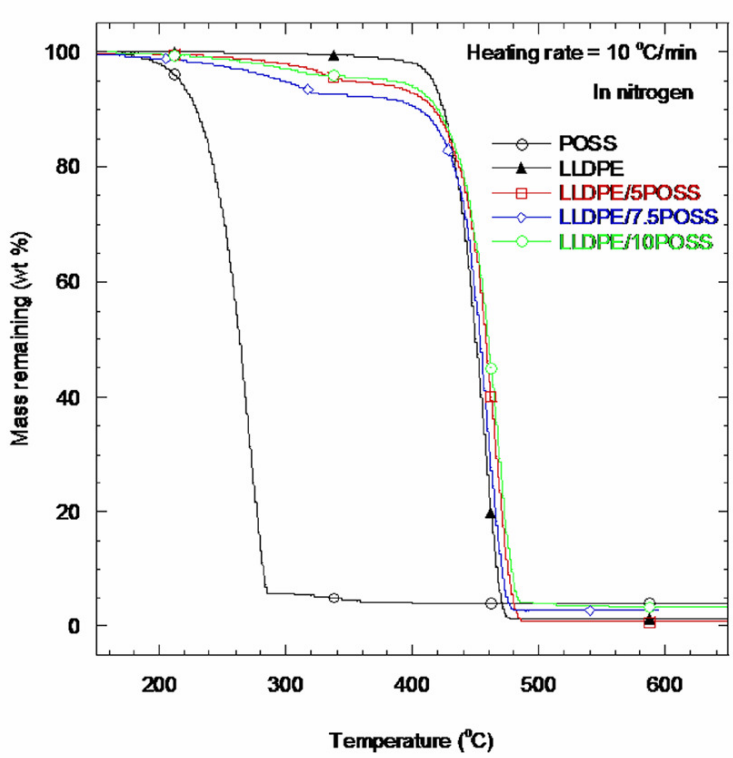

Figure 4.13 TGA curves of neat POSS, neat LLDPE and various nanocomposite samples obtained in nitrogen atmosphere

4.2.6 Dynamic mechanical analysis (DMA)

Dynamic mechanical analysis was used to measure the response to an oscillatory deformation in tension-torsion mode as a function of temperature for the LLDPE matrix before and after nanocomposite formation with POSS. The temperature dependence of the storage modulus (G') and the loss modulus (G'') of LLDPE upon nanocomposite formation was examined at three different POSS concentrations (Figures 4.14 and 4.15). It is evident that for both LLDPE/7.5POSS and LLDPE/10POSS nanocomposites a significant improvement in G', compared to that of neat LLDPE, is observed over the entire temperature range investigated, while the LLDPE/5POSS nanocomposite shows an improvement in the flexural storage modulus up to room temperature. This observation may be due to the potential formation of three-dimensional network-like structures in the nanocomposites with higher POSS contents [27]. The G' curves of both LLDPE/7.5POSS and LLDPE/10POSS nanocomposites show an enhanced rubbery plateau, which indicates that the addition of POSS particles induces a reinforcement effect which increases at very high temperatures. This behaviour indicates the enhancement of the thermomechanical stability of these materials at high temperatures.

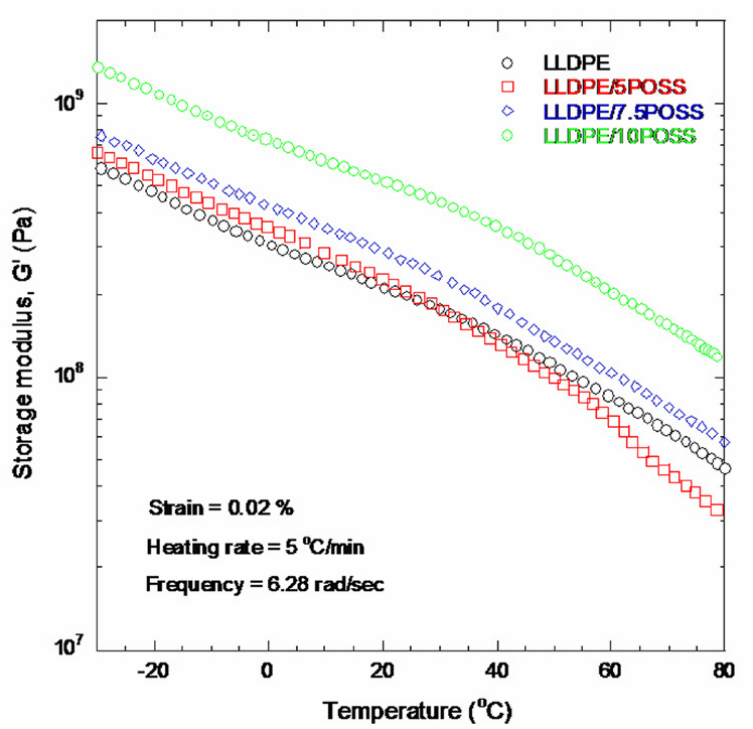

Figure 4.14 Temperature dependence of the storage modulus (G') of neat LLDPE and the nanocomposite samples

The incorporation of POSS particles into the LLDPE matrix also results in a substantial increase in G" (Figure 4.15). This observation suggests that the plastic behaviour of the LLDPE matrix increases in the presence of the POSS particles. It is interesting to note that all the samples show two distinguishable transitions in the G" curves. Generally, polyethylene exhibits three transitions in the DMA loss modulus or loss factor curves, designated as α, β, γ in decreasing order of temperature. The α-transition is found in the wide temperature range of 10 to 120 °C, the β-transition occurs in the temperature range of -30 to 10 °C, and the γ-transition in the temperature range of -150 to -120 °C [28,29]. The β-transition has been universally detected in branched polyethylenes [30,31]. In this study, it can be seen that all the samples exhibit only β- and α-transitions. Since LLDPE is a semi-crystalline polymer, crystalline structures coexist with amorphous parts. The first transition (β-transition) relates to the relaxation of the disordered structures (amorphous parts) along with small crystallites. The second broad transition (α-transition) is due to the crystalline part of the polymer [32-34]. In this study, the β-transition for LLDPE can be regarded as its glass transition temperature. The glass transition is where the chains in the amorphous regions start with coordinated large-scale motion. Although there is a controversy regarding the glass transition of polyethylenes [35], it is generally agreed that the β-transition is due to the transition of branch points.

Figure 4.16 shows the loss factor (G''/G') curves of the LLDPE and its nanocomposites. The loss factor provides information on the relative contributions of the viscous and elastic components of viscoelastic materials. It can be seen that all the samples exhibit β- and α-transitions. It is clear from Figures 4.15 and 4.16 that the presence of POSS did not change the T_g of LLDPE. This is probably the result of the relatively weak interaction between the LLDPE and the POSS particles as well as the lack of dispersion. It is, however, clear from the loss factor curves in Figure 4.16 that the α-transitions related to the crystalline parts of LLDPE were influenced by the presence of POSS. This may be the result of preferable crystallization of LLDPE around the POSS particles.

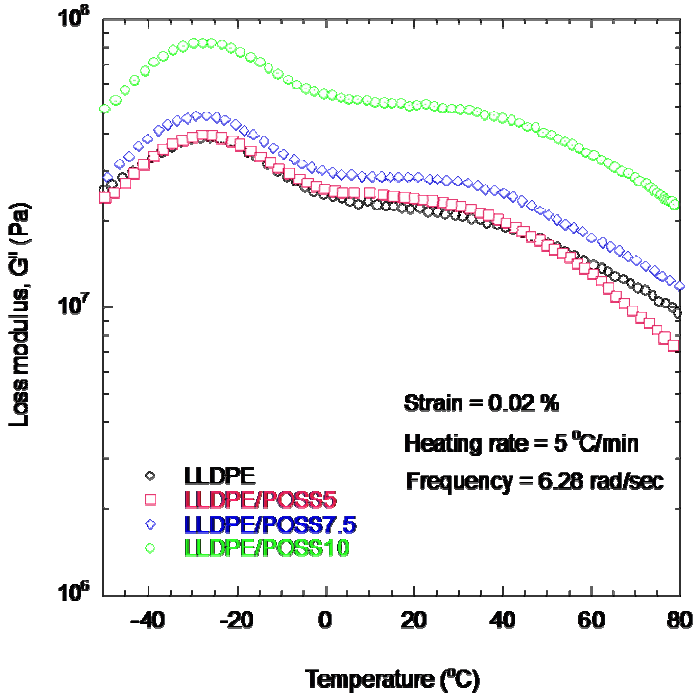

Figure 4.15 Temperature dependence of flexural loss modulus (G'') of neat LLDPE and the different nanocomposite samples

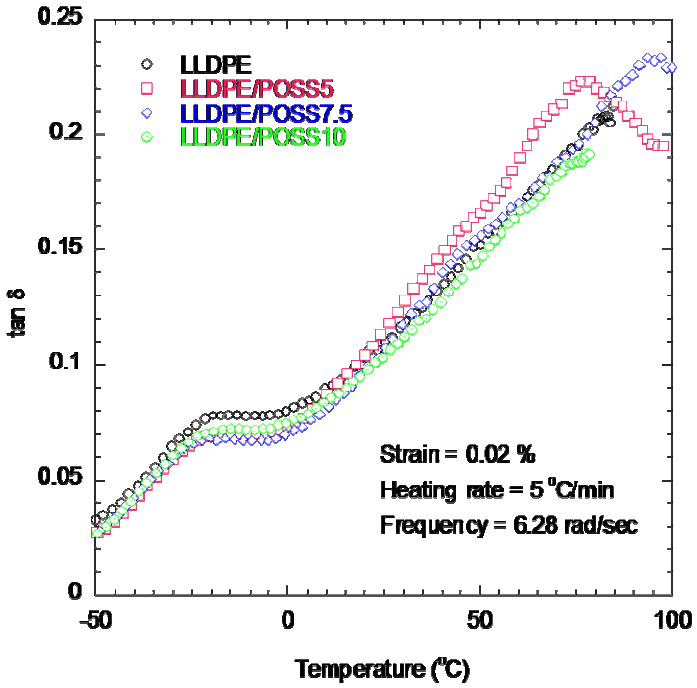

Figure 4.16 Temperature dependence of the loss factor of neat LLDPE and the different nanocomposite samples

4.3 Conclusions

In this chapter, the effect of the inorganic-organic hybrid POSS nanofiller loading on the thermal and thermomechanical properties of an LLDPE matrix was reported. POM and FE-SEM studies revealed a fairly homogeneous dispersion of POSS micro-aggregates in the LLDPE matrix. This micro-aggregation in the nanocomposite systems is due to the intrinsic chemical properties of both LLDPE and POSS, even though the POSS used had been modified with octamethyl chains.

Both conventional and temperature modulated differential scanning calorimetry were used to study the melting behaviour of the LLDPE and its nanocomposites. Multiple melting behaviour was observed for all the samples. This behaviour was attributed to partial melting, re-crystallization, and re-melting phenomena. DSC analysis showed a decrease in the overall crystallinity of the LLDPE matrix with POSS loading. This is associated with a homogeneous

dispersion of POSS micro-aggregates into the LLDPE matrix, which might hinder the local lamellar crystallization and leads to a decrease in the overall degree of crystallinity. However, POSS did not have any significant effect on the melting temperature of LLDPE.

The homogeneous dispersion of POSS micro-aggregates in the LLDPE matrix leads to a dramatic improvement in the elastic storage modulus at higher POSS concentrations. This is due to the potential formation of three-dimensional network-like structures. Two distinguishable transitions were observed in both the loss modulus and loss factor curves. The thermal stability of pure LLDPE and nanocomposite samples was also studied in air and inert atmospheres. Two degradation steps were observed for all the nanocomposite systems under inert atmosphere. The higher thermal stability of the nanocomposite samples observed in air in the high-temperature regions may be due to the dispersion of POSS particles in the LLDPE matrix, which decelerates the degradation of polymer chains *via* char formation.

4.4 References

1. J. Rong, Z. Jing, H. Li, M. Sheng. A polyethylene nanocomposite prepared via in-situ polymerization. Macromolecular Rapid Communications 2001; 22:329-334.
2. S. Sinha Ray, M. Bousmina. Poly(butylene succinate-co-adipate)/montmorillonite nanocomposites: effect of organic modifier miscibility on structure, properties and viscoelasticity. Polymer 2005; 46:12430-12430.
3. G. Qiu, Z.L. Tang, N.X. Huang, L. Gerking. Dual melting endotherms in the thermal analysis of poly(ethylene terephthalate). Journal of Applied Polymer Science 1998; 69:729-742.
4. S. Tan, A. Su, W. Li, E. Zhou. The crystallization behavior of the metastable melts of poly(ethylene terephthalate) from the multiple melting process. Macromolecular Rapid Communications 1998; 19:11-14.
5. E.M. Woo, T.Y. Ko. A differential scanning calorimetry on poly(ethylene terephthalate) isothermally crystallized at stepwise temperatures: multiple melting behaviour re-investigated. Colloid and Polymer Science 1996; 274:309-315.
6. C. Zhou, S.B. Clough. Multiple melting endotherms of poly(ethylene terephthalate). Polymer Engineering and Science 1988; 28:65-68.
7. Y. Kong, J.N. Hay. Multiple melting behaviour of poly(ethylene terephthalate). Polymer 2003; 44:623-633.

8. N.C. Andrews, A.J. McHugh, J.D. Schieber. Polyelectrolytes in shear and extensional flows: Conformation and rheology. Journal of Polymer Science Part B: Polymer Physics 1998; 36:1401-1417.
9. A.M.A. Qudah, A.A. Raheil. Surface morphology and annealing of poly(butylene terephthalate). Polymer International 1995; 38:375-380.
10. M.E. Nichols, R.E. Roberts. The multiple melting endotherms from poly(butylene terephthalate). Journal of Polymer Science Part B: Polymer Physics 1992; 30:755-768;
11. R.S. Stein, A. Misra. Morphological studies on poly(butylene terephthalate). Journal of Polymer Science Part B: Polymer Physics 1980; 18:327-342.
12. Y.Lu, D.M. Shinozaki, S. Herbert. Inhomogeneous deformation in welded high density polyethylene. Journal of Applied Polymer Science 2002; 86:43-52.
13. S. Hashemi, J.G. Williams. A fracture toughness study on low density and linear low density polyethylenes. Polymer 1986; 27:384-392.
14. R.K. Verma, V. Velikov, R.G. Kander, H. Marand. SAXS studies of lamellar level morphological changes during crystallization and melting of PEEK. Polymer 1996; 37:5357-5365.
15. A.M. Jonas, T.P. Russell, D.Y. Yoon. Synchroton x-ray scattering studies of crystallization of poly(ether-ether-ketone) from the glass and structural changes during subsequent heating-cooling processes. Macromolecules 1995; 28:8491-8503.
16. S. Sinha Ray, J. Bandyopadhyay, M. Bousmina. Thermal and thermomechanical properties of poly[(butylene succinate)-*co*-adipate] nanocomposite. Polymer Degradation and Stability 2007; 92:802-812.
17. W. Zhang, B.X. Fu, Y. Seo, E. Schrag, B. Hsiao, P.T. Mather, N.L. Yang, D. Xu, H. Ade, M. Rafailovich, J. Sokolov. Effect of methyl methacrylate/polyhedral oligomeric silsesquioxane random copolymers in compatibilization of polystyrene and poly(methyl methacrylate) blends. Macromolecules 2002; 35:8029-8038.
18. B.X. Fu, B. Hsiao, S. Pagola, P. Stephens, H. White, M. Rafailovich, Sokolov, P.T. Mather, H.G. Jeon, S. Phillips, J. Lichtenhan, J. Schwab. Structural development during deformation of polyurethane containing polyhedral oligomeric silsesquioxanes (POSS) molecules. Polymer 2001; 42:599-611.
19. B.X. Fu, B. Hsiao, H. White, M. Rafailovich. P.T. Mather, H.G. Jeon. Nanoscale reinforcement of polyhedral oligomeric silsesquioxane (POSS) in polyurethane elastomer. Polymer International 2000; 49:437-440.

20. J.A. Molefi, A.S. Luyt, I. Krupa. Comparison of the influence of Cu micro- and nano-particles on the thermal properties of polyethylene/Cu composites. Express Polymer Letters 2009; 3:639-649.
21. M. Joshi, B.S. Butola, G. Simon, N. Kukaleva. Rheological and viscoelastic behaviour of HDPE/octamethyl-POSS nanocomposites. Macromolecules 2006; 39:1839-1849.
22. P. Rizzo, F. Baione, G.G. Martinotto, L. Martinotto, E. Albizzati. Polyethylene unit cell and crystallinity variations as a consequence of different crosslinking processes. Macromolecules 2001; 34:5175-5179.
23. J. Heinemann, P. Reichert, R. Thomann, R. Mülhaupt. Polyolefin nanocomposites formed by melt compounding and transition metal catalyzed ethene homo- and copolymerization in the presence of layered silicates. Macromolecular Rapid Communications 1999; 20:423-430.
24. M. Joshi, B.S. Butola. Studies on nonisothermal crystallization of HDPE/POSS nanocomposites. Polymer 2008; 45:4953-4968.
25. A. Fina, D. Tabuani, A. Frache, G. Camino. Polypropylene-polyhedral oligomeric silsesquioxanes (POSS) nanocomposites. Polymer 2005; 46:7855-7866.
26. A. Fina, H.C.L. Abbenhuis, D. Tabuani, A. Frache, G. Camino. Polypropylene metal functionalised POSS nanocomposites: A study by thermogravimetric analysis. Polymer Degradation and Stability 2006; 91:1064-1070.
27. Y.H. Hyun, S.T. Lim, H.J. Choi, M.S. Jhon. Rheology of poly(ethylene oxide)/organoclay nanocomposites. Macromolecules 2001; 34:8084-8093.
28. N.G. McCrum, D.J. Meir. Molecular basis of transitions and relaxations, Gordon and Breach: New York (1978).
29. R.H. Boyd. Relaxation processes in crystalline polymers: molecular interpretation - A review. Polymer 1985; 26:1123-1133.
30. M.L. Cerrada, R. Benavente, B. Peña, E. Pérez. The effect of thermal treatment on the structure and relaxation processes of olefinic polymers synthesized with metallocene catalysts. Polymer 2000; 41:5957-5965.
31. M.L. Cerrada, R. Benavente, E. Pérez. Influence of thermal history on morphology and viscoelastic behaviour of ethylene-1-octene copolymers synthesized with metallocene catalysts. Journal of Materials Research 2001; 16:1103-1111.
32. V. Gaucher-Miri, S. Elkoun, R. Séguéla. On the plastic behavior of homogeneous ethylene copolymers compared with heterogeneous copolymers. Polymer Engineering and Science 1997; 37:1672-1683.

33. P. Starck, B. Lofgren. Thermal properties of ethylene/long chain α-olefin copolymers produced by metallocenes. European Polymer Journal 2002; 38:97-107.
34. R. Popli, M. Glotin, L. Madelkern, R.S. Benson. Dynamic mechanical studies of α and β relaxations of polyethylenes. Journal of Polymer Science: Polymer Physics Edition 1984; 22:407-448.
35. E.A Turi. Thermal Characterization of Polymer Materials, 2nd Edition. Academic Press: New York (1997).

CHAPTER 5

MELT-STATE VISCOELASTIC AND MATERIALS PROPERTIES OF POSS-CONTAINING LINEAR LOW-DENSITY POLYETHYLENE NANOCOMPOSITES

5.1 Introduction

In this chapter the effect of the incorporation of octamethyl-T_8-POSS nanoparticles on the melt-state rheological properties of LLDPE was investigated, since the measurement of the rheological properties of any polymeric material in the molten state is crucial to gain a fundamental understanding of the processibility of that material and of the degree of interfacial interactions between the polymer chains and the filler surface [1]. A series of LLDPE nanocomposites with different POSS loadings from 5 − 10 wt % were prepared through melt mixing. LLDPE nanocomposites with three different POSS loadings of 5, 7.5 and 10 wt. % were correspondingly abbreviated as LLDPE/5POSS, LLDPE/7.5POSS and LLDPE/10POSS. The effect of addition of POSS on the material properties of LLDPE were studied in detail.

5.2 Results and discussion

5.2.1 Melt-state rheology

When a small deformation sinusoidal strain [$\gamma(t) = \gamma_0 \sin(\omega t)$] is applied to any polymeric material in the linear viscoelastic (LVE) region, the resultant shear stress $\tau(t)$ is denoted by

$$\tau(t) = \gamma_0[G'(\omega) \sin(\omega t) + G''(\omega) \cos(\omega t)] \quad (5.1)$$

where t is the real time.

Figures 5.1 and 5.2, respectively, present the storage (G') and loss (G") moduli as a function of applied strain for pure LLDPE and the three different nanocomposites. It is clear from these figures that the neat LLDPE exhibits a Newtonian plateau up to 6 % strain. It is also

notable that both these moduli decrease after nanocomposites formation with different POSS loadings. Furthermore, the presence of POSS particles does not significantly change the onset of the nonlinear viscoelastic region of LLDPE. This observation can be attributed to the absence of strain-sensitive rigid network-like structures [2] between the POSS and the LLDPE matrix, which results in a decrease in the modulus values. The absence of strain-sensitive structures is due to a highly phase separated morphology between the POSS particles and the LLDPE as shown in Figure 4.1.

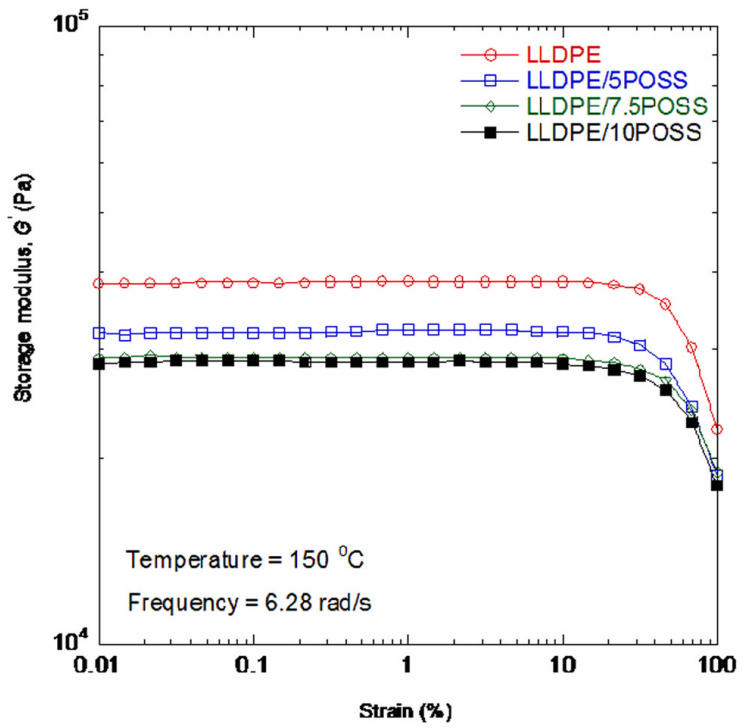

Figure 5.1 Strain amplitude sweep dependence of the storage modulus (G') of the LLDPE matrix and the three different LLDPE/POSS nanocomposites

For the neat LLDPE and its nanocomposites, in the LVE region, it can be seen that the viscous behaviour dominates the elastic one (i.e. G" > G'). This suggests the existence of a liquid-like behaviour for all the samples investigated. This is because of no chemical or physical network formation between the LLDPE chains and the POSS particles. For this reason, the samples are not form stable at rest since they creep or flow [3].

To further elucidate the effect of the POSS particles on the structure of the LLDPE matrix, frequency sweep experiments of the pure LLDPE and the LLDPE/POSS nanocomposites were conducted at 150 °C at a constant strain of 5 % and the results of G' and G" are shown in

Figures 5.3 and 5.4. It can be seen that the presence of the POSS particles in LLDPE does not cause any significant enhancement in both the storage modulus (G') or the loss modulus (G'') at all frequencies investigated. It is also notable that both moduli show a frequency dependence that is characteristic of liquid-like materials [4]. This is due to the lack of interaction between the LLDPE chains and the POSS particles as observed in the amplitude sweep results. Another possible reason for this behaviour is the lubrication effect of the POSS particles on the LLDPE matrix in the molten state [5].

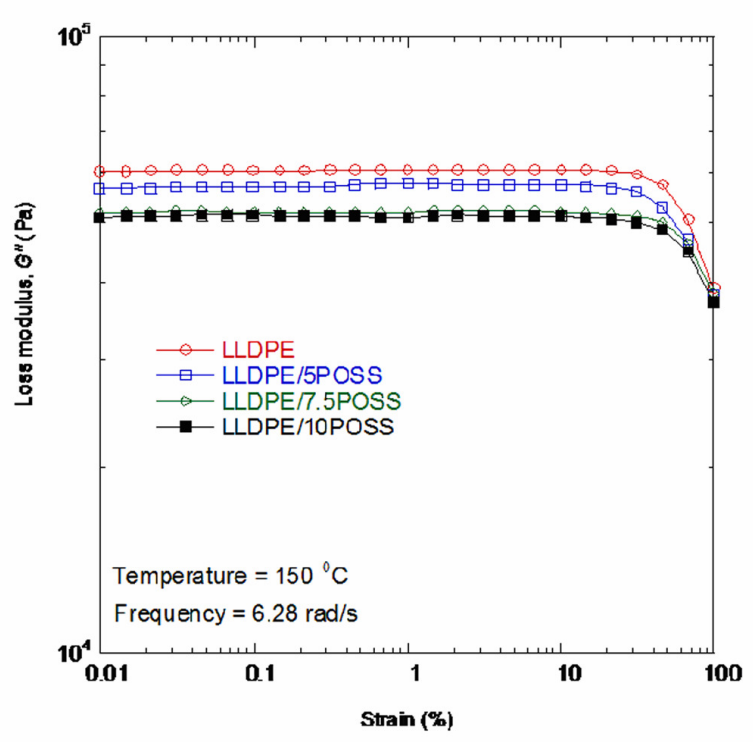

Figure 5.2 Strain amplitude sweep dependence of loss modulus (G'') of the LLDPE matrix and the three different LLDPE/POSS nanocomposites

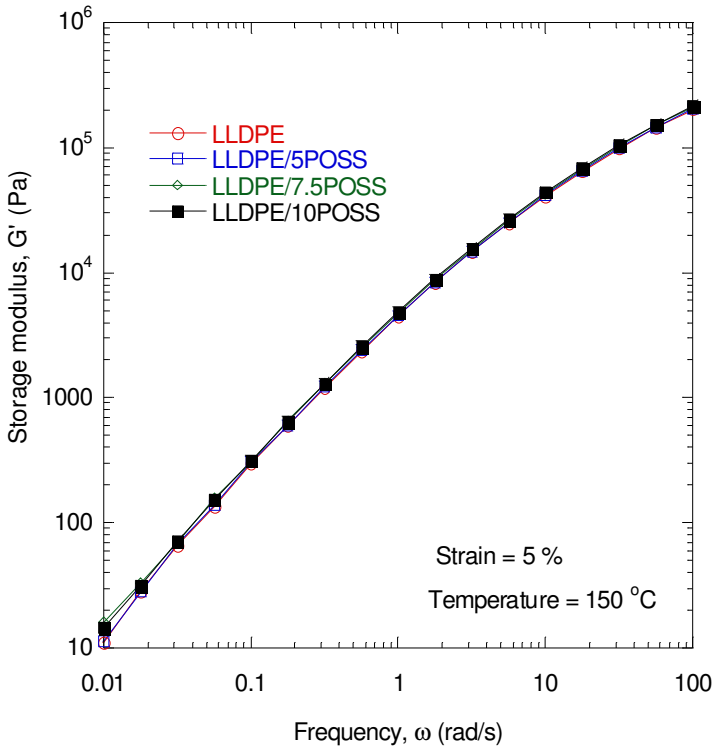

Figure 5.3 Frequency dependence of the storage modulus (G') of the pure LLDPE and the three different nanocomposite samples

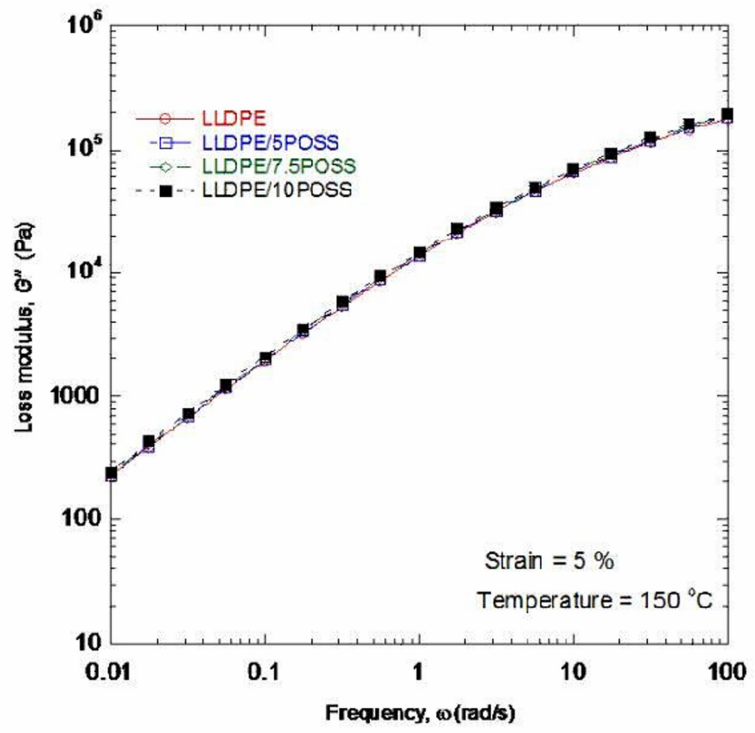

Figure 5.4 Frequency dependence of the loss modulus (G'') of the pure LLDPE and the three different nanocomposite samples

The frequency dependence of the dynamic complex viscosity, $|\eta^*|$ of LLDPE and various nanocomposites is shown in Figure 5.5. The value of $|\eta^*|$ of the neat LLDPE matrix shows almost no effect after nanocomposite formation with various POSS concentrations. These results also support the conclusion that there are almost no interactions between the POSS particles and the LLDPE matrix as revealed by SEM studies (see Figure 4.1). However, all the samples exhibit a shear thinning region in the high frequency range. In this region, there is limited relative motion in the entangled structures, because the cyclic motion of the rheometer is too fast for the polymer chains to react to the change in applied stress. The maximum part of the energy needed to deform the sample can therefore be stored at this high frequency region. This means that the amount of deformation energy lost by friction between the molecules because of relative motion is reduced, hence a decrease in $|\eta^*|$ was observed [6].

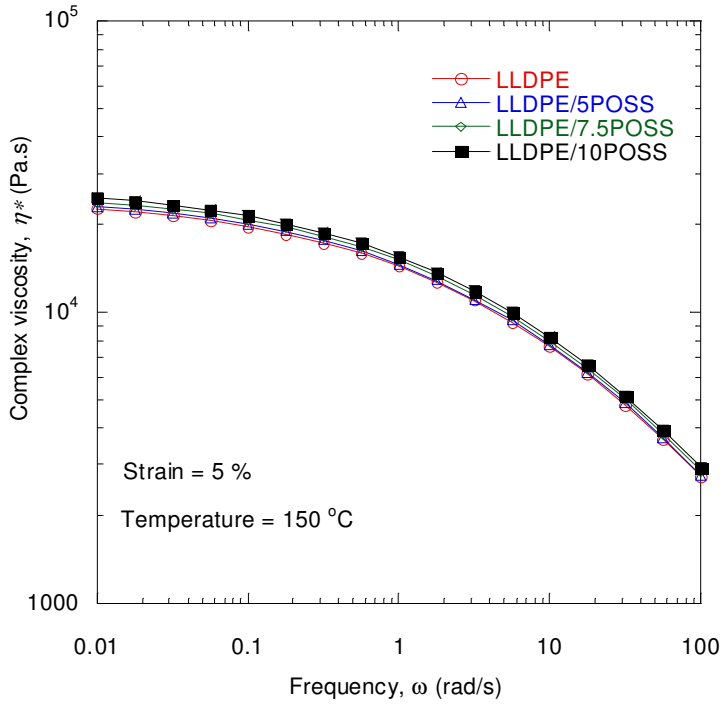

Figure 5.5 Frequency dependence of dynamic complex viscosity (η^*) of neat LLDPE and its nanocomposites at different POSS loadings

5.2.2 Tensile properties

To determine the interfacial interactions between the POSS particles and the LLDPE chains, the tensile properties of the pure LLDPE and the various nanocomposite samples were measured at room temperature and 42 % humidity. It is well known that the tensile properties

of a composite material are directly dependent on the interfacial interactions between the filler and the matrix as well as the dispersion of the filler particles. The values of Young's modulus (E), yield strength (σ_y), and elongation at break (ε_b) of all the samples are summarized in Figures 5.6 to 5.8. It is clear from Figure 5.6 that there is a very slight increase in Young's modulus with 5 wt % POSS loading. This is associated with the high degree of crystallinity of the sample in the presence of low POSS content. With an increase in POSS loading there was no improvement in the modulus, and in the case of the nanocomposite with 10 wt % POSS loading the modulus dropped to a value lower than that of LLDPE. These results are in good agreement with the work reported by Yoon *et al*. [7]. In their studies they observed a decrease in modulus for PET/POSS composites prepared by melt-mixing. This behaviour may either be due to the phase separated morphology of the LLDPE/POSS nanocomposites, or a decrease in the total crystallinity of the neat LLDPE matrix with an increase in POSS loading (Table 4.1).

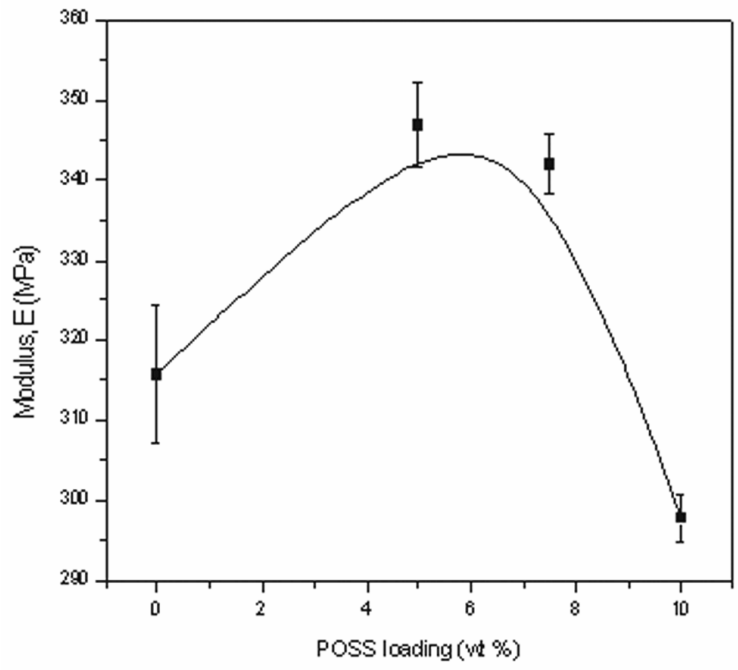

Figure 5.6 Young's modulus (E) as a function of POSS loading of pure LLDPE and the various LLDPE/POSS nanocomposites

Figure 5.7 shows the yield strength of neat LLDPE and three different LLDPE/POSS nanocomposites as a function of POSS loading. It is well known that the strength of a particulate composite is usually reduced with filler content following a power law in the case of poor polymer-filler interaction [8,9]. From the figure it is clear that the strength of the LLDPE matrix decreases after incorporation of POSS particles. This behaviour is the result of

the observed phase separated morphology, as well as the poor adhesion at the polymer-filler interface. The phase separated morphology is also responsible for the decrease in the elongation at break of the LLDPE matrix after nanocomposite formation with POSS (Figure 5.8). When there is phase separation in the nanocomposites, the material loses drawability and strain at break strongly decreases. Possible crack initiation can start at the domains of segregation of low molecular weight material. The number of chain ends, i.e. the number of dislocations, will increase with an increase in POSS content due to the spherical POSS particles that are difficult to form tie chains. This will induce a decrease in the strain at break.

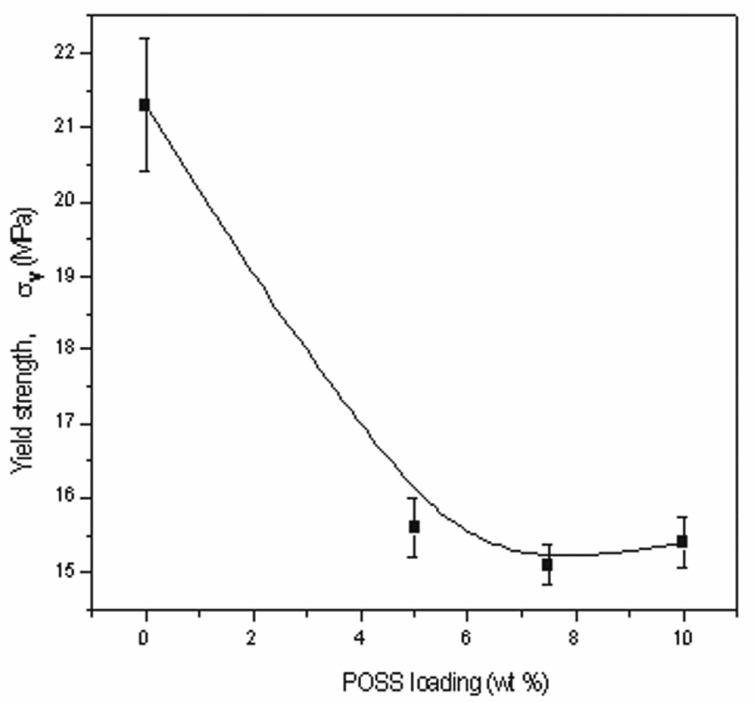

Figure 5.7 Yield strength (σ_y) as a function of POSS loading of pure LLDPE and the various LLDPE/POSS nanocomposites

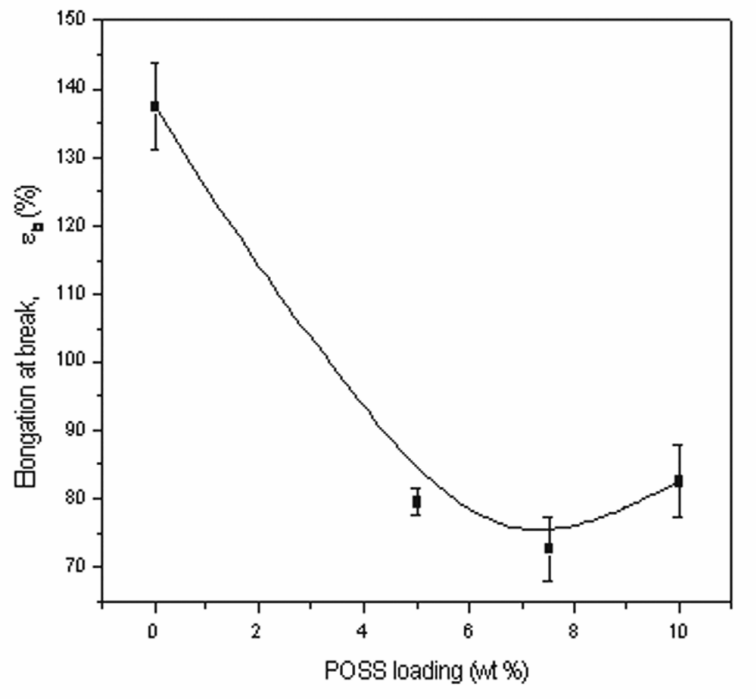

Figure 5.8 Elongation at break (ε_b) as a function of POSS loading of pure LLDPE and the various LLDPE/POSS nanocomposites

5.3 Charpy impact strength

Impact strength is defined as the ability of a material and its structure to survive impact induced damages during an impact event applied at a high speed. The impact properties of composites are directly related to their overall toughness. Composite fracture toughness is affected by factors such as interlaminar shear, matrix ductility, void content of the composites and interfacial strength parameters [10,11].

Figure 5.9 represents the results of the Charpy impact strength of pure LLDPE and its three different nanocomposites. The impact strength of the composite with 5 wt % POSS content is 105.2 kJ.m^{-2} compared to that of the neat LLDPE matrix (98.5 kJ.m^{-2}), implying that POSS at a lower content toughens the LLDPE matrix. The increase in impact behaviour is due to a number of deformation and failure mechanisms acting in the notch tip process zone and in the crack wake. Crack tip zone processes include plastic deformation of the thermoplastic such as nucleation, growth, and coalescence of micro-voids. A crack wake mechanism like crack bridging by highly ductile microscopic-sized ligaments of the polymer also contributes to such an enhancement in toughness [12]. With a further increase in POSS loading from 7.5 to

10 wt %, there is a considerable decrease in impact strength, indicating that a small amount of energy is needed to break the sample. This decrease is due to the phase separated morphology as well as poor adhesion at the polymer-filler interface (Figure 4.1). These results are in accordance with the tensile results reported above.

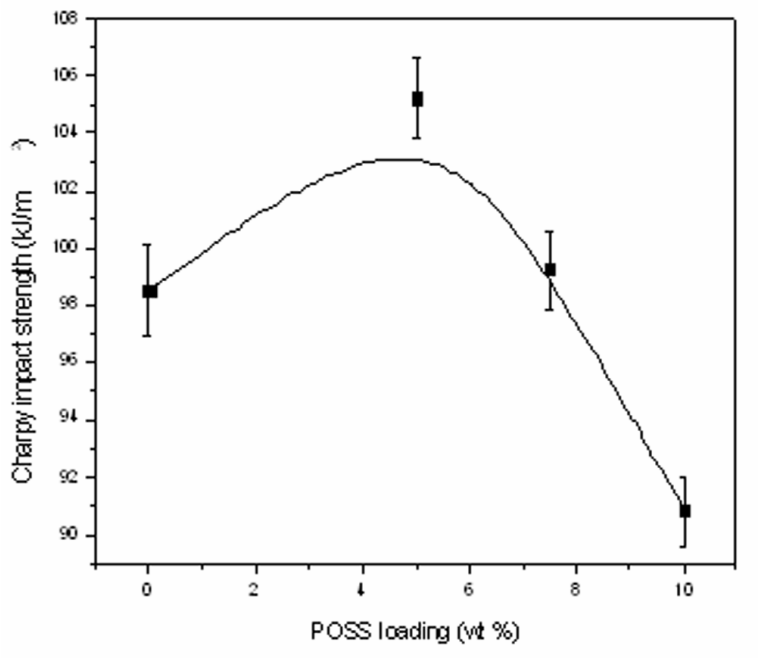

Figure 5.9 The notched Charpy impact strength at room temperature as a function of POSS loading of pure LLDPE and the various LLDPE/POSS nanocomposites

5.4 Heat distortion temperature (HDT)

Shown in Figure 5.10 are the heat distortion temperature results of the neat LLDPE matrix and its different nanocomposites. It can be seen that the HDT of the nanocomposites increased with increasing POSS loading. According to Nielsen's prediction regarding the behaviour of flexural modulus with filler loading [13], the increase of the HDT is attributed to a change in flexural modulus.

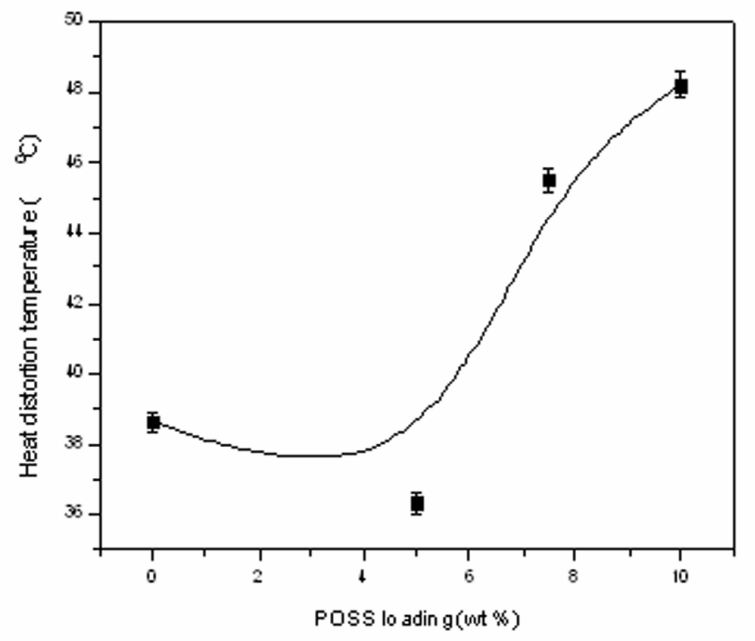

Figure 5.10 Heat distortion temperatures as a function of POSS loading of pure LLDPE and the various LLDPE/POSS nanocomposites

5.5 Conclusions

In this study, the influence of POSS nanofiller loading on the melt-state rheological properties of LLDPE was investigated. Strain and frequency sweep results show that the POSS particles are highly immiscible with the LLDPE matrix. Because of this phase-separated morphology, POSS-containing LLDPE composites do not show any improvement in tensile properties. A phase-separated morphology also gave rise to the decrease in impact properties of the LLDPE at higher POSS loadings. The heat distortion temperature of the samples increased with increasing the POSS loading in the polymer matrix. This observation was attributed to the potential formation of three-dimensional network-like structures in the nanocomposites.

5.6 References

1. L. Elias, F. Fenouillot, J.C. Majeste, Ph. Cassagnau. Morphology and rheology of immiscible polymer blends filled with silica nanoparticles. Polymer 2007; 48:6029-6040.

2. S. Sinha Ray. K. Okamoto, M. Okamoto. Structure-property relationship in biodegradable poly(butylene succinate)/layered silicate nanocomposites. Macromolecules 2003; 36:2355-2367.
3. T.G. Mezger. The Rheology Handbook, 2nd Ed. Hannoprint, Germany (2006).
4. A. Durmus, A. Kasgoz, C.W. Macosko. Linear low density polyethylene (LLDPE)/clay nanocomposites. Part I: Structural characterization and quantifying clay dispersion by melt rheology. Polymer 2007; 48:4492-4502.
5. M. Joshi, B.S. Butola, G. Simon, N. Kukaleva. Rheological and viscoelastic behaviour of HDPE/octamethyl-POSS nanocomposites. Macromolecules 2006; 39:1839-1849.
6. J. Bandyopadhyay, S. Sinha Ray, M. Bousmina. Viscoelastic properties of clay-containing nanocomposites of thermotropic liquid-crystal polymer. Macromolecular Chemistry and Physics 2008; 210:161-171.
7. K.H. Yoon, M.B. Polk, J.H. Park, B.G. Min, D.A. Schiraldi. Properties of poly(ethylene terephthalate) containing epoxy-functionalized polyhedral oligomeric silsesquioxane. Polymer International 2005; 54:47-53.
8. D.N. Bikiaris, A. Vassiliou, E. Pavlidou, G.P. Karayannidis. Compatibilization effect of PP-g-MA copolymer on *i*-PP/SiO_2 nanocomposites prepared by melt mixing. European Polymer Journal 2005; 41:1965-1978.
9. S. Sun, C. Li, L. Zang, H.L. Du, J.S. Burnell-Gray. Effects of surface modification of fumed silica on interfacial structures and mechanical properties of poly(vinyl chloride) composites. European Polymer Journal 2006; 42:1643-1652.
10. A.K. Bledzki, J. Gassan, W. Zhang. Impact properties of natural fibre-reinforced epoxy foams. Journal of Cellular Plastics 1999; 19:550-562.
11. S. Mishra, A.K. Mohanty, L.T. Drzal, M. Misra, S. Parija, S.K. Nayak, S.S. Tripathy. Studies on mechanical perfomance of biofibre/glass reinforced polyester hybrid composites. Composites Science and Technology 2003; 63:1377-1385.
12. T.S. Srivatsan, P.C. Lam, J. Krause. The impact toughness characteristics of steel wire-reinforced polymer composites. Materials Letters 1999; 39:324-328.
13. L.E. Nielsen. Mechanical Properties of Polymer Composites, Vol.2. Marcel Dekker, New York (1974).

CHAPTER 6

THE EFFECT OF POSS ON THE THERMAL AND THERMOMECHANICAL PROPERTIES OF POLY(METHYL METHACRYLATE) MATRIX

6.1 Introduction

This chapter describes the morphology, thermal, thermomechanical and rheological properties of PMMA filled POSS nanocomposites. PMMA nanocomposites with various POSS loadings of 5, 10, 15 and 25 wt %, were prepared through melt mixing and are correspondingly abbreviated as PMMA/5POSS, PMMA/10POSS, PMMA/15POSS and PMMA/25POSS.

6.2 Results and discussion

6.2.1 Scanning electron microscopy (SEM)

The morphologies of the nanocomposites were studied by field-emission SEM (FE-SEM) analysis of the fracture surfaces of the nanocomposites, in order to investigate the dispersion degree and the compatibility between the POSS particles and the PMMA matrix. Figure 6.1 shows the FE-SEM images of the pure PMMA matrix and its nanocomposites containing different POSS loadings. No clear distinction could be made between the PMMA matrix and the POSS nanoparticles in the images, probably because of the small difference between the optical absorbances of POSS and PMMA. The scales of the images are also such that it will be difficult to locate individual nanoparticles in the polymer matrix on the images, and therefore it is difficult to draw any conclusions about the dispersion of the POSS in the PMMA matrix from the FE-SEM results.

6.2.2 Differential scanning calorimetry (DSC)

The conventional DSC curves of pure PMMA and the different PMMA/POSS nanocomposites are shown in Figure 6.2. No exothermic peaks are observed in the curves, which indicate that no reactive methyl methacrylate (MMA) monomer residues were present

in the nanocomposites. All the samples show a single glass transition temperature (T_g) and these values are presented in Table 6.1. The T_g slightly decreased and the glass transition region broadened with increasing POSS content in the matrix. There are several factors that contribute to the variation of the T_g of POSS-containing polymer hybrids [1,2]. These factors

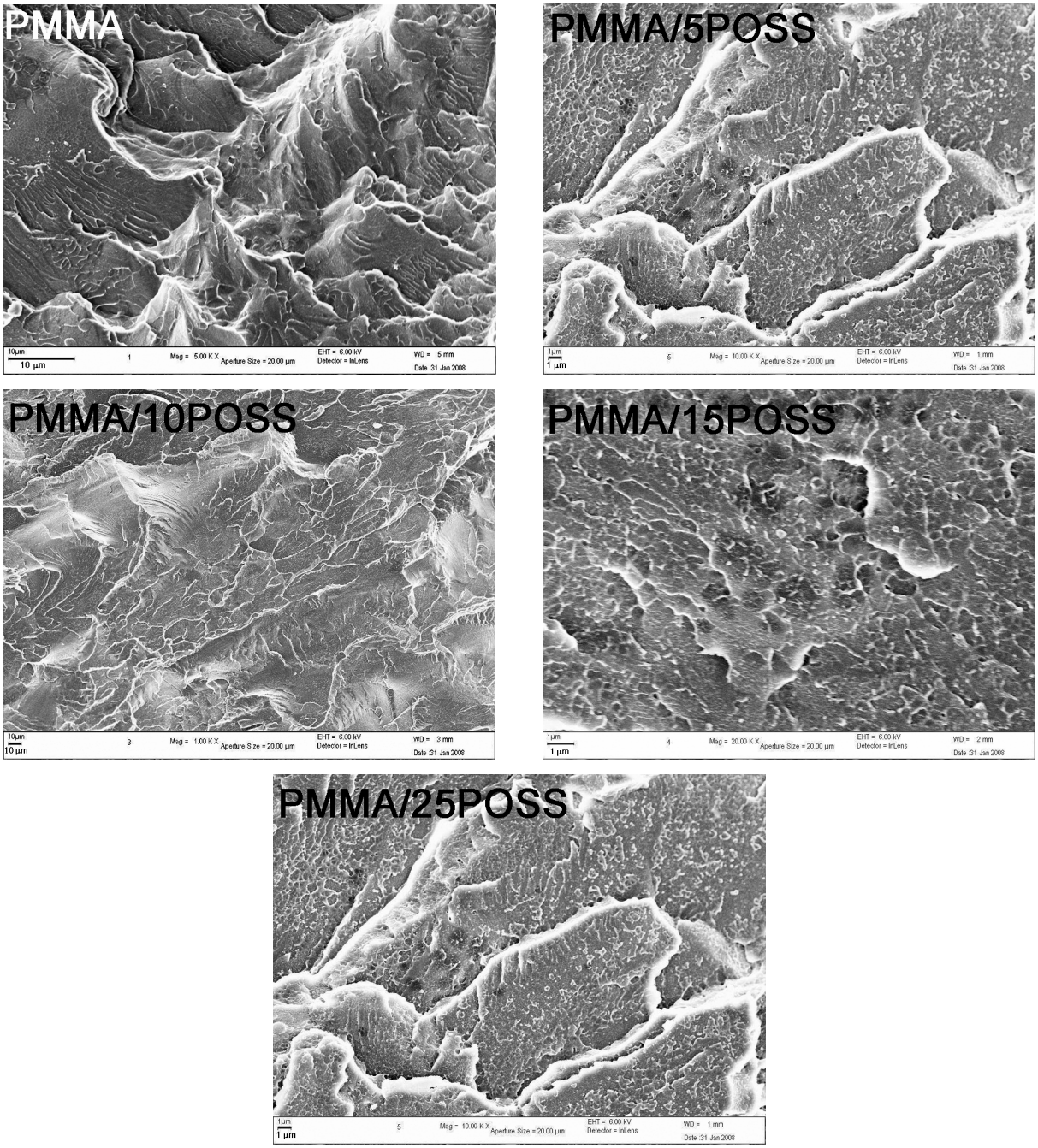

Figure 6.1 FE-SEM images of the freeze-fractured surfaces of pure PMMA and its different nanocomposite samples

include POSS species, POSS loading and different structures of the hybrids. In this work, we attribute the T_g depression of the nanocomposites to an internal plasticization effect of the

well-dispersed POSS cages within the PMMA matrix, where the side groups increase the interchain spacing and free volume, V_f [3], which facilitate the motion of the PMMA chains.

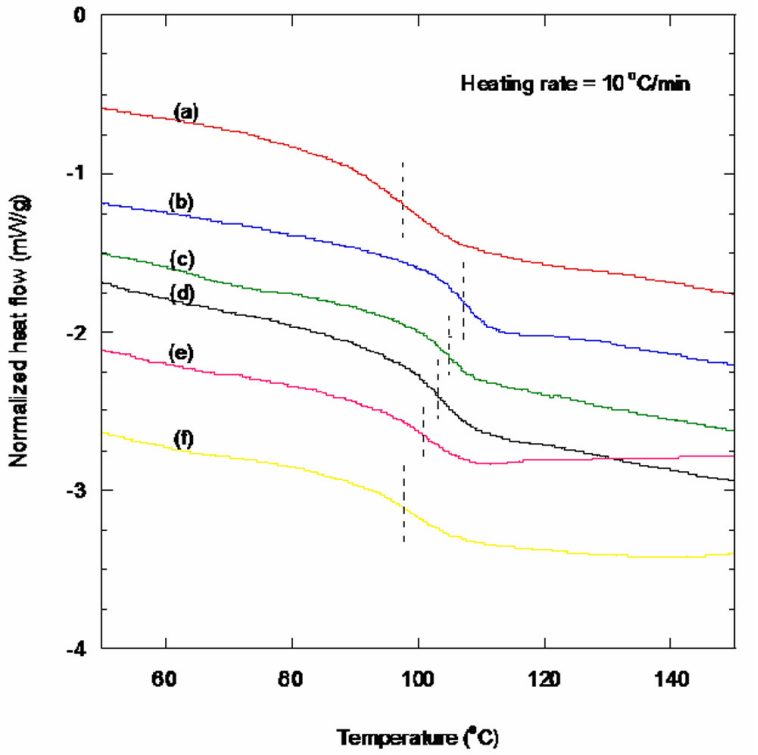

Figure 6.2 DSC curves of (a) pure POSS, (b) pure PMMA, (c) PMMA/5POSS, (d) PMMA/10POSS, (e) PMMA/15POSS and (f) PMMA/25POSS nanocomposites

Table 6.1 Glass transition temperature of pure POSS, PMMA and different PMMA/POSS nanocomposites

Sample	T_g (°C)
POSS	97.3
PMMA	107.7
PMMA/5POSS	104.2
PMMA/10POSS	102.9
PMMA/15POSS	100.8
PMMA/25POSS	98.4

Different authors observed a decrease in the T_g for epoxy/POSS nanocomposites [4,5]. They reported that this behaviour was due to the separation of the polymer chains caused by the bulkiness of the POSS cages where chain separation additionally prevented interchain

hydrogen bonding in epoxy systems [6,7]. Xu *et al*. [8] observed that for poly(hydroxystyrene-*co*-vinylpyrolidone-*co*-isobutylstyryl polyhedral oligosilsesquioxane) the T_g of the hybrids decreased as the POSS loading increased. They reported that the interactions between the copolymers reduced the original dipole-dipole interaction within the polymers. Kim *et al*. [9] reported that the flexible siloxane spacer unit appended to two of the apexes of the POSS cube led to a more flexible molecular environment, which finally reduced the T_g.

6.2.3 X-ray diffraction (XRD)

X-ray diffraction studies were carried out to characterize the dispersion of POSS within the PMMA matrix. Figure 6.3 shows the diffraction patterns of the pure POSS, PMMA and different PMMA/POSS nanocomposites. A broad peak is observed between $2\theta = 11°$ and 16° for pure PMMA and POSS. This broad peak is characteristic of an amorphous nature. Similar characteristic diffraction patterns for PMMA were observed by Elasmawi and Hakeem [10] at $2\theta = 14.8°$ and 35°. Two shoulder peaks are observed at $2\theta = 8.1°$ and 19.4° for POSS. The two peaks correspond to *d*-spacings of 1.16 nm [11] and 0.46 nm [12]. In this study, the peak at the higher 2θ value is not pronounced and it has been observed by other researchers for most POSS crystals [13-15]. The broadness of the peak observed between $2\theta = 11°$ and 16° in the nanocomposites can be attributed to the hybrid formation due to the presence of POSS inorganic segments. In the case of different nanocomposite systems, similar diffraction patterns were observed after addition of POSS into a PMMA matrix. However, the location of the main diffraction peak of the PMMA ($2\theta = 14.8°$) slightly shifts towards higher *d*-spacing (smaller 2θ angle) with increasing POSS concentration, suggesting that POSS nanoparticles are distributed throughout the matrix. This means that the POSS nanoparticles push the PMMA chains apart and shift the peak to a smaller 2θ angle. This is due to the overlapping signal of the POSS peak observed at $2\theta = 19.4°$. This does not allow the precise location of the PMMA matrix to be determined upon nanocomposite formation with POSS [16]. The broad PMMA diffraction peak, which appears at a higher 2θ scattering angle, remains in the same position in the presence of different POSS loadings.

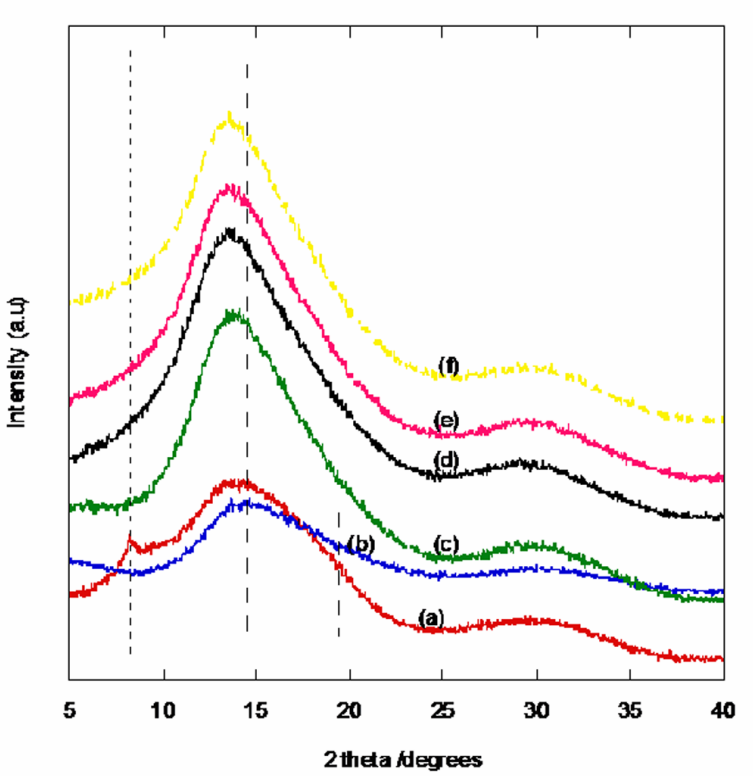

Figure 6.3 X-ray diffraction patterns of (a) pure POSS, (b) pure PMMA, (c) PMMA/5POSS, (d) PMMA/10POSS, (e) PMMA/15POSS and (f) PMMA/25POSS nanocomposite samples

6.2.4 Thermogravimetric analysis (TGA)

Figure 6.4 presents the TGA curves for pure PMMA and different PMMA/POSS nanocomposite samples, performed under nitrogen atmosphere. The TGA curve of pure POSS shows two degradation steps. The first degradation step at 182 °C is attributed to the organic fraction of the POSS [17], while the second step could probably be due to further degradation of the methyl methacrylate fraction of POSS. The pure POSS exhibits much lower thermal stability compared to that of the pure PMMA and the nanocomposite samples. The lower thermal stability of POSS may be associated with its sublimation behaviour at lower temperatures [18-20]. The thermal stability of the PMMA matrix decreases with increasing POSS content. The decrease is the result of the lower thermal stability of the POSS. However, at 25 wt % POSS loading the onset of degradation is still more than 100 °C higher than that of pure POSS. It seems as if the presence of PMMA inhibits the POSS degradation, probably because of the intimate contact between the PMMA and the POSS which to a certain extent

isolates the POSS and retards its thermal degradation. Moreover, all the samples exhibited a 100 % weight loss, indicating that no silicates were formed upon POSS thermal treatment.

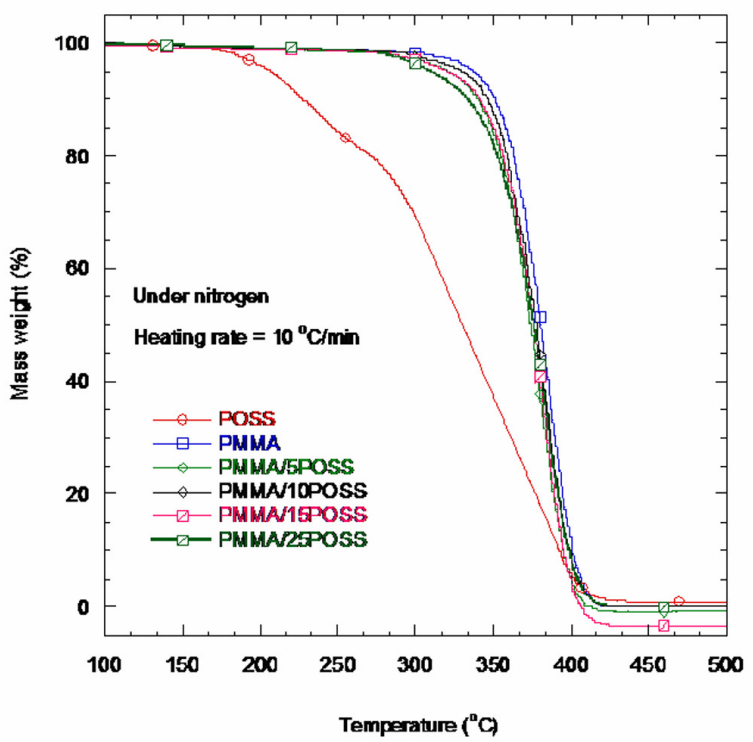

Figure 6.4 TGA curves of pure POSS, pure PMMA and the different nanocomposites obtained in nitrogen atmosphere

Lichtenhan [21] observed that polymers reinforced with polyhedral silsesquioxanes show higher decomposition temperatures, due to the ceramic nature of the silsesquioxane component, which creates a glassy layer during pyrolysis and retards the rate of diffusion of decomposition gases.

6.2.5 Melt-state rheology

To determine the effect of the POSS concentration on the structural modification of the PMMA matrix with changing the strain amplitude, strain amplitude tests were conducted at 180 °C on the different nanocomposites. Figures 6.5 and 6.6 depict the storage modulus (G') and loss modulus (G") as a function of applied strain, γ (0.01 to 100 %). All the samples show a Newtonian plateau up to 8 % strain, and the incorporation of different POSS loadings into the polymer matrix shows an increase in G' and G". Furthermore, the presence of the POSS particles does not significantly change the onset of the nonlinear viscoelastic region of the

PMMA. This behaviour can be attributed to the absence of the formation of a strain-sensitive rigid network-like structure [22] between the POSS and the PMMA, which results in higher moduli values. The absence of strain-sensitive structures may be due to well dispersed POSS particles within the matrix, although such a dispersion could not be conclusively established. In the linear viscoelastic region the elastic behaviour dominates the viscous one (i.e. G' > G'') for all the samples investigated, indicating the formation of a gel-like behaviour of PMMA and its nanocomposites. Even if this is a weak gel-like structure, these samples exhibit a certain form-stability [23].

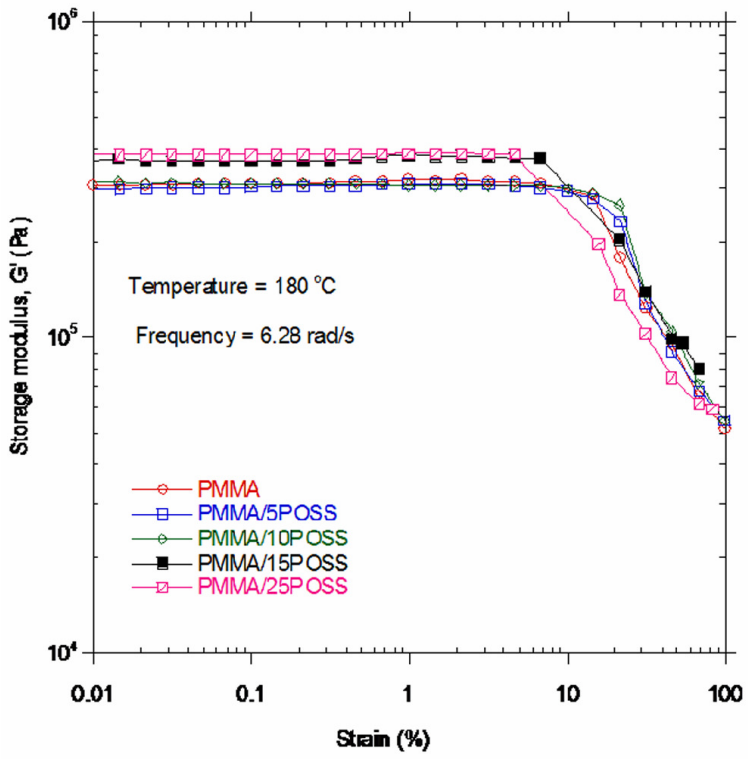

Figure 6.5 Strain amplitude sweep dependence of storage modulus (G') of the PMMA matrix and the different PMMA/POSS nanocomposites

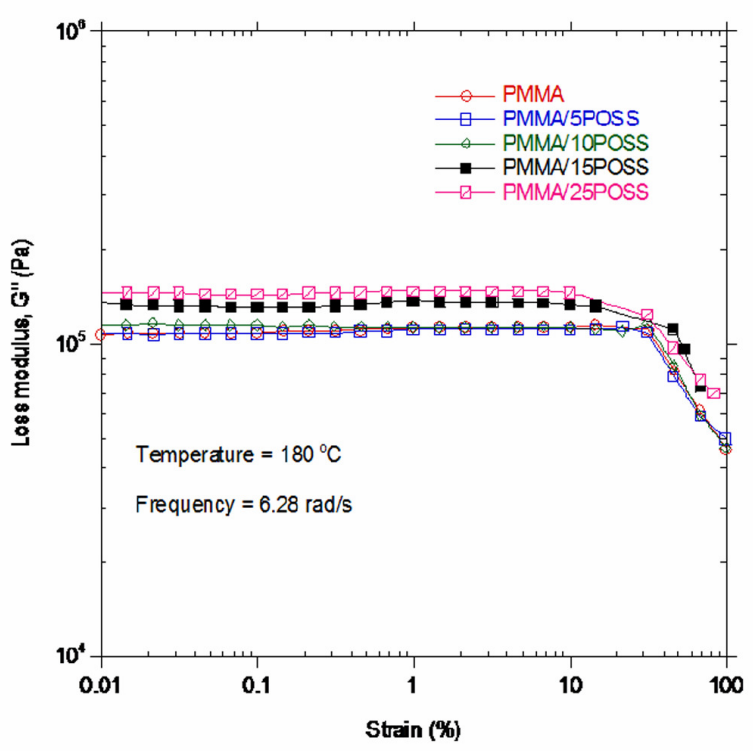

Figure 6.6 Strain amplitude sweep dependence of the loss modulus (G'') of the PMMA matrix and its nanocomposites

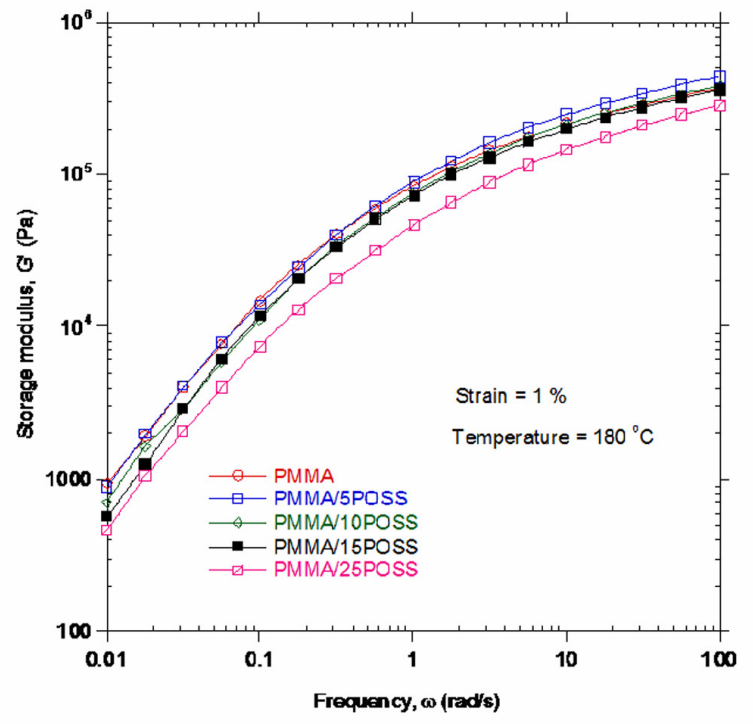

Figure 6.7 Frequency dependence of the storage modulus (G') of pure PMMA and the PMMA/POSS nanocomposites

The frequency sweep tests of the samples were performed in a dynamic oscillation mode at a constant oscillation strain of 1 % at 180 °C to investigate the time-dependent shear behaviour of the pure PMMA and its nanocomposites simulated by rapid motion (high frequencies) and by slow motion (low frequencies) as shown in Figures 6.7 and 6.8. By increasing the frequency, the structure of the temporary network-of-entanglements of the PMMA shows more inflexibility and rigidity. Under these circumstances more deformation energy dissipated by friction between the molecules, because of the reduced relative motion between their chains, can be accumulated. Therefore, both G' and G" are increasing with dominant elastic behaviour. The moduli show an increase up to 5 wt % POSS loading in PMMA, particularly at higher frequencies. A decrease in the modulus with increasing the content of POSS in the polymer matrix was observed. This was probably due to the dispersion of the POSS particles within the matrix. The presence of POSS particles within the matrix resulted in a viscous behaviour of the samples [22], suggesting a decrease in the value of the complex viscosity, η^* (Figure 6.9).

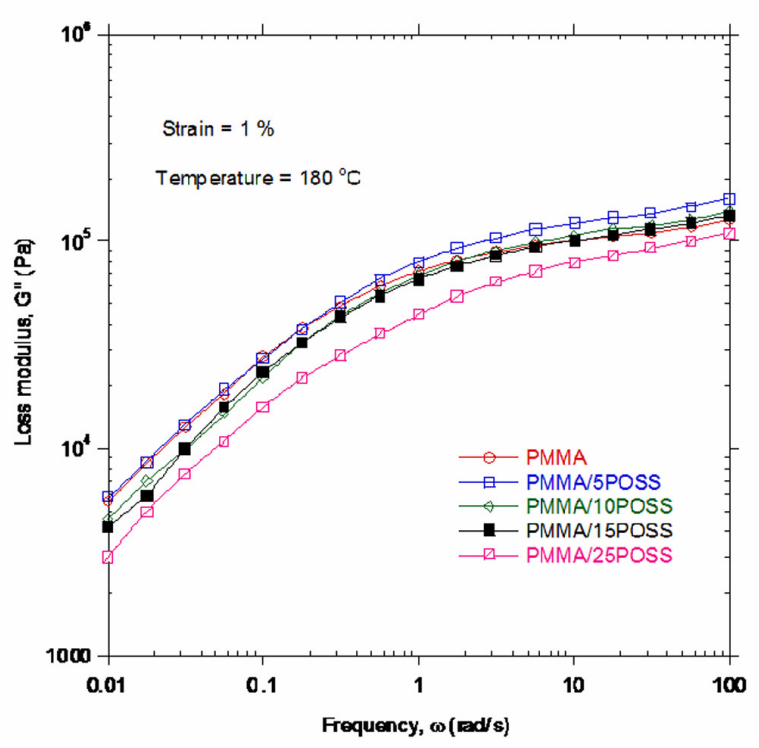

Figure 6.8 Frequency dependence of loss modulus (G'') of pure PMMA and the PMMA/POSS nanocomposites

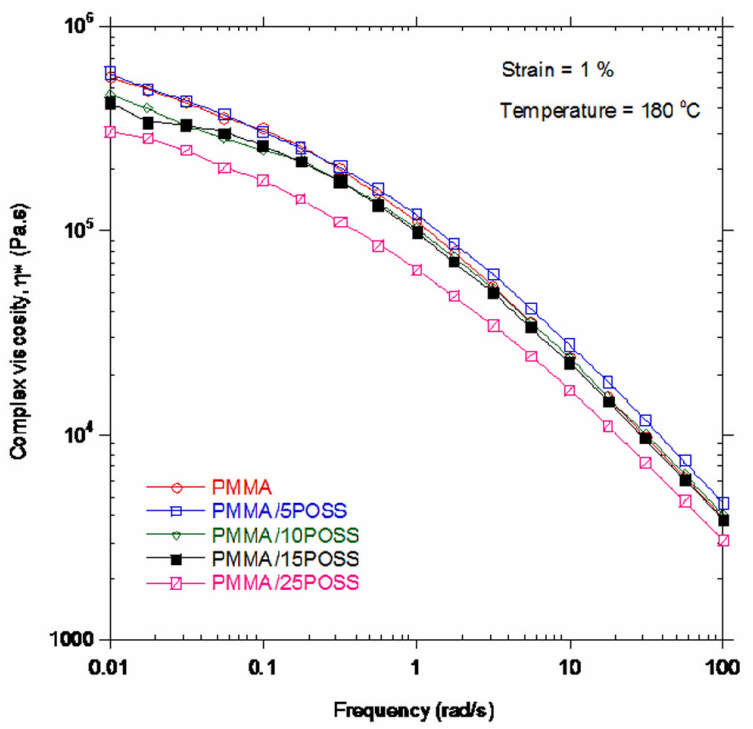

Figure 6.9 Frequency dependence of the dynamic complex viscosity (η*) of pure PMMA and the PMMA/POSS nanocomposites

Kopesky *et al.* [24] reported the rheological behaviour of POSS-filled homopolymers. A slight decrease in the viscosity for POSS loadings $\phi < 0.05$ was observed. This decrease was attributed to a small amount of molecularly-dispersed POSS particles that plasticized the matrix in the molten state at small loadings.

6.2.6 Dynamic mechanical analysis (DMA)

DMA studies were conducted to further confirm the plasticization effect of POSS on the PMMA matrix. The storage modulus (E') curves as a function of temperature are illustrated in Figure 6.10. One can clearly see that the E' for the nanocomposite containing 5 wt % POSS was slightly higher than that of the pure PMMA in the glassy state over the investigated temperature range. The increase in modulus could be attributed to various factors such as the reinforcement effect of the dispersed spherical and rigid particles of POSS on the PMMA. Another probable reason is that the PMMA matrix could simultaneously be reinforced by part of the POSS cages, indicating that the PMMA nanocomposites have a much higher dimensional thermal stability than the pure PMMA at lower temperatures. However, with increasing the POSS content up to 25 wt %, a decrease in E' was observed. Since the POSS

particles do not have any influence on the stiffening of the PMMA matrix when high loadings of POSS were used, this clearly shows that the POSS is molecularly dispersed within the polymer matrix [24]. It is interesting to note that the storage modulus in the rubbery state ($T > T_g$) of the PMMA nanocomposites containing POSS are closer or lower than that of the pure PMMA, despite the presence of nanoreinforcement by the small amount of POSS. This behaviour is attributed to plasticization effect of POSS particles on the PMMA matrix.

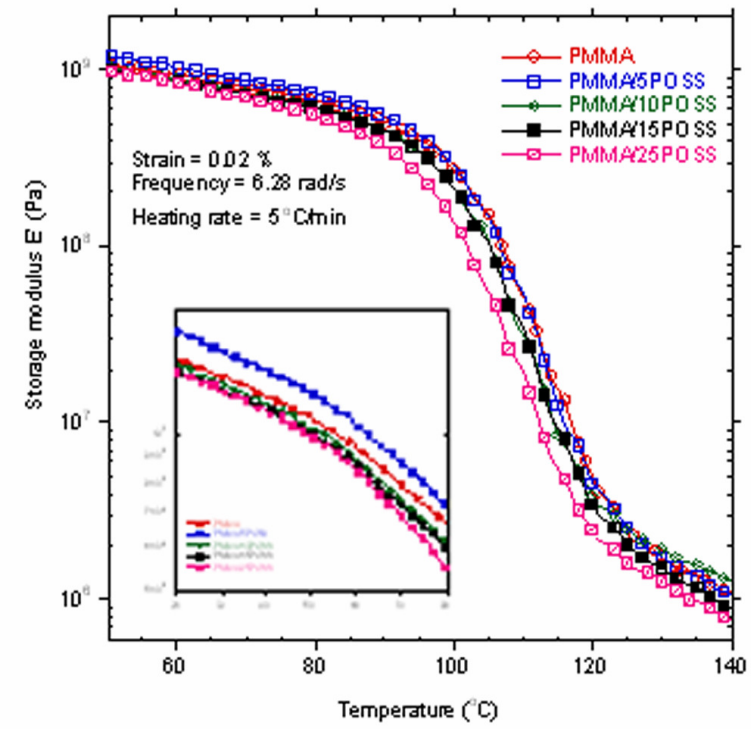

Figure 6.10 Temperature dependence of the storage modulus, E' of pure PMMA and PMMA/POSS nanocomposites

The tan δ curves as a function temperature of the pure PMMA and its nanocomposites are shown in Figure 6.12, in which the T_g is defined as the maximum of tan δ peak. The tan δ curve of the pure PMMA matrix shows a well-defined relaxation peak centered at 125 °C, which is ascribed to the glass-rubbery transition of the PMMA matrix. The T_g values of the PMMA/5POSS, PMMA/10POSS, PMMA/15POSS and PMMA/25POSS nanocomposites are 120, 116, 116 and 113 °C, respectively. The decrease in the T_g with increasing POSS content is attributed to the plasticization effect of the POSS on the PMMA.

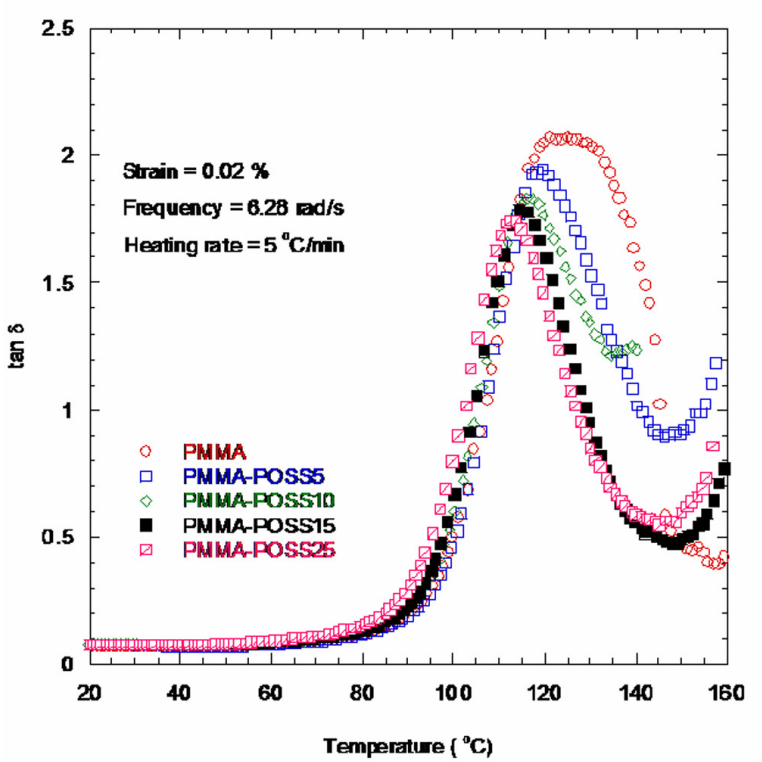

Figure 6.11 Temperature dependence of loss factor curves of pure PMMA matrix and different nanocomposite samples

6.3 Conclusions

This chapter discussed the effect of the addition of different contents of POSS on the morphological, thermal and thermomechanical properties of the PMMA matrix. The dispersion of the POSS particles in the PMMA matrix could not be conclusively established from the FE-SEM results, but the x-ray diffraction studies indicated that the POSS particles were dispersed throughout the PMMA matrix. Both differential scanning calorimetry and dynamic mechanical analysis show a single glass transition for all the investigated samples. A decrease in the glass transition temperature was observed with increasing POSS loading in the polymer matrix, which was attributed to the plasticization effect of POSS on the PMMA. The rheological studies showed a gel-like character for all the investigated samples. An increase in the storage modulus for the 5 wt % POSS containing sample was observed. This behaviour was due to the reinforcement effect of the well dispersed, spherical and rigid POSS particles in the matrix.

6.4 References

1. H. Weickmann, R. Delto, R. Thomann, R. Brenn, W. Döll, R. Mülhaupt. PMMA nanocomposites and gradient materials prepared by means of polysilsesquioxane (POSS) self-assembly. Journal of Materials Science 2007; 42:87-92.
2. Z. Zhang, G. Liang, X. Wang. The effect of POSS on the thermal properties of epoxy. Polymer Bulletin 2007; 58:1013-1020.
3. S. Rogers, L. Mandelkern. Glass transitions of the poly(n-alkyl methacrylates). Journal of Physical Chemistry 1957; 61:985-991.
4. Y. Ni, S. Zheng, K. Nie. Morphology and thermal properties of inorganic–organic hybrids involving epoxy matrix and polyhedral oligomeric silsesquioxanes. Polymer 2004; 45:5557-5568.
5. G.Z. Li, L. Wang, H. Toghiani, T.L. Daulton, K. Koyama, C.U. Pittman, Jr. Viscoelastic and mechanical properties of epoxy/multifunctional polyhedral oligomeric silsesquioxane nanocomposites and epoxy/ladderlike polyphenylsilsesquioxane blends. Macromolecules 2001; 34:8686-8693.
6. H. Xu, S.W. Kuo, J.S. Lee, F.C. Chang. Preparations, thermal properties, and T_g increase mechanism of inorganic/organic hybrid polymers based on polyhedral oligomeric silsesquioxanes. Macromolecules 2002; 35:8788-8793.
7. S.H. Phillips, T.S. Haddad, S.J. Tomczak. Developments in nanoscience: polyhedral oligomeric silsesquioxane (POSS)-polymers. Current Opinion in Solid State and Materials Science 2004; 8:21-29.
8. H. Xu, S.W. Kuo, J.S. Lee, F.C. Chang. Glass transition temperatures of poly(hydroxystyrene-*co*-vinylpyrrolidone-*co*-isobutylstyryl polyhedral oligosilses-quioxanes). Polymer 2002; 43:5117-5124.
9. G.M. Kim, H. Qin, X. Fang, F.C. Sun, P.T. Mather. Hybrid epoxy-based thermosets based on polyhedral oligosilsesquioxane: cure behavior and toughening mechanisms. Journal of Polymer Science Part B: Polymer Physics 2003; 41:3299-3313.
10. I.S. Elashmawi, N.A. Hakeem. Effect of PMMA addition on characterization and morphology of PVDF. Polymer Engineering and Science 2008; 48:895-901.
11. T. Seçkin, S. Köytepe, H.I. Adigüzel. Molecular design of POSS core star polyimides as a route to low-κ dielectric materials. Materials Chemistry and Physics 2008; 112:1040-1046.

12. L. Zheng, A.J. Waddon, R.J. Farris, E.B. Coughlin. X-ray characterization of polyethylene polyhedral oligomeric silsesquioxane copolymers. Macromolecules 2002; 35:2375-2379.
13. L. Cui, J.P. Collet, G. Xu, L. Zhu. Supramolecular self-assembly in a disk-cube dyad molecule based on tryphenylene and polyhedral oligomeric silsesquioxane (POSS). Chemistry of Materials 2006; 18:3503-3512.
14. A.J. Waddon, E.B. Coughlin. Crystal structure of polyhedral oligomeric silsesquioxane (POSS) nanomaterials: A study by x-ray diffraction and electron microscopy. Chemistry of Materials 2003; 15:4555-4561.
15. Y.C. Sheen, C.H. Lu, C.F. Huang, S.W. Kuo, F.C. Chang. Synthesis and characterization of amorphous octakis-fucntionalized polyhedral oligomeric silsesquioxanes for polymer nanocomposites. Polymer 2008; 49:4017-4024.
16. E.T. Kopesky, T.S. Haddad, G.H. McKinley, R.E. Cohen. Miscibility and viscoelastic properties of acrylic polyhedral oligomeric silsesquioxane–poly(methyl methacrylate) blends. Polymer 2005; 46:4743-4752.
17. E. Markovic, S. Clarke, J. Matisons, G.P. Simon. Synthesis of POSS−methyl methacrylate-based cross-linked hybrid materials. Macromolecules 2008; 41:1685-1692.
18. A. Fina, D. Tabuani, F. Carniato, A. Frache, E. Boccaleri, G. Camino. Polyhedral oligomeric silsesquioxane (POSS) thermal degradation. Thermochimica Acta 2006; 440:36-42.
19. J. Zeng, C. Bennett, W.L. Jarrett, S. Iyer, S. Kumar, L.J. Mathias, D.A. Schiraldi. Structural changes in trisilanol POSS during nanocomposite melt processing. Composites Interfaces 2005; 11:673-685.
20. R.A. Mantz, P.F. Jones, K.P. Chaffee, J.D. Lichtenhan, J.W. Gilman, I.M.K. Ismail, M.J. Burmeister. Thermolysis of polyhedral oligomeric silsesquioxane (POSS) macromers and POSS-siloxane copolymers. Chemistry of Materials 1996; 8:1250-1259.
21. J.D. Lichtenhan. Polyhedral oligomeric silsesquioxane: building blocks for silsesquioxanes-based polymers and hybrid materials. Comments on Inorganic Chemistry 1995; 17:115-130.
22. T. Qcwabaza, S. Sinha Ray, W.W. Focke, A. Maity. Morphology and properties of nanostructured materials based on polypropylene/poly(butylene succinate) blend and organoclay. European Polymer Journal 2009; 45:353-367.
23. T.G. Mezger. The Rheology Handbook, 2nd Ed. Hannoprint: Germany (2006).

24. E.T. Kopesky, T.S. Haddad, R.E. Cohen, G.H. McKinley. Thermomechanical properties of poly(methyl methacrylate) containing tethered and untethered polyhedral oligomeric silsesquioxanes. Macromolecules 2004; 37:8992-9004.

CHAPTER 7

CONCLUSIONS, PUBLICATIONS AND CONFERENCE PRESENTATIONS

7.1 Conclusions

The purpose of the study was to prepare polymer nanocomposites based on thermoplastic (LLDPE) and amorphous (PMMA) resins with different types and loadings of POSS nanoscale fillers. The influence of POSS loadings on the morphology, thermal, mechanical, microstructure, thermomechanical and rheological properties was investigated through two different systems, namely LLDPE/octamethyl-T_8-POSS and PMMA/poly((propylmethacryl-heptaisobutyl-POSS)-*co*-(methyl methacrylate)) nanocomposites.

Polarized optical microscopy and FE-SEM studies revealed a fairly homogeneous dispersion of octamethyl-T_8-POSS micro-aggregates in the LLDPE matrix. This micro-aggregation in the nanocomposite systems was due to the intrinsic chemical properties of both LLDPE and POSS, even though the POSS used had been modified with octamethyl chains.

Both conventional and temperature modulated differential scanning calorimetry exhibited multiple melting behaviour of the LLDPE and its nanocomposites at all POSS loadings. This behaviour was attributed to partial melting, re-crystallization, and re-melting phenomena. A homogeneous dispersion of POSS micro-aggregates into the LLDPE matrix resulted in a decrease in the overall crystallinity of the LLDPE matrix with POSS loading. However, POSS did not have any significant effect on the melting temperature of LLDPE.

The homogeneous dispersion of POSS micro-aggregates in the LLDPE matrix led to a dramatic improvement in the elastic storage modulus at higher POSS concentrations. This was due to the potential formation of three-dimensional network-like structures. Two distinguishable transitions were observed in both the loss modulus and loss factor curves. The thermal stability of pure LLDPE and the nanocomposite samples was also studied in air and inert atmospheres. Two degradation steps were observed for all the nanocomposite systems under inert atmosphere. The higher thermal stability of the nanocomposite samples observed

in air in the high-temperature regions may be due to the dispersion of POSS particles in the LLDPE matrix, which decelerated the degradation of the polymer chains *via* char formation.

The melt-state rheological property measurements showed that the POSS particles were highly immiscible with the LLDPE matrix. Because of this phase-separated morphology, POSS-containing LLDPE composites did not show any improvement in tensile properties. A phase-separated morphology also gave rise to a decrease in impact properties of the LLDPE at higher POSS loadings. The heat distortion temperature of the samples increased with increasing the POSS loading in the polymer matrix. This observation was attributed to the potential formation of three-dimensional network-like structures in the nanocomposites.

In the case of PMMA/POSS nanocomposites, the FE-SEM results did not give any information about the dispersion of the POSS particles in the PMMA matrix. However, the x-ray diffraction studies indicated that the POSS particles were dispersed throughout the PMMA matrix. Both differential scanning calorimetry and dynamic mechanical analysis showed a single glass transition for all the investigated samples. A decrease in the glass transition temperature was observed with increasing POSS loading in the polymer matrix, which was attributed to the plasticization effect of the POSS on the PMMA. The rheological studies showed a gel-like character for all the investigated samples. An increase in the storage modulus for the 5 wt % POSS containing sample was observed, which was due to the reinforcement effect of the well dispersed, spherical and rigid POSS particles in the matrix.

7.2 Publications from this project

1. M.J. Hato, S. Sinha Ray, A.S. Luyt. Nanocomposites based on polyethylene and polyhedral oligomeric silsesquioxanes: 1 - Microstructure, thermal and thermomechanical properties. Macromolecular Materials and Engineering 2008; 293:752-762.
2. M.J. Hato, S. Sinha Ray, A.S. Luyt. The effect of POSS nanoparticles on the melt-state viscoelastic and mechanical properties of linear low-density polyethylene nanocomposites. Journal of Nanoscience and Nanotechnology, accepted (2010).
3. M.J. Hato, S. Sinha Ray, A.S. Luyt. The effect of POSS nanoparticles on the thermal and thermomechanical properties of poly(methyl methacrylate). Advanced Science Letters, submitted (2010).

7.3 Conferences presentations

1. Preparation, characterization and viscoelastic properties of LLDPE/POSS nanocomposites. NanoAfrica 2009 Conference, Pretoria, 1-4 February 2009, RSA.
2. Preparation, characterization and viscoelastic properties of linear low-density polyethylene/POSS nanocomposites. 2nd Southern African Conference on Rheology, Cape Peninsula University of Technology, Cape Town, 6-8 October 2008, RSA.
3. Properties of linear low density polyethylene/polyhedral oligomeric silsesquioxanes nanocomposites. 236th American Chemical Society (ACS) meeting and exposition, Philadelphia, PA, 17-21 August 2008, USA.